Statistical analyses of the meteorological observation and numerical weather forecasting datasets to understand severe dust events and extreme wind speed in Iran

マーモウディ, レイラ

https://hdl.handle.net/2324/7329513

出版情報：Kyushu University, 2024, 博士（学術）, 課程博士
バージョン：
権利関係：

Statistical analyses of the meteorological observation and numerical weather forecasting datasets to understand severe dust events and extreme wind speed in Iran

By

Leila Mahmoudi

A THESIS SUBMITTED IN PARTIAL FULFILMENT OF THE REQUIREMENTS FOR THE DEGREE OF

Doctor of Philosophy (PhD)

in

Interdisciplinary Graduate School of Engineering Sciences

Kyushu University

(Fukuoka, Japan)

九州大学

KYUSHU UNIVERSITY

Supervisor: Professor Dr. Naoki Ikegaya

June 2024

ABSTRACT

Understanding the fundamental mechanisms of sand and dust transports is crucial for grasping the diverse causes and impacts of dust events in Iran, which occur in various forms such as suspended dust, rising dust, and dust storms. These events exhibit distinct characteristics and frequencies across different regions in the entire regions of Iran. By understanding the frequency of different dust events in various regions, we can quantify the impact of dust events on buildings, transportation, and human beings. In addition, predicting dust storms requires accurate estimation of weather conditons such as wind speed distributions. Improving our understanding of wind dynamics is crucial for refining predictions and mitigating the impacts of dust storms. Therefore, this thesis deals with both meteorological observation and numerical weather forecasting datasets. The meteorological datasets were employed to quantify the present status of the dust events in Iran over last ten years in terms of the occurrence frequency, strength, types, and spatial distributions of the dust events. Accordingly, to clarify the effect of strong wind speeds on the dust events, numerical weather forcasing was employed to predict wind speed distributions thoroughout a year. By scrutinizing the meteorological datasets and weather forecasting wind distributions, this thesis clarify the spatial distributons of the dust events and wind speeds in the entire regions of Iran. The summaries of the thesis are as follows:

In Chapter 1, we introduced the research background, declared the research gap and purpose, outlined the thesis structure, and provided fundamental preliminary information essential for this research.

Chapter 2 explores the environmental dynamics of the dry belt region, particularly focusing on the Middle East. It discusses the climatic and anthropogenic parameters influencing sand and dust storms. The chapter highlights Iran's susceptibility to dust events due to its geographical conditions and examines the impact of dry lake beds on dust generation. Additionally, it discusses predictive modeling of dust storms and their impact on various sectors, emphasizing the importance of proactive measures in mitigating adverse effects.

Chapter 3 explores an extensive examination of sand and dust storms within the geographical context of Iran. The primary objective is to comprehensively analyze the occurrence patterns, spatial distribution, and long-term trends of these atmospheric phenomena. The chapter meticulously examines the frequency and duration of dust events across Iran based on the analysis of long-term meteorological datasets. By categorizing dust events into three main types—

suspended dust, rising dust, and dust storms—the chapter clarifies the varying characteristics and prevalence of each category. This categorization aids in understanding the spatial and temporal distribution of dust events, offering insights into the regions most affected and the severity of these events. Furthermore, by uncovering seasonal patterns and trends in the frequency and duration of dust events across different seasons, the chapter explores long-term trends of dust events, utilizing historical data to discern patterns and changes over time.

Chapter 4 provides a comprehensive analysis of the prediction accuracy of wind speeds using both numerical weather forecasting (NWF) and statistical models across various stations in Iran. This chapter describes the methodology employed to investigate wind patterns in Iran. It begins by explaining the study region, providing comprehensive details regarding the implementation of the NWF model. Furthermore, it introduces a statistical model, namely the Gram-Charlier series (GCS) model, aimed at refining the approximation of wind speed probability density functions (PDFs). Moreover, this chapter scrutinizes the relationship between fundamental statistics for both the numerical weather model and observational outputs for estimating extreme wind speeds. Subsequently, the analysis proceeds to compare PDFs at specific stations, thereby accentuating the applicability of the statistical GCS model prediction of extreme wind values using the mentioned model. Thereby, assessing the effectiveness and utility of the GCS model in this context.

Chapter 5 offers concise summaries of the key findings and results from each preceding chapter, accompanied by insights into potential future research directions for further exploration and development.

ACKNOWLEDGEMENTS

First, I would like to extend my sincere gratitude to Prof. Naoki Ikegaya for his immense knowledge, invaluable advice, and most importantly, his unwavering support during my three-year doctoral program. His patient leadership and timely support during the most challenging moments have been instrumental in my academic and personal growth. I could not have reached this milestone without his continuous support and mentorship.

Secondly, I would like to extend my profound gratitude to Prof. Hagishima, who provided me with the opportunity to continue my studies in Japan. I am deeply appreciative of her continuous guidance and encouragement.

Additionally, I would like to thank both Prof. Hagishima and Prof. Sugihara for their valuable comments and advice, which have significantly helped me improve my thesis.

My doctoral program would not have been possible without the financial support for tuition and stipend provided by the MEXT scholarship. I am very grateful for the valuable opportunity offered by the Japanese government.

My deep thanks go to my beloved family for their boundless love and encouragement throughout my time studying abroad. Their consistent respect for my decisions and support have been a source of great strength and motivation.

When youth departs, May wisdom prove enough.

Winston Churchill

TABLE OF CONTENTS

LIST OF FIGURES

LIST OF TABLES

CHAPTER 1: BACKGROUND OF STUDY

1.1. MOTIVATION

Climate is unstable and it always changing. In recent decades it has turned into a concern among countries, and it has been considered as the biggest challenge of the 21st century. Climate change induce the dust storm even though it is natural elements of earth bio-chemical cycles, but they have been increased in recent decades through human activities and climate change (Jish Prakash Et al. 2015). Drivers of dust storms are both natural and anthropogenic. major place that these events happen is deserts. Thus, the frequency of occurrence of dust and sandstorms are high in arid and semi-arid regions. However, Deserts are not only source of aeolian particles, volcanic eruptions, marine terraces, and coastal dunes, dry lakes bed, riverbeds, glacial and periglacial deposits, and ocean spray are other important sources which shows that they are not limited to deserts areas and happens in other regions of world (Chen et al. 2018).

Aeolian particles originate from the Earth's surface and is carried by the wind into the air. It is transported both vertically and horizontally before finally falling back to the Earth's surface in different scales. It is called sand and dust storm which happen in different areas in world and different parameters effects it (Yamamoto et al. 2007). There is no standard definition for sand and dust events, and the distinction between sandstorms and dust-storms is not clear. However, these events can be characterized mainly by their duration, widespread coverage, and the concentration of particulates (Gandham et al. 2020). Additionally, they can be categorized based on a continuum of particle sizes: clay-sized (<4 µm in diameter), silt-sized (4–62.5 µm), and sand-sized (62.5 µm to 2 mm) (FAO, 2023). Chemically, sand and dust are composed of silicon dioxide (SiO_2), aluminum oxide (Al_2O_3), iron oxides (Fe_2O_3 and FeO), calcium oxide (CaO), magnesium oxide (MgO), and potassium oxide (K_2O). The relative abundance of these compounds varies depending on the sediment in the source area (Krueger et al. 2004). Dust particles may also contain various salts, organic matters, microorganisms (including fungi, bacteria, and viruses, some of which can be pathogenic), and pollutants from human activities such as agriculture and industry, and particles of biogenic origin, and fragments from living organisms (such as pollen and spores), also include elements derived from plant and animal matter (Yang et al. 2007).

Nine regions generate global dust production: North Africa (Sahara), South Africa, the Arabian Peninsula, Central Asia, Western China, Eastern China, North America, South America, and Australia and among these, North Africa, the Middle East, Southwest Asia, and Northeast Asia experience the highest dust frequencies which known as Dust Belt (World Bank. 2019).

Planetary-scale climate indices, such as ENSO, IOD, NAO, AMO, and AO, influence dust emissions across various regions through teleconnections. ENSO affects East Asia dust storms via the winter monsoon, while IOD impacts Middle Eastern and Southwest Asian dust emissions by altering local rainfall and winds. NAO and AMO control Sahel dust emissions by modifying rainfall, and AO influences East Asian dust storms by affecting atmospheric instability and Central Asian dust emissions by regulating the Siberian high (Feng et al. 2016).

Global warming, linked to sea surface temperature (SST) anomalies, affects dust emissions over the dust belt. Shifts in ENSO phases correspond with warming trends on Eurasian and North American continents. A slowdown in SST warming in the Indian Ocean reduced dust in Southwest Asia, while warmer North Atlantic SSTs decreased dust in the Sahel by increasing rainfall (Shi et al. 2021).

Besides, land tenure and management systems across the Dust Belt are intricate and multifaceted. Smallholder field crop cultivation is primarily conducted on private arable lands, whereas livestock management in marginal drylands, such as rangelands and steppes, typically takes place on governmental or public lands.

Additionally, Dust emissions in the Middle East are strongly linked to the semi-permanent anticyclone situated over North Africa and extending to Eastern Europe, as well as the Monsoon trough affecting Iraq, southern Iran, Pakistan, and the Indian subcontinent and in Central Asia, dust emissions are influenced by the Caspian high and the Hindu-Kush low.

Wind erosion predominantly occurs in the northern hemisphere within the dust belt. About 40% of the solid or liquid particles suspended in the troposphere are dust particles from wind erosion, leading to a higher frequency of sand and dust storms in this expansive region compared to other parts of the world where such events are notably less common (Muhs et al. 2014).

Impacts of sand and dust storms are widespread, and they directly affect poverty, hunger, health, safe water, clean energy, economic growth, Industry innovation and infrastructure, Sustainable cities and communities, Climate action, life below water, life on land. Sand and dust storm can cause poverty since it causes desertification and damage to crops and livestock as well as agricultural infrastructure and food quality. Sand and dust storm can cause respiratory problems. Sand and dust storm can pollutant clean waters since they carry micro-organisms and salt. They can cause damages to energy infrastructures, roads, cities and hampering the cities effort to become safe and resilient. They have both negative and positive impacts on life under water; However, they effect life on land mostly in negative way (FAO. 2023).

Recent findings reveal that Arctic amplification is causing changes in wind circulation, reducing dust transport to certain regions, according to Gao Meng from Hong Kong Baptist University. Conversely, in Pakistan, dust has worsened air quality in cities like Karachi and Lahore and significantly altered rainfall patterns, says Khan Alam from the University of Peshawar. Dust particles can increase extreme rainfall, and Alam's team is exploring a possible link between dust and the severe floods in Pakistan in 2022 (Ahmadzai. 2023).

Approximately 80 percent of the populations in Turkmenistan, Pakistan, Uzbekistan, Tajikistan, and Iran are exposed to poor air quality due to sand and dust storms, according to ESCAP reports. Among these countries, Iran is also projected to experience high levels of water stress by 2030, leading to extreme drought conditions and consequently increasing the risk of sand and dust storms in the future. Additionally, simulation modelling indicates that emissions of dust into the atmosphere caused by the combined impact of land use and climate change have increased by 25–50 percent globally since 1900 (Shepherd et al. 2016; Vukovic et al. 2021).

Managing the risks associated with sand and dust storms may also become essential in areas not previously recognized as source areas. Effective management of sand and dust sources begins with accurately identifying their locations. Thus, sand and dust storms represent an important emerging issue for policymakers. Alternatively, our understanding of how these storms interact with society and the environment is still limited by considerable uncertainties.

Strengthening capacities in proactive disaster preparation for effective response and recovery at all levels is essential due to the anticipated increase in sand and dust risk in many parts of the Dust Belt. As climate change and human activities continue to influence weather patterns and land use, the frequency and intensity of these events are expected to rise. This requires a comprehensive approach that emphasizes early warning systems and accurate forecasting, along with community preparedness programs and effective recovery plans to mitigate the impact of sand and dust storms (World Bank. 2019).

Within these dryland areas, sources of sand and dust storms are often highly localized and specific. Within Key physical factors that influencing soil erosion are wind speed and wind direction and wind turbulence. Turbulence over a loose and unstable surface, influenced by wind structure, contributes to the rise of dust and sand particles from the soil. In most regions, dust storms begin when wind speeds reach 10–12 m/s. Thus, wind speed (in meters per second) and duration (in hours) are used to estimate the severity of sand and dust storms. Because severity of dust storm has connection with transport of particles in various modes (Duniway et al. 2019).

The transport of soil particles by wind can thus be crudely separated into several physical regimes but these regimes change continuously into the next with changing wind speed, particle size, and soil size distribution. The mentioned divisions also help to understand the occurrence frequency of sand and dust events (Goossens et al. 2002).

Besides, seasonal variations in wind patterns can lead to significant changes in the frequency and magnitude of dust events, with some regions experiencing more intense and frequent events during particular times of the year. By understanding the frequency and characteristics of different dust events in various regions, we can develop more effective strategies to protect affected areas and mitigate their effects. It also helps to identify sources of sand and dust storms whether they are local, regional, or transboundary.

Numerous studies have analyzed dust events across various regions in Iran. they indicate that a significant portion of dust originates from transboundary sources. Recent environmental changes in neighboring countries have manifested as an increased frequency and intensity of dust events over Iran.

Middleton. (1986) conducted a preliminary study on the frequency and seasonality of dust events in Iran using ground station observations. He suggested that the highest frequency of dust events occurs at the borders of Iran, Pakistan, and Afghanistan. This region, known as Dasht-e Margo, includes the Sistan Basin, the Registan Desert, and northwestern Baluchistan.

This region experiences the 'wind of 120 days' from mid-May to mid-September. Another high-frequency source of dust identified by Middleton. (1986) is the Makran Desert along the coastal plain of the Oman Sea. Subsequently, Furman. (2003) examined the temporal characteristics of dust storms in the Middle East using synoptic data spanning 21 years, from 1973 to 1993. Furman's study revealed distinct seasonal variations in peak dust activity across different areas of the Middle East. He identified clear seasonal variations in peak dust activity across different areas of the Middle East. In the Mediterranean region, the peak occurred in winter and spring. Further southeast, over western Iraq, Syria, and the northern Arabian Peninsula, the peak was in spring. Meanwhile, in Mesopotamia, Iran, and the southern Arabian Peninsula, the peak dust activity was observed during the summer.

Few studies within Iran have analyzed the frequency of dust events across the country, often relying on data from a limited number of stations and regions. Consequently, these analyses have generally been narrow in scope compared to the vast and diverse areas of Iran and the wide range of dust event categories. For example, studies by Beyranvand et al., Baghbanan et al., Mesbahzadeh et al., Modarres, and Sadeghi have used limited data sets, while those employing a high number of stations, such as Alizadeh-Choobari et al. (2016), have focused on only a few dust categories and have not fully explored the variety of dust events.

This study aims to address this gap by analyzing data from all available meteorological stations across Iran to comprehensively assess the most significant dust categories within a recent time frame.

As mentioned previously, wind speed plays a crucial role in the development of sand and dust storms. However, the relationship between wind speed and sand and dust storm development is complex and not straightforward. Various factors, such as soil moisture, vegetation cover, and land surface conditions, also significantly influence the initiation and intensity of these storms. Predicting dust storms accurately is challenging due to flaws in current forecasting methods, particularly when it comes to estimating wind speed. Numerical weather models, which are essential tools for forecasting sand and dust storm, often struggle to provide precise wind speed measurements (Akhlaq et al. 2012). These inaccuracies can result in unreliable predictions of dust events, leading to either underestimation or overestimation of their severity. This discrepancy is due to numerical weather models not fully considering local terrain, weather conditions, and surface features that affect wind patterns. Consequently, improving wind speed estimation in weather models is critical for enhancing the accuracy of dust storm forecasts. The weather research and forecast (WRF) is one of widely used model in Iran for both research and operational weather forecasting. It is favored for its high resolution and ability to simulate local weather phenomena. However, the accuracy of predictions from the WRF model remains uncertain, with several studies indicating a tendency to overestimate wind speed (Prósper et al. 2019; Saadatabadi et al. 2023; Hamzeh et al. 2023), particularly during extreme wind events (Mohammadi et al. 2024).

To examine the outcomes derived from numerical weather models such as WRF, many statistical models or parametric methods have been developed to estimate wind speed distribution. Knowledge of the wind speed frequency distribution is a very important factor to evaluate the wind potential. The probability density function (PDF) provides a comprehensive representation of the wind speed distribution, capturing the frequency and intensity of different wind speeds within a given area. By examining the PDF, researchers can better understand the local flow patterns and the variability in wind speeds. The shape of the PDF, which is influenced by various parameters, helps in accurately fitting the observed wind speed data, allowing for more reliable predictions and assessments of wind potential. Several parametric estimation methods can be used in wind studies (Palutikof et al 1999; Huang et al. 2018).

Weibull, Gamma, and Rayleigh distributions are commonly used as probability distribution functions for estimating wind power potential. Among these, researchers have established that the Weibull distribution is more accurate in capturing the skewness of wind speed distributions, making it the preferred choice in many studies. The Weibull distribution relies on two key parameters to define its PDF and cumulative distribution function (CDF).

The two parameters are k and c. The parameter k, known as the shape factor, is dimensionless and describes the distribution's form. The parameter c, known as the scale factor, is measured in units of wind speed (m/s) and influences the distribution's scale. Understanding the shape parameter is crucial for determining the wind characteristics in a particular region, especially since wind direction is a significant factor. Meanwhile, the scale parameter is vital for assessing the wind energy potential, as it indicates the typical wind speed magnitude in the area (Shi et al. 2021).

Previous studies have indicated that extreme wind speeds have minimal impact on the parameter values of the Weibull distribution (Wang et al. 2015). When wind speeds surpass a certain threshold, the Weibull model becomes ineffective. This ineffectiveness results in significant errors in estimating the maximum annual wind speed distribution and the return period, thereby compromising the risk assessment of extreme winds (Perrin et al. 2006). To address this issue, an alternative approach to modeling the PDF of wind speeds, a modified Gaussian distribution known as the Gram-Charlier series (GCS), has recently been employed. The GCS is acknowledged as series expansion of the Gaussian distribution function, incorporating higher-order statistics to precisely estimate PDFs. Extreme wind speeds can be estimated by GCS because the GCS method adjusts the Gaussian distribution by incorporating a term based on higher-order statistics, allowing it to describe PDFs that meet the specified statistical requirements.

In recent years, several studies have analyzed low-occurrence wind events at pedestrian levels in idealized scenarios, utilizing the GCS model to determine PDFs from time-series wind speed data. However, the application of the GCS model has been limited to these pedestrian-level studies and has not been extended to meteorological studies. Our research aims to bridge this gap by applying the GCS model to meteorological data, providing a novel approach to estimating low-occurrence extreme wind speeds.

This study aims to enhance the accuracy of dust storm forecasts in Iran by comprehensively analyzing data from all available meteorological stations and applying the numerical weather and statistical model to estimate low-occurrence extreme wind speeds. By doing so, the prediction of dust events will be improved by integrating advanced wind speed estimation techniques with extensive meteorological data analysis.

1.2. OBJECTIVE OF DISSERTATION

(1) Analyze the temporal and spatial variations of dust events in Iran highlighting key regions with high dust activity and identifying trends over recent decades.

(2) Apply the statistical model to meteorological data and simulation data to estimate PDF of extreme wind speeds, aiming to improve the accuracy of wind speed predictions and, consequently, dust storm forecasts.

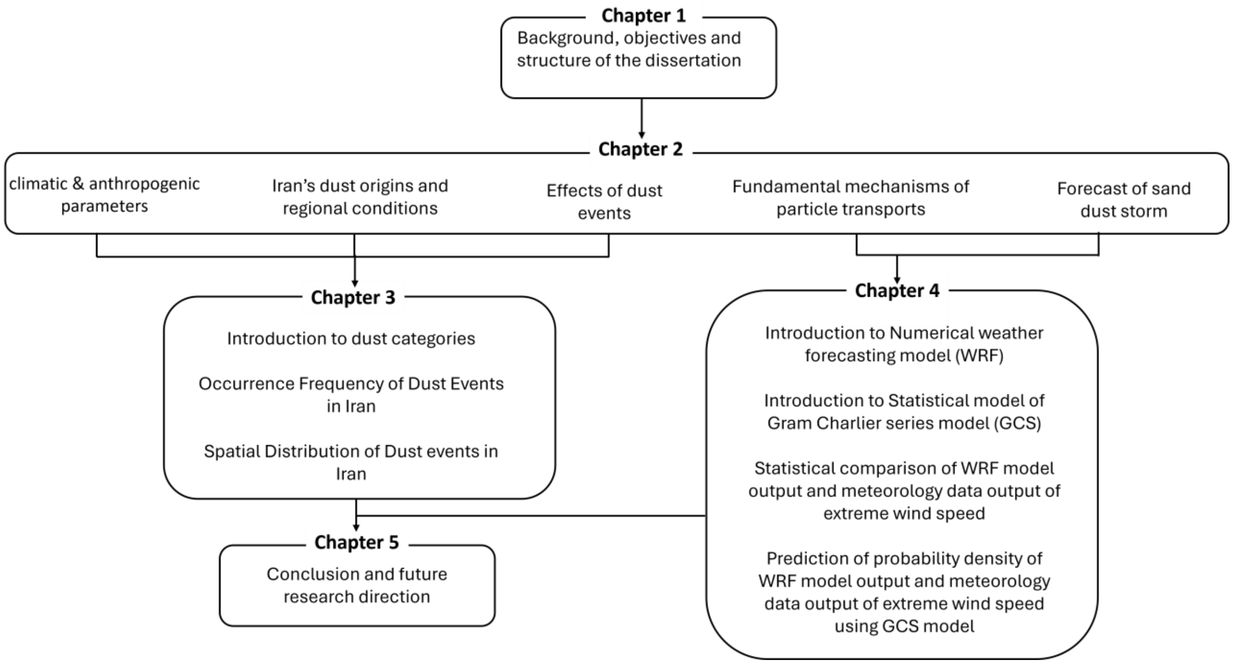

Figure 1.1 Diagram of dissertation structure.

1.3. STRUCTURE OF DISSERTATION

This dissertation is structured in accordance with the following chapters, which collectively encompass the objectives mentioned earlier:

- Chapter 2 explores the environmental dynamics of the dry belt region, particularly focusing on West Asia, known as the Middle East. It discusses the climatic and anthropogenic parameters influencing sand and dust storms. The chapter highlights Iran's susceptibility to dust events due to its geographical conditions and examines the impact of dry lake beds on dust generation. Additionally, it discusses predictive modeling of dust storms and their impact on various sectors, emphasizing the importance of proactive measures in mitigating adverse effects.
- Chapter 3 explores an extensive examination of sand and dust storms within the geographical context of Iran. The primary objective is to comprehensively analyze the occurrence patterns, spatial distribution, and long-term trends of these atmospheric phenomena. The chapter meticulously examines the frequency and duration of dust events across Iran based on the analysis of long-

term meteorological datasets. By categorizing dust events into three main types of suspended dust, rising dust, and dust storms the chapter clarifies the varying characteristics and prevalence of each category. This categorization aids in understanding the spatial and temporal distribution of dust events, offering insights into the regions most affected and the severity of these events. Furthermore, by uncovering seasonal patterns and trends in the frequency and duration of dust events across different seasons, the chapter explores long-term trends of dust events, utilizing historical data to discern patterns and changes over time.

- Chapter 4 provides a comprehensive analysis of the prediction accuracy of wind speeds using both numerical weather forecasting (NWF) and statistical models across various stations in Iran. This chapter describes the methodology employed to investigate wind patterns in Iran. It begins by explaining the study region, providing comprehensive details regarding the implementation of the NWF model. Furthermore, it introduces a statistical model, namely the Gram-Charlier series (GCS) model, aimed at refining the approximation of wind speed probability density functions (PDFs). Moreover, this chapter scrutinizes the relationship between fundamental statistics for both the numerical weather model and observational outputs for estimating extreme wind speeds. Subsequently, the analysis proceeds to compare PDFs at specific stations, thereby accentuating the applicability of the statistical GCS model prediction of extreme wind values using the mentioned model. Thereby, assessing the effectiveness and utility of the GCS model in this context.
- Chapter 5 offers concise summaries of the key findings and results from each preceding chapter, accompanied by insights into potential future research directions for further exploration and development.

1.4. REFERENCES

Ahmadzai H. (2023). The impact of sand and dust storms on agriculture in Iraq. Middle East Development Journal, 15(1), 50-65.

Akhlaq M, Sheltami TR, Mouftah HT. (2012). A review of techniques and technologies for sand and dust storm detection. Reviews in Environmental Science and Bio/Technology, 11, 305-322.

Alizadeh-Choobari O, Ghafarian P, Owlad E. (2016). Temporal variations in the frequency and concentration of dust events over Iran based on surface observations. International Journal of Climatology, 36(4), 2050-2062.

Beyranvand A, Azizi G, Alizadeh-Choobari O, Darvishi Boloorani A. (2019). Spatial and temporal variations in the incidence of dust events over Iran. Natural Hazards, 97, 229-241.

Chen S, Jiang N, Huang J, Xu X, Zhang H, Zang Z, Huang K, Xu X, Wei Y, Guan X, Zhang X. (2018). Quantifying contributions of natural and anthropogenic dust emission from different climatic regions. Atmospheric Environment, 191, 94-104.

Duniway MC, Pfennigwerth AA, Fick SE, Nauman TW, Belnap J, Barger NN. (2019). Wind erosion and dust from US drylands: a review of causes, consequences, and solutions in a changing world. Ecosphere, 10(3), e02650.

Feng J, Liao H, Li J. (2016). The impact of monthly variation of the Pacific–North America (PNA) teleconnection pattern on wintertime surface-layer aerosol concentrations in the United States. Atmospheric Chemistry and Physics, 16(8), 4927-4943.

Furman HK. (2003). Dust storms in the Middle East: sources of origin and their temporal characteristics. Indoor and Built Environment, 12(6), 419-426.

Gandham H, Dasari HP, Langodan S, Karumuri RK, Hoteit I. (2020). Major changes in extreme dust events dynamics over the Arabian Peninsula during 2003–2017 driven by atmospheric conditions. Journal of Geophysical Research: Atmospheres, 125(24), e2020JD032931.

Goossens D, Gross J. (2002). Similarities and dissimilarities between the dynamics of sand and dust during wind erosion of loamy sandy soil. Catena, 47(4), 269-289.

Hamzeh NH, Abadi AR, Kaskaoutis DG, Mirzaei E, Shukurov KA, Sotiropoulou RE, Tagaris E. (2023). The Importance of Wind Simulations over Dried Lake Beds for Dust Emissions in the Middle East. Atmosphere, 15(1), 24.

Huang M, Li Q, Xu H, Lou W, Lin N. (2018). Non-stationary statistical modeling of extreme wind speed series with exposure correction. Wind Struct, 26(3), 129-146.

Krueger BJ, Grassian VH, Cowin JP, Laskin A. (2004). Heterogeneous chemistry of individual mineral dust particles from different dust source regions: the importance of particle mineralogy. Atmospheric Environment, 38(36), 6253-6261.

Liu Y, & Westphal, D. L. (2001). Dust Storms: A Review of Meteorological and Climatological Aspects. Journal of Climate, 14(5), 997-1010.

Middleton NJ. (1986). A geography of dust storms in South-west Asia. Journal of Climatology, 6(2), 183-196.

Mohammadi MH, Meshkatee AH, Ghader S, Azadi M. (2024). Wind gust forecasting by post-processing the WRF model outputs using ANN. Dynamics of Atmospheres and Oceans, 105, 101425.

Muhs DR, Prospero JM, Baddock MC, Gill TE. (2014). Identifying sources of aeolian mineral dust: Present and past. In Mineral dust: A key player in the earth system (pp. 51-74).

Palutikof JP, Brabson BB, Lister DH, Adcock ST. (1999). A review of methods to calculate extreme wind speeds. Meteorological Applications, 6(2), 119-132.

Prósper MA, Otero-Casal C, Fernández FC, Miguez-Macho G. (2019). Wind power forecasting for a real onshore wind farm on complex terrain using WRF high resolution simulations. Renewable Energy, 135, 674-686.

Shepherd G, Terradellas E, Baklanov A, Kang U, Sprigg W, Nickovic S, Boloorani AD, Al-Dousari A, Basart S, Benedetti A, Sealy A. Global assessment of sand and dust storms. UNEP, WMO, UNCCD. 2016 Sep 1.

Shi H, Dong Z, Xiao N, Huang Q. (2021). Wind speed distributions used in wind energy assessment: a review. Frontiers in Energy Research, 9, 769920.

Shi L, Zhang J, Yao F, Zhang D, Guo H. (2021). Drivers to dust emissions over dust belt from 1980 to 2018 and their variation in two global warming phases. Science of The Total Environment, 767, 144860.

Stenchikov G, Kalenderski S, Osipov S, Bangalath H. (2015). The impact of dust storms on the Arabian Peninsula and the Red Sea. Atmospheric Chemistry and Physics, 15(1), 199-222.

Vukovic Vimic A, Cvetkovic B, Giannaros TM, Shahbazi R, Sehat Kashani S, Prieto J, Kotroni V, Lagouvardos K, Pejanovic G, Petkovic S, Nickovic S. (2021). Numerical simulation of Tehran dust storm on 2 June 2014: A case study of agricultural abandoned lands as emission sources. Atmosphere, 12(8), 1054.

Wang J, Qin S, Jin S, Wu J. (2015). Estimation methods review and analysis of offshore extreme wind speeds and wind energy resources. Renewable and Sustainable Energy Reviews, 42, 26-42.

World Bank. 2019. Sand and Dust Storms in the Middle East and North Africa Region—Sources, Costs, and Solutions. Washington, DC.

Yamamoto T, Yoshino M, Suzuki J. (2007). The relationship between occurrence of dust events and synoptic climatological condition in East Asia, 1999-2003. Journal of the Meteorological Society of Japan, 85(2), 81-99.

Yang X, Liu Y, Li C, Song Y, Zhu H, Jin X. (2007). Rare earth elements of aeolian deposits in Northern China and their implications for determining the provenance of dust storms in Beijing. Geomorphology, 87(4), 365-377.

CHAPTER 2: PRESENT SITUATIONS OF DUST EVENTS IN IRAN FOR SEEKING NUMERICAL PREDICTIONS

2.1. CLIMATE AND DUST DYNAMICS OF WEST ASIA

West Asia, commonly known as the Middle East, encompasses a climatically sensitive region that spans from the eastern Mediterranean Sea to the Arabian Peninsula, including Syria, Iraq, Iran, and other neighboring areas. This area is located in the world dry belt, an expansive region characterized by diverse landscapes, ranging from the Sahara and the deserts of the Arabian Peninsula to the Thar Desert, the Iranian highlands, and further eastward to the Karakum and Kyzylkum deserts of Central Asia. Extending over 15,000 kilometers from the Atlantic coast to northern China, the Sahara–Gobi Desert belt is a defining feature of this region. Precipitation is low in the dry belt, and it is most concentrated in the southeastern part of Asia, gradually decreasing towards the west. Encompassing various desert ecosystems such as the Taklamakan and the Gobi in Mongolia and China, this vast belt underscores the climatic intricacies and environmental diversity of West Asia and its surroundings (Sharifi et al. 2018). Thus, these regions are the most dust-prone areas in the world. However, the Sahara is considered the main source of dust, generating between 61 and 366 million tons annually among these regions (Swap et al. 1996).

2.2. CLIMATIC PARAMETERES

Precipitation, wind speed, temperature, vegetation cover, soil moisture and porosity in sand sources exert a direct influence on the manifestation of sand and dust events.

The decrease in precipitation affects soil moisture and vegetation rates. Soil moisture increase the cohesion between soil and gran particles and prevent them from moving by wind.

Low coverage of vegetation on the surface makes it susceptible to wind erosion (Awadh et al. 2023). Therefore, the height and density of vegetation should be considered as effective factors. On the other hand, increased precipitation leads to higher soil humidity, enhancing soil particle cohesion. This increased cohesion enables the soil to resist wind erosion (Awadh et al. 2023). Dust events, shaped by both wind speed and particle size, determining the distance and area over which they occur. They can either emerge locally, affecting nearby regions, or travel across vast distances to affect areas far beyond their origin.

soil grain size also effective factor and if the soil grains become small the dust is blown up easily into air by wind.

2.3. ANTHROPOGENIC PARAMETERS

Even though climatic and terrestrial parameters are the main reasons of development of sand and dust storms, but anthropogenic parameters also induce these events. Most of the sand and dust storms in the Middle East come from a complex mixture of both natural and anthropogenic sources particularly hydrologic sources. Hydrologic dust sources, including ephemeral water bodies, contribute to 31% of worldwide dust emissions, with 15% being natural and 85% anthropogenic. Globally, 20% of dust emissions originate from vegetated surfaces, predominantly desert shrublands and agricultural lands. The emissions from anthropogenic dust sources are influenced by land use and ephemeral water bodies, both of which are connected to the hydrological cycle (Ginoux et al. 2012).

2.4. IRAN GEOMETRICAL AND REGIONAL CONDITIONS

Iran, located within a dry belt in the northern hemisphere, is surrounded by several countries having large deserts. For example, the Karakum desert with an area of 350,000 km^2 is located in Turkmenistan, the northeast area of Iran. Margo (Dasht-e Margo) and Registan deserts spread in the southeast of Iran with an area of 150,000 km^2 in Afghanistan. In addition, the Arabian desert in southwest across the Persian Gulf of Iran consists of three deserts (Rub al Khali, ad-Dahna, and An-Nafud). The area of 2,330,000 km^2 covers not only Saudi Arabia but also Jordan, Iraq, Oman, Yemen, and United Arab Emirates. In Iran as well, there are also deserts such as Dasht-e Kavir and Lut deserts covering the wide ranges of the land of Iran. Since the main problems caused by the dust and sand transports are related to the sands traveling in the air and drifting on the ground from the surrounding deserts, it can be said that Iran is located in susceptible regions influenced by the dust transport and dust events (Maghsoudi. 2020).

Although Iran spans in vast latitude and is categorized into different types of climate zones, the inland is also affected by morphological conditions. In the east-west and northwest-southeast regions, Alborz and Zagros mountains extend, respectively. These mountains act as barriers preventing humid air from the Caspian Sea and the Persian Gulf to be introduced into the central parts of the country. Although most parts of Iran lie in sub-tropical regions, Precipitation in Iran has a high spatial and time variability. There are regions in the south of the Caspian Sea, which receive up to 2000 mm of annual precipitation, whereas portions of the central and eastern parts of the country get less than 50 mm (Some'e BS et al. 2012). Due to these synoptical and morphological conditions, the overall land of Iran is considerably dry. According to the DeMarton classification, 64% of the whole country is arid. and 20% semiarid. Accordingly, the Mediterranean to per humid climate type is only limited to 16% (Tegen et al. 2004).

2.5. IRAN’S DUST ORIGINS

2.5.1. Salt Deserts

Dasht-e Lut, or the 'Emptiness Plain,' is a salt desert located in the provinces of Kerman and Sistan-Baluchestan, Iran, and is one of Iran's prominent dust sources. Another area is Dasht-e Kavir, also known as the Great Salt Desert, which sprawls across central and northern Iran, claiming the title of the country's largest desert. Within its expanse, a network of drainage channels crisscrosses the terrain, leading to the formation of ephemeral lakes and marshes. These water bodies, though temporary, host rich deposits of dust-sized sediments. These two deserts have been recognized as sources of sand and dust storms in numerous studies. Ginoux et al. (2012) identified Dasht-e Kavir and the Sistan Basin as two major sources of dust in the interior of Iran based on Moderate Resolution Imaging Spectroradiometer (MODIS) data and land use information. In another study, Walker et al. (2009) utilized high-resolution satellite imagery to identify small, eroding point sources and dust plumes originating from the Lut Desert.

2.5.2. Dry Lakes Bed

Iran has been experiencing long cycles of drought for the last 50 years, and recent droughts in the Middle East have weakened the water sources of the region (Duniway et al. 2019). Water scarcity in Iran, along with low rainfall, has caused the expansion of barren lands and the abandonment of agricultural lands. Temporary lakes have created favorable conditions for the occurrence of dust events over the region, with many of these lakes serving as the main source of such events. They receive enough runoff in the winter and spring seasons, but in summer, the shortage of water causes them to dry up. Zucca et al. (2021) analyzed over eighteen lakes known as dust sources due to desiccation or anthropogenic activities, with four of them located within Iran's borders. The drivers of desiccation for these lakes vary, but as mentioned before, over 80% of dust events originate from dried wetlands. Therefore, Iran is one of the areas exposed to the serious situation of dried lakebed erosion, especially near the edges of the lakes, caused by winds (Beyranvand et al. 2023).

The lakes within Iran contributing to the spread of dust are listed below:

Hamoun Lake in the Sistan region is a temporary lake. Most of the watershed of the lake is located in Afghanistan, and therefore, the runoff of this lake originates from Afghanistan. The Iranian part of this lake is arid. It dries during certain months from April to September. This drought coincides with the phenomenon of strong winds lasting 120 days, which blow in a north-southern direction between June and August. Dust and sand storms reach their maximum in summertime in this area, turning it into the dustiest area in Iran. Hamoun Lake's water level varied significantly during the last decades depending on precipitation and runoff. Long droughts in 1999 affected this region and dried up the Hamoun lakes, leaving deflatable soil material easily uplifted by intense local winds. Consequently, sand and dust storm activity increased in this area both in frequency and severity (Rashki et al. 2013). Thus, Hamoun has been considered to be one of the most active dust source regions in Southwest Asia in much research (Choobari et al., 2014; Rashki et al., 2012).

Hawr-al-Azim, the largest wetland in Iran spanning an area of 3000 km2, is primarily nourished by two rivers, the Karkheh and Tigris. However, the construction of dams on these rivers and activities related to oil production have led to a reduction in its size, with parts of it drying up and transforming into sources of sand and dust storms (Attiya & Jones. 2020). Adib et al. (2018) observed that the peak dust discharge from the Hawr-al-Azim wetland occurs in June and July, with the dust dispersing northwestwards towards densely populated areas of Iran. Khusfi Ebrahimi et al. (2022) noted a notable inverse relationship between reductions in wetland water area and dust pollution in cities situated near this wetland. Furthermore, Mirian et al. (2024) conducted research assessing the impact of the Hawr-al-Azim marshland drying on wind erosion in the region. Their analysis of soil characteristics across various land uses revealed a significant negative correlation between wind erodibility and soil moisture. In another study by Sedaghat & Nazaripour (2020), the temporal-spatial variations of soil moisture in the Hawr-al-Azim marshes were examined using remote sensing data and its correlation with the frequency of dust events in southwestern Iran. The results indicated a decrease in vegetation density and an increase in land surface temperature, leading to a rise in the frequency of sand and dust storms in the region. This underscores the critical importance of maintaining soil moisture levels and restoring marshland water to mitigate wind erosion.

Another significant source of dust is the Jazmurian seasonal lake, situated within the Jazmurian basin between Kerman, Sistan, and Baluchestan provinces. Covering an area of over 6900 km2, this lake is fed by two rivers; however, their contribution is limited due to diversion for agricultural purposes (Rashki et al. 2017). Annual precipitation in the western part of the basin averages around 200 mm, with even drier conditions prevailing in other areas, where average annual precipitation falls below 100 mm. Conversely, evaporation rates soar to approximately 2500 mm per year, propelled by the intensely hot climate characteristic of the region (Gholami et al. 2020). Since the early 2000s, the lake has progressively dried up due to extensive drought and increasing water demand in the region, thereby contributing to sand and dust storm occurrences. Sand and dust storm activity at Jazmurian peaks during the spring months (March–May) and extends into July, with the lowest activity observed during autumn and winter. Erosion predominantly affects the eastern, western, and southern parts of the lake. Dust generated by Jazmurian primarily impacts southeastern Iran, southern Pakistan, and Oman.

Urmia lake with an area of 5200 km^2 is located in the northwest of Iran and it is known as the largest hypersaline lake and the biggest lake in Iran. Urmia lake is located between two highly populated cities in northwest of Iran. Desiccation of the lake has increased from 2005 to 2013. This drought is more identified in southern shore of it which lead to local dust events. The desiccation of this lake has been debated. Poor water management and climatic factors are the two main reasons. The result showed particle concentration of dust has been increased not only in Urmia and Tabriz cities but also in Igdir Turkey (Ghale et al. 2021). Mobarak Hassan et al. (2023)

has examined dust phenomena in the Urmia basin over a 30-year period. It finds that the annual number of dusty days has increased over time, with peaks in May and October. Tabriz experiences the highest number of dusty days. Synoptic systems and decreased precipitation drive dust events in autumn, while drying soil leads to May dust emissions.

Gavkhouni wetland, located in Isfahan province, is a saline wetland fed by the Zayandehrod River (Fig 2.1). However, paradoxically, runoff from this river plays a significant role in the wetland's drying process. In spring, the wetland flourishes, but by summer, it often dries up. Research indicates an inverse relationship between the drought of this lake and dust events in the nearby city of Isfahan. Azadi et al. (2022) has concluded that Since 2000, the Gavkhouni wetland has become progressively drier, experiencing near-complete dryness in 2009, 2011, 2015, and 2017. This dryness significantly affects the local climate, leading to an increase in mean seasonal air temperatures of approximately 1.6°C in spring and 1°C in summer.

2.5.3. Dust Hotspots

The Khuzestan Plain, situated in the southwest of Iran, is characterized by numerous relatively small dust sources, including demolished pastures, abandoned rain-fed agricultural lands, uncultivated areas, dried wetlands, and ponds, and irrigated agricultural lands (Heidarian et al. 2018). To the north and east of Khuzestan lies the Zagros Mountain range. However, the elevation of the province gradually decreases towards the southwest, transitioning to forms of sand dunes. Khuzestan is primarily affected by dust from sources outside the province, with local dust comprising only 27% of the total dust in the area, originating from wind erosion distributed in Ram hormoz, Ahvaz, Omidiyeh, and Shush. However, intra-provincial wind erosion contributes minimally to sand and dust storm formation due to the size of the sand particles, which exhibit saltation or creeping movements (Mehrizi. 2022).

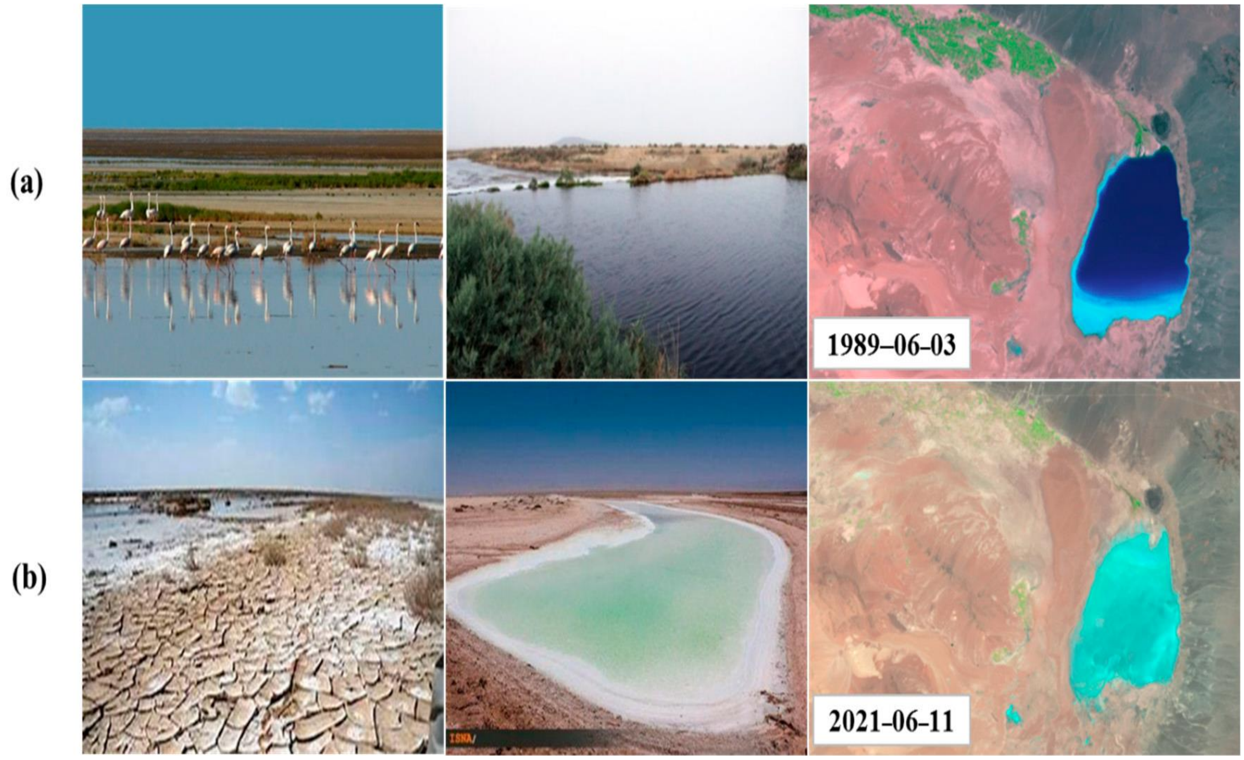

Figure 2.1. The situation of the Gavkhouni wetland: (a) in 1989; (b) in 2021 (Azadi et al. 2020).

Another area prone to sand and dust storms within Iran is Sarakhs County in the northeast, near the Turkmenistan border. Its proximity to the Turkmenistan desert, flat topography, and low average precipitation elevates Sarakhs to our list of regions experiencing a high frequency of dust events within Iran.

The Makran coastline desert is another potential source of dust events. However, its impact extends beyond Iran itself, and dust plumes from this area can surpass the Persian Gulf and reach to Oman (Fig 2.2).

Another coastline that can be considered a source of dust events is the Persian coastal plain in Hormozgan province. While this region contains dust sources, it is more severely affected by dust plumes originating from Saudi Arabia than by the dust sources within it (Choobari et al. 2016).

Figure 2.2. NASA's Terra satellite captured a dust storm off Iran and Pakistan on October 30, 2007. The storm intensified along the Iran-Pakistan border compared to the previous day, with reduced activity to the east. https://earthobservatory.nasa.gov/images/19270/dust-off-iran-and-pakistan

2.5.4. External Origins of Dust events

Although there are many dust sources inside Iran, a considerable number of recorded dust and sandstorms within the country originate from outside sources. Most sand and dust storms that occur in Iran come from eastern Syria, Iraq, and the Arabian Peninsula (Cao et al. 2015).

In the western neighboring countries, including Iraq, Syria, and Saudi Arabia, were determined as potential dust sources (Fig 2.3). Iraq and the eastern part of Syria, with an approximate contribution of 70 to 95%, have the most influence on PM10 levels in the receptor cities. This region mainly encompasses the basin of the Tigris-Euphrates Rivers, which includes anthropogenic and natural non-hydrological sources in most parts and, as an active dust source, plays a significant role in raising PM10 levels at receptor stations (Sotoudeheian et al. 2016). The Tigris-Euphrates basin in the Mesopotamian area dries up in spring and summer seasons, but the important factor that causes sand and dust storms is the Shamal dust winds, which mostly occur during warm seasons. The Shamal wind is a strong north-to-northwesterly wind that is capable of lifting dust mainly from the Tigris-Euphrates basin. The wind system can transport dust particles to the Persian Gulf, the Arabian Peninsula, and the west and southwest of Iran (Abadi et al. 2022).

Figure 2.3. shows the geographical distribution of deserts inside Iran and across (Aryanfar et al. 2021)

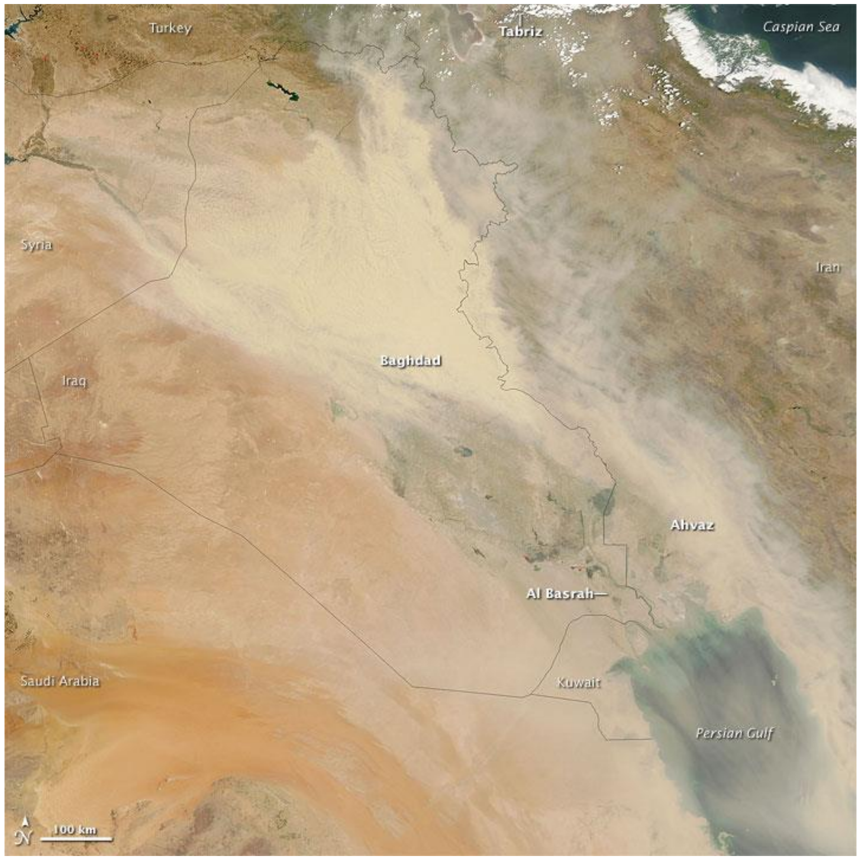

Figure 2.4. Massive Dust Storm Over Iraq, Iran, and Persian Gulf on July 4, 2009
https://earthobservatory.nasa.gov/images/39204/dust-storm-over-iraq

Saudi Arabia is another significant source of sand and dust storms. In the winter, coastal regions of southern Iran are impacted by frontal dust storms originating from the southern Arabian Peninsula and traveling across the Persian Gulf (Cao et al. 2015) Frontal dust storms associated with the frontal system mostly occur in cold seasons; however, the frequencies of frontal dust storms are much lower than Shamal dust storms. Studies have shown that Central Iraq, western and southwestern Iran, and northeastern Saudi Arabia are the regions most affected by frontal dust storms, with dust plumes observed more prominently in these areas compared to others in the Middle East. The most severe frontal dust storms occur during March and April (Fig 2.4).

In northeast of Iran, in Turkmenistan there is persistent dust activity because of Karakum desert which reach its high activity in summertime and effect northeast of Iran. Under intense high-pressure conditions, powerful northerly winds, ranging from north-westerlies to north-easterlies, transport dust from the Central Asian deserts (including the Caspian depressions, Aralkum, Kyzylkum, and Karakum) southward towards southern Turkmenistan and northeastern Iran (Mohammadpour et al. 2022).

In the east, Margo and Registan deserts in Afghanistan are also one of the main sources of dust affecting Khorasan and Sistan and Baluchestan provinces in eastern Iran (Rashki et al. 2018).

2.6. FUNDAMENTAL MECHANISMS OF PARTICLE TRANSPORTS

In Iran, located in semi-arid areas with low mean annual precipitation, wind erosion surpasses water erosion in significance. The soil remains relatively dry for extended periods throughout the year, diminishing the adhesion power between water and soil particles and rendering the soil more susceptible to transportation. Surface wind emerges as a crucial indicator of soil erosion (Mozaffari & Rezaei. 2021).

Surface wind impacts both the soil and vegetation. Rough, cloddy, or vegetated surfaces alter the wind speed at the soil surface, diminishing the wind's energy and reducing its capacity to erode the soil. However, if the wind speed reaches sufficient levels, it can initiate soil particle movement. Soil attributes exhibit high heterogeneity and are not consistently well characterized. However, there are three phases of soil particle movement: saltation, creep, and suspension. this dynamic is illustrated in Figure 2.5 (Presley & Tatarko. 2009).

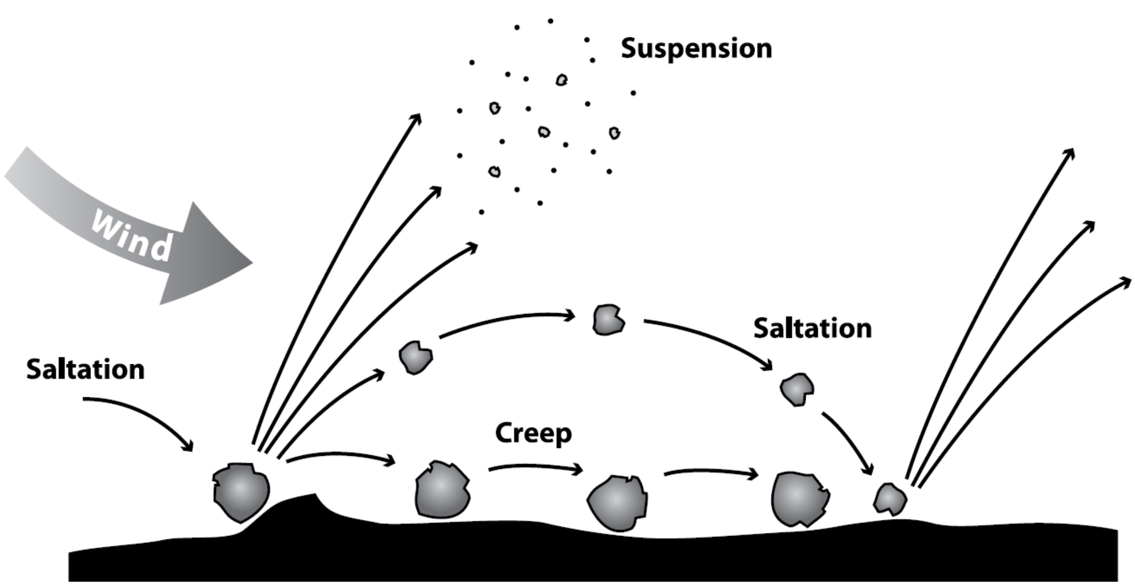

Figure 2.5. Soil particles can move through saltation, creep, and suspension (Presley & Tatarko. 2009).

Some particles have diameters between 0.5 and 3 mm. Consequently, they are too heavy to be lifted, and the wind can only roll them along the surface, resulting in what is known as surface creep. Generally, 5 to 25% of soil texture is lost and carried by wind through this creeping process. This type of movement can transport soil for only a few meters and deposit it within a localized area.

Another process is called saltation. The size of particles lifted by saltation ranges between 0.1 and 0.5 mm. They are light enough to be picked up by the wind but too large to remain suspended in the air. Therefore, after being lifted, they strike the ground and are then lifted again. This repetitive process causes abrasion on the surface by breaking larger particles and crusts into smaller pieces. Between 50 and 75% of lost soil is carried by wind in this manner. Like particles involved in creep movement, saltating particles continue to move until the wind slows or they are trapped in sheltered areas (Jarrah et al. 2020).

The last process is suspension. Some particles are too small to settle and remain suspended. Their size does not exceed 0.01 mm in diameter, and they are known as PM10 particles. These particles can reach high altitudes, stay in the atmosphere for extended periods, and travel long distances without falling unless precipitated. Additionally, the ratio of soil lost by suspension is 3 up to 4%. Particles in the suspension category may cause health problems when inhaled (Gillette. 1978).

2.7. EFFECTS OF SAND AND DUST STORMS

Sand and dust storms can cause various damages to human health, the environment, climate, and the economy. For example, they can increase the risk of respiratory diseases, affect cloud lifetime causing a significant change in the climate, and impair plant growth resulting in less productivity in farm products. The impacts of sand and dust storms depend on regional relations between urban areas and potential source locations, landscape, wind speed, and socio-economic activities.

Many studies in Iran have demonstrated the relationship between dust events and their impact on human health. Aghababaeian et al. (2021) revealed a positive correlation between occurrences of dust events and cardiovascular and respiratory mortality rates in Dezful city, Iran, from 2014 to 2019. Furthermore, research conducted by Khaniabadi et al. (2017) found that dust events can lead to increased hospital admissions and respiratory mortality rates in southwest regions of Iran, particularly affecting Khuzestan province. A study in Sanandaj by Ebrahimi et al. (2014) linked dust storms to increased cardiovascular emergency admissions. Dust events from 2009 to 2010 were analyzed alongside PM10 levels and health data. Results found a correlation between PM10 levels and cardiovascular emergencies, but not respiratory issues.

Kalankesh et al. (2022) found that residents in central regions of Iran experience respiratory, cardiovascular, cancer, and infectious diseases, largely attributed to environmental issues such as chemical and microbial pollution from air and water sources, respectively. Particularly, the prevalence of cancers such as skin, stomach, bladder, prostate, and colorectal cancer, alongside respiratory and cardiovascular diseases, is notably higher in arid and semi-arid zones like Kerman and Yazd compared to other provinces. Recent studies have highlighted the impacts of sand and dust storms on human health, but research on the type and size of dust particles has yielded contradictory results regarding their role in disease causation or exacerbation. Additionally, synergistic effects between human-made pollutants and dust particles have been explored, adding complexity to the issue. Sand and dust storms can also affect indoor air quality due to the entrainment of particles from gaps and openings in building walls. Since people spend over 80 percent of their time inside buildings, the effects of sand and dust storms are indirect but considerably important for human health. Miri et al. (2023) investigated indoor and outdoor bacterial concentrations in two cities, Zahak and Zabol, exposed to dust events in Iran. It was shown that indoor air quality correlated strongly with outdoor air quality, with both affected by increasing PM10 concentrations. Results suggest that the morning poses the highest risk to respiratory health.

In another study by Soleimani et al. (2016), bioaerosol concentrations and composition inside and outside a hospital in Ahvaz, Iran, were investigated. Results show increased bioaerosol concentrations during dust events, with dominant bacterial constituents.

In addition, the entry of dust particles into indoor areas can cause damage to electronic equipment and shorten the lifetime of furniture. Miri & Middleton. (2022) evaluated that over 60 million US dollars had been spent for cleaning and repairing electrical furniture for four years in the Sistan region because of the physical damages due to the entrained dust particles.

Another aspect is the effects on the commercial sectors. Studies have been conducted to analyze the effects of sand and dust storms on various factors in the transportation sectors, such as aviation, travel speed, the traffic volume of vehicles, traffic accidents, damages to roads and facilities, and impacts on railway transport, in southeast regions of Iran over seven years. The total damage cost caused by sand and dust storms were estimated at approximately 46 million US dollars. The road transport sector was estimated to incur the most damage among other sectors. Additionally, over 103 flights were canceled during storms in Zabol and Zahedan cities, which were the main factors contributing to the economic damage in the aviation sector (Fig 2.6 - Fig 2.9).

Physical damages from sand and dust storms to traffic roads in the Sistan region were revealed, with road paths critically affected by sand and dust storms resulting in total reconstruction costs exceeding 300 million Rial (Shahreki Kaftargi et al. 2021). Additionally, sand and dust storms with saline particles affect agricultural lands, turning them into barren lands. Therefore, the impacts of sand and dust storms are more severe in rural than urban areas (Miri et al. 2007).

Sand and dust storms also affect agriculture, reducing the photosynthesis process and weakening it, causing loss of plant tissue due to sandblasting (Ibrahim & El-Gaely. 2012). Maleki et al. (2017) studied the effects of sand and dust storms in Kermanshah province, Iran, and found that dust affects various types of agricultural producers differently, with orchard farmers and beekeepers being the most impacted. In another study by MalAmiri et al. (2023) in Khuzestan province on the effect of sand and dust storms on the economy, agriculture, and health sectors, the cost of damages amounted to around $39 million in the mentioned three sectors in different time periods.

Figure. 2.6. Asphalt Surface Weathered by Dust Storm (Miri & Middleton. 2022).

Figure. 2.7. Remarking Road surface and repairing bridge fences after dust storm (Miri & Middleton. 2022).

Figure. 2.8. Sand deposition on the rails and cleaning (Miri & Middleton. 2022).

.

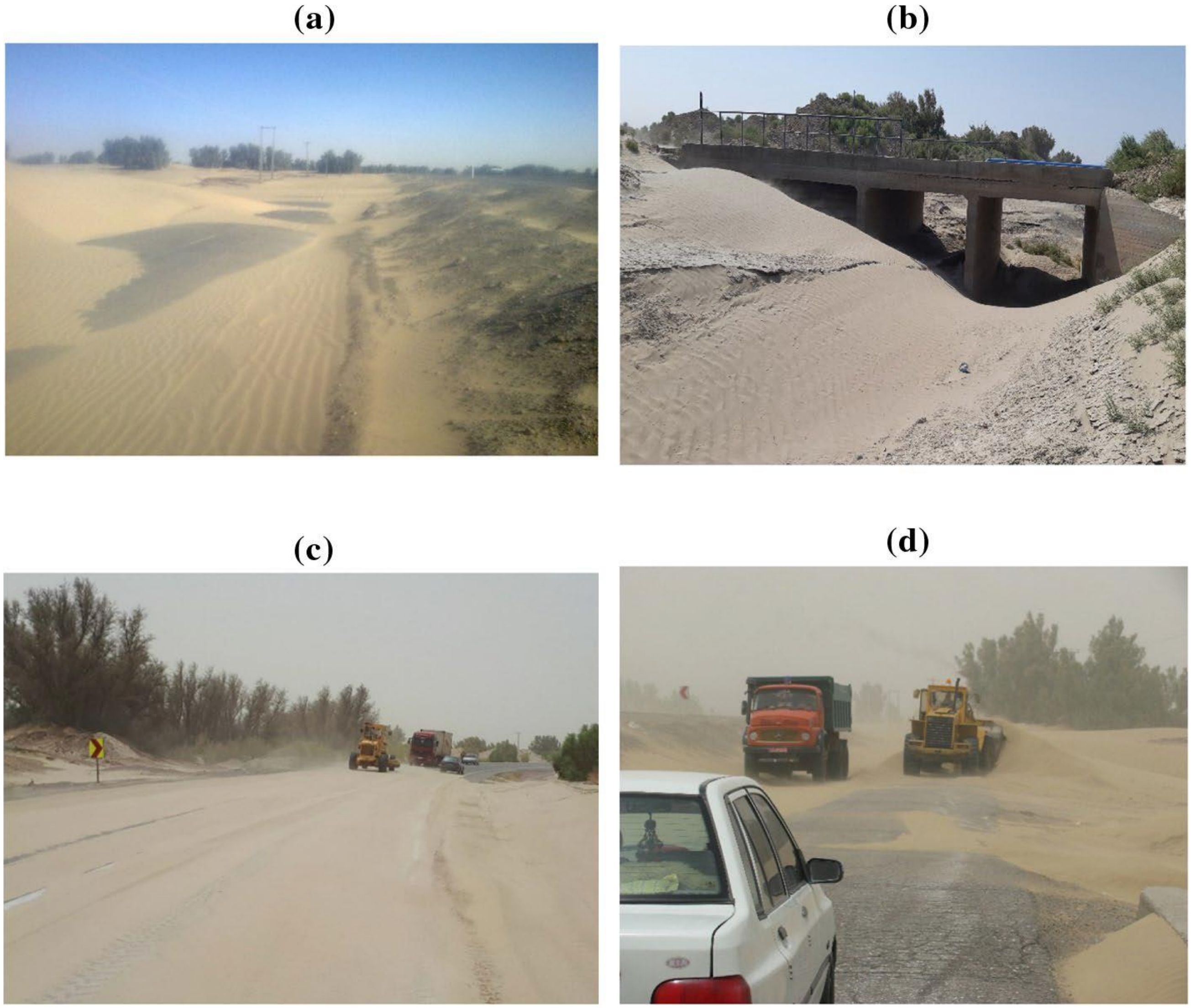

Figure. 2.9. Sediment Deposition on Roads (a) and Bridges (b), Cleanup Operations on the Road (c), and Sediment Clearance to Restore Road Access (d) (Miri & Middleton. 2022).

2.8. FORECAST OF SAND AND DUST STORM

Early warning systems, incorporating detection, monitoring, analysis, and forecasting components, empower individuals, communities, governments, businesses, and organizations to take timely action, mitigating the impact of storms and enabling proactive measures to reduce disaster risks and potential impacts on affected areas.

At the moment, monitoring and forecasting sand and dust storms is limited but possible through various methods, such as satellite remote sensing, ground-based lidars, and radar systems technology, by monitoring them at different spatial and temporal resolutions, as well as predicting their transport pathways. Satellite remote sensing is characterized by wide coverage and observation, which can play an important role in sand and dust storm monitoring. However, few satellites can capture the continuous process, and besides, they cannot detect sand and dust storms under the clouds.

Another method is ground-based monitoring stations, but these stations cannot detect dust at high altitudes and its intensity. Ground-based lidar can be supplementary for ground-based monitoring because lidar can detect the vertical distribution of aerosols. However, individual lidars cannot detect the whole dust event in three dimensions. Thus, for comprehensive monitoring, more lidar systems are needed to detect the pattern of transport. Additionally, lidar waves will experience serious signal attenuation during storms (Yang et al. 2022).

Radio Detection and Ranging (Radar) system is similar to lidar technique, but it uses laser pulses, while in radar systems, radio waves are used to detect the particles and determine their distance in the atmosphere. Atmospheric particles get charged when they are transported by wind. Charged particles can affect the detection results of the radar system (Xie et al. 2017).

Overall, while these methods provide valuable insights, challenges remain in achieving comprehensive dust storm monitoring. Observations of sand and dust storms offer limited monitoring capabilities, primarily assisting in evaluating the progression of sand and dust storms only a few hours in advance through simplified spatial and temporal extrapolation of their characteristics.

Over the past decade, numerous numerical modeling systems have been developed specifically to forecast sand and dust events. The dust emission flux algorithm depicted in Figure 2.10 establishes the interconnections between various components of the dust model, meteorological data inputs, and geographical characteristics. It integrates information such as threshold friction velocity, wind speed, and both horizontal and vertical dust emission flux to simulate the release of dust particles into the atmosphere. By utilizing this algorithm, the dust model effectively incorporates meteorological conditions and surface features to accurately predict dust emissions from various sources.

Dust particle transportation and deposition are standard features in these models, with the dust mass conservation equation included as a fundamental governing equation (Najafpour et al. 2023).

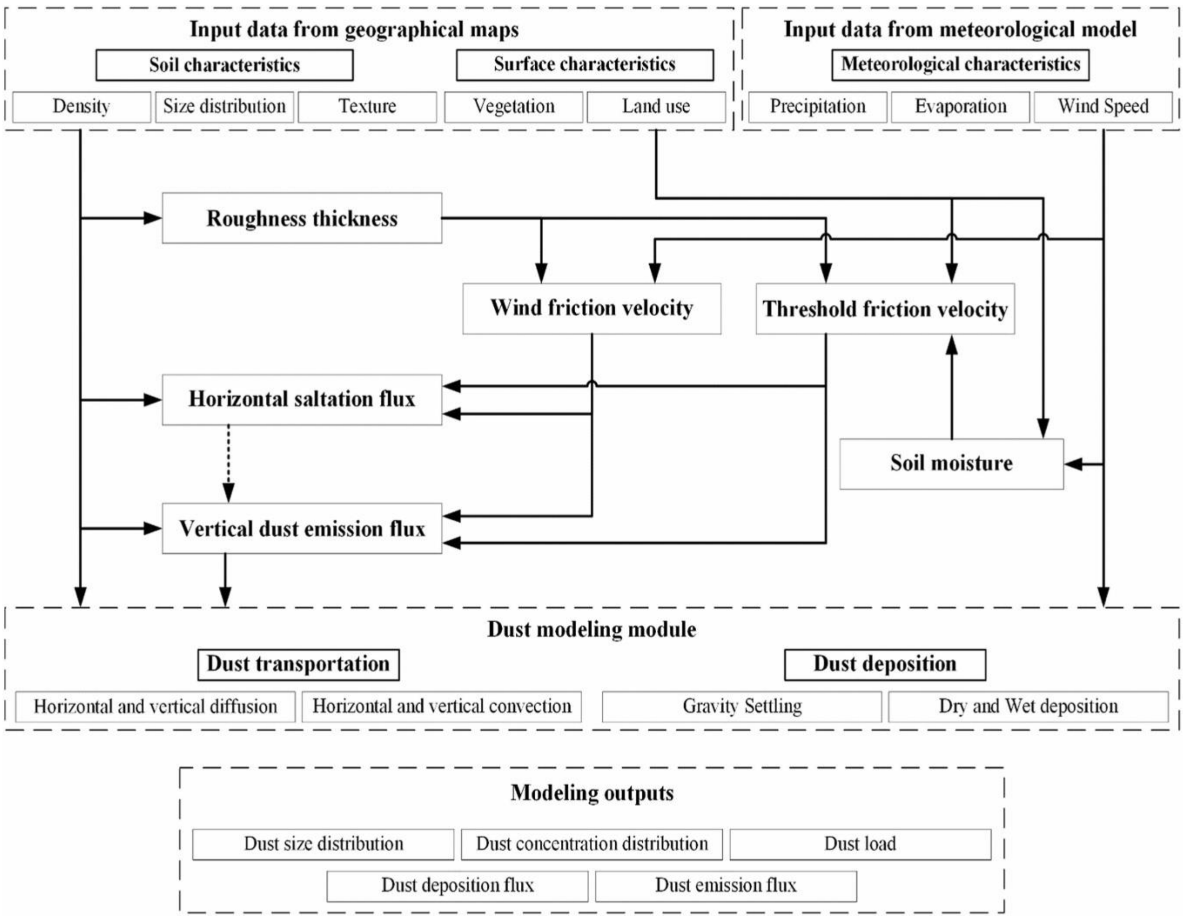

Figure 2.10. shows the algorithm for dust emission flux within the dust models (Najafpour et al. 2023).

Some forecasting systems additionally integrate satellite and ground-based observations to enhance their understanding of the initial dust content, leading to more precise predictions of its evolution. The number and complexity of atmospheric models for dust have experienced a significant rise for both research and operational purposes. Table 2.1 shows some global and regional sand and dust storm models. These models are primarily categorized into two main groups: regional and global. Regional climate models focus on smaller parts of the Earth's surface, using more detailed grids ranging from 1 to 50 kilometers. However, global models have grid spacings varying between 100 and 300 kilometers (Diallo 2006).

Dust models encounter several challenges due to the intricate nature of the system, notably the limited comprehension of the physical mechanisms driving the dust cycle, particularly concerning dust emission processes. There is a shortage of suitable dust observations available for model development, evaluation, and assimilation, especially for desert dust sources. Soil conditions, which influence dust emission, vary widely and are not always well-characterized in potential dust source areas, adding complexity to modeling efforts. Additionally, wind, a key factor in dust production, exhibits significant variability in both space and time, posing challenges for accurately representing its effects on dust emission.

Table 2.1. Shows Global and Regional Models for Sand and Dust Storm Prediction

model	institution	domain	Data assimilation
CAMS-ECMWF	ECMWF	Global	MODIS-AOD
MetUM	Met Office	Global	MODIS/Aqua
GEOS-5	NASA	Global	MODIS
NGAC	NOAA National Centers for Environmental Prediction (NCEP)	Global	NO
SILAM	Finnish Meteorological Institute (FMI)	Global	NO
MASINGAR	Meteorological Research Institute of the Japan Meteorological Agency (MRI/JMA)	Global	Yes
NAAPS and ICAP ensemble	U.S. Naval Research Laboratory (NRL)	Global	YES
WRF-Chem	National Center for Atmospheric Research (NCAR), the National Oceanic and Atmospheric Administration (NOAA)	Regional	NO
BSC-DREAM8b_c2	Barcelona Supercomputing Center	Regional	NO
DREAM8-NMME-CAMS	South East European Virtual Climate Change Center (SEEVCCC)	Regional	YES
NMMB/MONARCH	Barcelona Supercomputing Center	Regional	NO
EMA REG CM4	Egyptian Meteorological Authority (EMA)	Regional	NO

LOTOS-EUROS	TNO	Regional	NO
ICON-ART	Deutscher Wetterdienst (DWD)	Regional	YES
CUACE	China Meteorological Administration (CMA)	Regional	three-dimensional variational (3D-VAR)
ADAM3	National Institute of Meteorological Sciences of the Korea Meteorological Administration (NIMS/ KMA)	Regional	Optimal interpolation (OI)

2.9. REFERENCES

Abadi AR, Hamzeh NH, Chel Gee Ooi M, Kong SS, Opp C. Investigation of two severe shamal dust storms and the highest dust frequencies in the south and southwest of Iran. Atmosphere. 2022 Nov 28;13(12):1990.

Adib A, Oulapour M, Chatroze A. Effects of wind velocity and soil characteristics on dust storm generation in Hawr-al-Azim Wetland, Southwest Iran. Caspian Journal of Environmental Sciences. 2018 Dec 1;16(4):333-47.

Aghababaeian H, Ostadtaghizadeh A, Ardalan A, Asgary A, Akbary M, Yekaninejad MS, Sharafkhani R, Stephens C. Effect of dust storms on Non-Accidental, cardiovascular, and respiratory mortality: A Case of Dezful City in Iran. Environmental health insights. 2021 Nov;15:11786302211060152.

Ahmadzai H. The impact of sand and dust storms on agriculture in Iraq. Middle East Development Journal, 15(1), 50-65.

Akhlaq M, Sheltami TR, Mouftah HT. A review of techniques and technologies for sand and dust storm detection. Reviews in Environmental Science and Bio/Technology, 11, 305-322.

Alizadeh-Choobari O, Ghafarian P, Owlad E. Temporal variations in the frequency and concentration of dust events over Iran based on surface observations. International Journal of Climatology, 36(4), 2050-2062.

Alizadeh-Choobari O, Zawar-Reza P, Sturman A. The “wind of 120 days” and dust storm activity over the Sistan Basin. Atmospheric research. 2014 Jun 15;143:328-41.

Aryanfar A, Gholami A, Pourgholi M, Zandi MZ, Khosravi A. A type-2 fuzzy-based multi-criteria decision-making method for sustainable development of wind power plants in Iran. Renewable Energy Research and Applications. 2021 Jul 1;2(2):147-55.

Attiya AA, Jones BG. Climatology of Iraqi dust events during 1980–2015. SN Applied Sciences. 2020 May;2(5):845.

Awadh SM. Impact of North African sand and dust storms on the Middle East using Iraq as an example: Causes, sources, and mitigation. Atmosphere. 2023 Jan 13;14(1):180.

Azadi S, Yazdanpanah H, Nasr-Esfahani MA, Pourmanafi S, Dorigo W. The Gavkhouni wetland dryness and Its impact on air temperature variability in the eastern part of the Zayandeh-Rud River Basin, Iran. Water. 2022 Jan 9;14(2):172.

Beyranvand A, Azizi G, Alizadeh O, Darvishi Boloorani A. Dust in Western Iran: the emergence of new sources in response to shrinking water bodies. Scientific Reports. 2023 Sep 27;13(1):16158.

Beyranvand A, Azizi G, Alizadeh-Choobari O, Darvishi Boloorani A. Spatial and temporal variations in the incidence of dust events over Iran. Natural Hazards, 97, 229-241.

Cao H, Liu J, Wang G, Yang G, Luo L. Identification of sand and dust storm source areas in Iran. Journal of Arid Land. 2015 Oct;7:567-78.

Chen S, Jiang N, Huang J, Xu X, Zhang H, Zang Z, Huang K, Xu X, Wei Y, Guan X, Zhang X. Quantifying contributions of natural and anthropogenic dust emission from different climatic regions. Atmospheric Environment, 191, 94-104.

Duniway MC, Pfennigwerth AA, Fick SE, Nauman TW, Belnap J, Barger NN. Wind erosion and dust from US drylands: a review of causes, consequences, and solutions in a changing world. Ecosphere. 2019 Mar;10(3)

.

Duniway MC, Pfennigwerth AA, Fick SE, Nauman TW, Belnap J, Barger NN. Wind erosion and dust from US drylands: a review of causes, consequences, and solutions in a changing world. Ecosphere, 10(3), e02650.

Ebrahimi SJ, Ebrahimzadeh L, Eslami A, Bidarpoor F. Effects of dust storm events on emergency admissions for cardiovascular and respiratory diseases in Sanandaj, Iran. Journal of Environmental Health Science and Engineering. 2014 Dec;12:1-5.

Ebrahimi-Khusfi Z, Roustaei F. Dust storm index anomaly for sand-dust events monitoring in western Iran and its association with the NDVI and LST anomalies. Environmental Science and Pollution Research. 2021 Jun 14:1-5.

Feng J, Liao H, Li J. The impact of monthly variation of the Pacific–North America (PNA) teleconnection pattern on wintertime surface-layer aerosol concentrations in the United States. Atmospheric Chemistry and Physics, 16(8), 4927-4943.

Furman HK. Dust storms in the Middle East: sources of origin and their temporal characteristics. Indoor and Built Environment, 12(6), 419-426.

Gandham H, Dasari HP, Langodan S, Karumuri RK, Hoteit I. Major changes in extreme dust events dynamics over the Arabian Peninsula during 2003–2017 driven by atmospheric conditions. Journal of Geophysical Research: Atmospheres, 125(24), e2020JD032931.

Ghale YA, Tayanc M, Unal A. Dried bottom of Urmia Lake as a new source of dust in the northwestern Iran: Understanding the impacts on local and regional air quality. Atmospheric Environment. 2021 Oct 1;262:118635.

Gillette D. A wind tunnel simulation of the erosion of soil: Effect of soil texture, sandblasting, wind speed, and soil consolidation on dust production. Atmospheric Environment (1967). 1978 Jan 1;12(8):1735-43.

Ginoux P, Prospero JM, Gill TE, Hsu NC, Zhao M. Global-scale attribution of anthropogenic and natural dust sources and their emission rates based on MODIS Deep Blue aerosol products. Reviews of Geophysics. 2012 Sep;50(3).

Gholami H, Mohamadifar A, Sorooshian A, Jansen JD. Machine-learning algorithms for predicting land susceptibility to dust emissions: The case of the Jazmurian Basin, Iran. Atmospheric Pollution Research. 2020 Aug 1;11(8):1303-15.

Goossens D, Gross J. Similarities and dissimilarities between the dynamics of sand and dust during wind erosion of loamy sandy soil. Catena, 47(4), 269-289.

Hamzeh NH, Abadi AR, Kaskaoutis DG, Mirzaei E, Shukurov KA, Sotiropoulou RE, Tagaris E. The Importance of Wind Simulations over Dried Lake Beds for Dust Emissions in the Middle East. Atmosphere, 15(1), 24.

Heidarian P, Azhdari A, Joudaki M, Khatooni JD, Firoozjaei SF. Integrating remote sensing, GIS, and sedimentology techniques for identifying dust storm sources: a case study in Khuzestan, Iran. Journal of the Indian Society of remote sensing. 2018 Jul;46(7):1113-24.

Huang M, Li Q, Xu H, Lou W, Lin N. Non-stationary statistical modeling of extreme wind speed series with exposure correction. Wind Struct, 26(3), 129-146.

Ibrahim MM, El-Gaely GA. Short-term effects of dust storm on physiological performance of some wild plants in Riyadh, Saudi Arabia. African Journal of Agricultural Research. 2012 Nov 13;7(47):6305-12.

Jarrah M, Mayel S, Tatarko J, Funk R, Kuka K. A review of wind erosion models: Data requirements, processes, and validity. Catena. 2020 Apr 1;187:104388.

Kalankesh LR, Rodriguez-Couto S, Alami A, Khosravan S, Meshki M, Ahmadov E, Mohammadpour A, Bahri N. Socio-Environmental Determinants and Human Health Exposures in Arid and Semi-Arid Zones of Iran—Narrative Review. Environmental Health Insights. 2022 Apr;16:11786302221089738.

Khaniabadi YO, Fanelli R, De Marco A, Daryanoosh SM, Kloog I, Hopke PK, Conti GO, Ferrante M, Mohammadi MJ, Babaei AA, Basiri H. Hospital admissions in Iran for cardiovascular and respiratory diseases attributed to the Middle Eastern Dust storms. Environmental science and pollution research. 2017 Jul;24:16860-8.

Krueger BJ, Grassian VH, Cowin JP, Laskin A. Heterogeneous chemistry of individual mineral dust particles from different dust source regions: the importance of particle mineralogy. Atmospheric Environment, 38(36), 6253-6261.

Liu Y, & Westphal, D. L. Dust Storms: A Review of Meteorological and Climatological Aspects. Journal of Climate, 14(5), 997-1010.

Maghsoudi M. Desert landscapes and landforms of Iran. Springer Nature; 2020 Sep 29.

MalAmiri N, Rashki A, Azarmdel H, Kaskaoutis D, Al-Dousari A. Socioeconomic impacts of the dust storms in southwest Iran.

Maleki T, Sahraie M, Sasani F, Shahmoradi M. Impact of dust storm on agricultural production in Iran. International Journal of Agricultural Science, Research and Technology in Extension and Education Systems (IJASRT in EESs). 2017 Jun 1;7(1):19-26.

Mehrizi E. An Investigation of Sources of Dust Storms in the Southeast and Southwest Regions of Iran. InFirst International Conference on Dust Storms 2022 Jan 20.

Miri A, Ahmadi H, Ghanbari A, Moghaddamnia A. Dust storms impacts on air pollution and public health under hot and dry climate.

Miri A, Middleton N. Long-term impacts of dust storms on transport systems in south-eastern Iran. Natural Hazards. 2022 Oct;114(1):291-312.

Miri A, Shirmohammadi E, Sorooshian A. Impacts of dust storms on indoor and outdoor bioaerosol concentration in the Sistan region of Iran. Journal of Building Engineering. 2023 Oct 1;76:107302.

Mirian I, Pahlavanravi A, Khalilimoghadam B. Effects of Land Use Change on Soil Wind Erodibility in the Horul Azim Marshland. Eurasian Soil Science. 2024 Jan 31:1-5.

Mobarak Hassan E, Fattahi E, Habibi M. Temporal and Spatial Variability of Dust in the Urmia Basin, 1990–2019. Atmosphere. 2023 Nov 29;14(12):1761.

Mohammadi K, Rashki A, Kaskaoutis DG. Impacts of dust storms on transportation and infrastructure in Sistan, southeastern Iran. Environmental Earth Sciences. 2018 Jul;77(14):1-16.

Mohammadpour K, Sciortino M, Kaskaoutis DG, Rashki A. Classification of synoptic weather clusters associated with dust accumulation over southeastern areas of the Caspian Sea (Northeast Iran and Karakum desert). Aeolian Research. 2022 Feb 1;54:100771.

Mozaffari H, Rezaei M, Ostovari Y. Soil sensitivity to wind and water erosion as affected by land use in southern Iran. Earth. 2021 Jun 6;2(2):287-302.

Najafpour N, Afshin H, Firoozabadi B. Sensitivity study and comparative evaluation of WRF-Chem over Iran: Available and embedded dust emission schemes. Atmospheric Pollution Research. 2023 Dec 1;14(12):101930.

Presley D, Tatarko J. Principles of wind erosion and its control. Kansas State University Agricultural Experiment Station and Cooperative Extension Service; 2009 Oct 1.

Rashki A, Arjmand M, Kaskaoutis DG. Assessment of dust activity and dust-plume pathways over Jazmurian Basin, southeast Iran. Aeolian Research. 2017 Feb 1;24:145-60.

Rashki A, Arjmand M, Kaskaoutis DG, Kahn RA. Dryness of ephemeral lakes and consequences for dust activity: the case of the Hamoun drainage basin, southeastern Iran. Science of the total environment. 2013 Oct 1;463:552-64.

Rashki A, Kaskaoutis DG, Goudie AS, Gherboudj I, Khadim F. Aerosol characteristics during the Middle Eastern dust storm period over the Arabian Peninsula. Atmospheric Environment, 128, 129-139.

Rashki A, Kaskaoutis DG, Goudie AS, Middleton N. The role of Hamoun Wetlands in dust emissions in southwestern Asia. The Holocene, 24(3), 353-364.

Rashki A, Kaskaoutis DG, Sepehr A. Statistical evaluation of the dust events at selected stations in Southwest Asia: From the Caspian Sea to the Arabian Sea. Catena. 2018 Jun 1;165:590-603.

Sadaghat, Nazaripour. Monitoring soil moisture changes in the Hoor Al-Azim wetland and its relationship with dust storms in southwestern Iran. "Sephār" Geographical Information Scientific Research Quarterly. 2020 Aug 22;29(114):133-45.

Shahreki Kaftargi O, Miri A, Nori S, Ahmadpoor Borazjani M. The damage cost of dust storms on roads in the Sistan region during 2017-2019. Journal of Natural Environmental Hazards. 2021 Dec 22;10(30):203-14.

Sharifi A, Murphy LN, Pourmand A, Clement AC, Canuel EA, Beni AN, Lahijani HA, Delanghe D, Ahmady-Birgani H. Early-Holocene greening of the Afro-Asian dust belt changed sources of mineral dust in West Asia. Earth and Planetary Science Letters. 2018 Jan 1;481:30-40.

Soleimani Z, Goudarzi G, Sorooshian A, Marzouni MB, Maleki H. Impact of Middle Eastern dust storms on indoor and outdoor composition of bioaerosol. Atmospheric environment. 2016 Aug 1;138:135-43.

Sotoudeheian S, Salim R, Arhami M. Impact of Middle Eastern dust sources on PM10 in Iran: Highlighting the impact of Tigris-Euphrates basin sources and Lake Urmia desiccation. Journal of Geophysical Research: Atmospheres. 2016 Dec 16;121(23):14-018.

Swap R, Ulanski S, Cobbett M, Garstang M. Temporal and spatial characteristics of Saharan dust outbreaks. Journal of Geophysical Research: Atmospheres. 1996 Feb 20;101(D2):4205-20.

Tegen I, Werner M, Harrison SP, Kohfeld KE. Relative importance of climate and land use in determining present and future global soil dust emission. Geophysical research letters. 2004 Mar 16;31(5).

United Nations Convention to Combat Desertification (UNCCD). 2022. Sand and Dust Storms Compendium: Information and Guidance on Assessing and Addressing the Risks. Bonn, Germany.

Walker AL, Liu M, Miller SD, Richardson KA, Westphal DL. Development of a dust source database for mesoscale forecasting in southwest Asia. Journal of Geophysical Research: Atmospheres. 2009 Sep 27;114(D18).

Xie L, Gao X, Qin J. Effect of charges carried by atmospheric particles on radar power ratio. Atmospheric Measurement Techniques Discussions. 2017 Nov 28;2017:1-3.

Yang L, Zhang S, Tao H, Yang Y, Wang L, Cui Y, Xu Y, Li X. Comprehensive Analysis of a Dust Storm by a Lidar Network Combined With Multiple Data. Frontiers in Environmental Science. 2022 Apr 26;10:832710.

Zucca C, Middleton N, Kang U, Liniger H. Shrinking water bodies as hotspots of sand and dust storms: The role of land degradation and sustainable soil and water management. Catena. 2021 Dec 1;207:105669.

CHAPTER 3: IDENTIFYING THE DISTRIBUTION AND FREQUENCY OF DUST EVENTS IN IRAN BASED ON LONG-TERM OBSERVATIONS FROM OVER 400 WEATHER STATIONS

3.1. INTRODUCTION

Sand and dust storms are atmospheric phenomena that result from the process of wind blowing small particles from the land surface (Middleton & Kang. 2017). The transformation of these particles depends on various factors, such as the physical properties of the soil, wind speed, particle size, and land cover. Physical features of the soil, such as soil texture, soil fertility, cohesiveness of particles, and soil moisture, can determine whether the particles can be aerosolized (Mahmoudi & Ikegaya. 2022). wind can decrease soil humidity, leading to a loss of particle cohesiveness. In addition, land cover or land surface conditions, such as vegetation cover and surface roughness, are other important factors that affect the emission of particles. The lack of vegetation is a critical factor that can cause dust emissions, as it leads to a lack of protein and humidity in the soil, making it more prone to erosion. In short, the combination and interaction of different factors cause soil erosion, which ultimately leads to sand and dust storms. In addition to numerous factors causing soil erosion, the particle formation is also complex physical phenomena. The size of sand particles is determined by their diameter, affecting how high and how long the wind can carry the particles (Bagnold. 1941).

These complex phenomena also hinder employing numerical predictions of the dust events as well as highlight the importance of the investigation of the field measurement datasets. Sand and dust storms are recognized as major hazards due to their numerous and wide-ranging impacts, which are not limited to arid areas. These storms have both natural and anthropogenic effects, and their impacts are not always negative; they can also have positive effects, such as providing minerals to oceans and terrestrial ecosystems (Cuevas Agulló. 2013). However, the negative effects of dust storms, such as desertification, degradation of landscapes, and crop loss, cannot be ignored (Sivakumar et al. 2005; Ke et al. 2023; Huang et al. 2023). As a result, they have become a global concern in recent decades, as they can impede the sustainable development of developing countries (Middleton & Kang. 2017). Therefore, it is crucial to address the impacts of sand and dust storms on socio-economy, human health, and the environment, to mitigate their effects and ensure sustainable development.

The Middle East experiences significant dust emissions from the Arabian Peninsula, Iraq, and Syria, impacting neighboring regions. Desertification and drought are on the rise, notably in Iraq and Syria, due to both natural processes and human activities like river control and dam construction (Francis et al. 2023; Ginoux et al. 2012). Iran is situated in the middle east which has an arid and semi-arid climate except for northern coastal areas and some parts of the west. Summers (from June to August) are hot and warm with little rainfall and relatively low humidity. Monthly precipitation is less than 40 mm even in the winter season, showing the very arid weather condition throughout a year. The climate of the region is characterized as continental, exhibiting hot and dry summers along with cold winters. The annual temperature range spans from 22 ◦C to 26 ◦C. In terms of precipitation, the average annual amount is approximately 240 mm. However, significant variations exist among different areas. with the north receiving the highest amounts and the Zagros slopes considerably less (https://climateknowledgeportal.worldbank.org).

Iran's drylands and deserts, characterized by aeolian processes, contribute to significant wind-eroded mineral dust. Desiccated lakes are major sources of dust events. Studies highlight the role of shrinking water bodies, particularly in Iran, in triggering dust storms.

Thus, sand and dust storms in Iran can be classified into two types: direct and indirect. Indirect storms occur in neighboring countries and enter Iran, while direct storms are created within Iran due to local factors. The increasing frequency of direct and indirect sand and dust storms in Iran underscores the need to examine the long-term trends, inter-seasonal to inter-annual variations, and temporal evolution of dust events in Iran, which hold great significance. In short, Iran is located in the regions where dust events can easily occur in terms of local climate conditions as well as geographical conditions.

Numerous studies have indicated that Syria and Iraq are the primary sources of sand and dust storms in the western part of Iran. Boloorani et al. (2014) used multiple methods to determine the source of sand and dust storms that affect the western part of Iran and concluded that they originate from Iraq, the Iraq–Jordan borders, and Syria. Javadian et al. (2019) revealed that southern and central Iraq are the main sources of sand and dust storms in the western part of Iran, using the HYSPLIT model. The Arabian Peninsula is also a significant source of sand and dust storms in the Middle East, with a large proportion of its land area consisting of desert plains, which can cause sand and dust storms over the Persian Gulf and southern areas of Iran

(Rezazadeh et al . 2013). Recent studies have concluded that the Arabian Peninsula ranks second, after the Sahara Desert, as a major source of sand and dust storms in the dry belt. Numerous studies have been conducted to investigate sand and dust storms in Iran, utilizing various methodologies such as remote sensing techniques, mineral dust sampling, and statistical and spatial analysis. Hamzeh et al. (2021) examined dust events at five meteorology stations in the southwest of Iran and concluded that a significant portion of dust events originate from transboundary sources, rather than from within Iran. Modarres and Sadeghi. (2018) analyzed the number of dusty days occurring in 22 stations in the desert regions of Iran and found that the highest variation of dust days was observed in the southeastern part of the country, with a high frequency in the summer and spring seasons. Mesbahzadeh et al. (2022) analyzed 35 meteorology stations across Iran and determined that Zabol and Zahedan were the stations most affected by dust events, while Mesbahzadeh et al. (2020) analyzed 37 meteorology stations from 1999 to 2018 and found that dust days were most common in the summer and spring seasons, with Zabol, Zahedan, and Arak stations experiencing ahigh frequency of dusty days. Further, Baghbanan et al. (2020) examined 44 stations across Iran and concluded that the highest frequency of dust storm occurrence was observed in the months of July, June, and May, with spring and summer being the peak seasons for dust storms. Additionally, Beyranvand et al. (2019), investigating dust events over Iran between1987 and 2016 for 44 stations, found that the frequency of suspended dust was particularly high in the southwest region of Iran, with Zabol station experiencing a high frequency of rising dust and dust storms in the eastern regions. Finally, a comprehensive analysis by Alizadeh-Choobari et al. (2016) of more than 300 stations across Iran from 1991 to 2010 revealed that suspended dust occurred more frequently in the western part of the country compared to other areas and that it was particularly prevalent during the spring season. Although these studies provide valuable insights into the prevalence and characteristics of sand and dust storms in Iran, two aspects are missing to entirely understand sand and dust storms in the region. The first is that these studies have analyzed the datasets obtained at a small number of meteorology stations located in well-known dust-storm areas. To understand the comprehensive situation of sand and dust storms within the nation, weather stations covering the entire nation need to be considered. The second is that continued monitoring is essential to understand the long-term trend. Therefore, this study aims to investigate dust events of three categories of suspended dust, rising dust, and dust storm at 427 stations over Iran covering a period of 12 years.

3.2. METHODOLOGY

3.2.1. Meteorological Stations and Datasets

The meteorology data for a period from 2010 to 2021, with a 3 h interval, for 427 stations were obtained from the meteorology organization of Iran. Figure 3.1 depicts the location of the stations. The data collection encompasses a range of additional physical quantities, including temperature, precipitation, wind speed, evaporation, relative humidity, soil temperature, sea level pressure, cloud height, and others. These fundamental weather variables are systematically gathered and recorded. In addition to these essential meteorological measurements, the datasets also incorporate the classification codes associated with dust events. Those are data pertaining to suspended dust, rising dust, and dust storm, with present weather codes of 06, 07, and 33–35, respectively, were included. The selection of dust event data was based on the definition of the World Meteorological Organization (WMO). The details of the dust classification are explained in the next section.

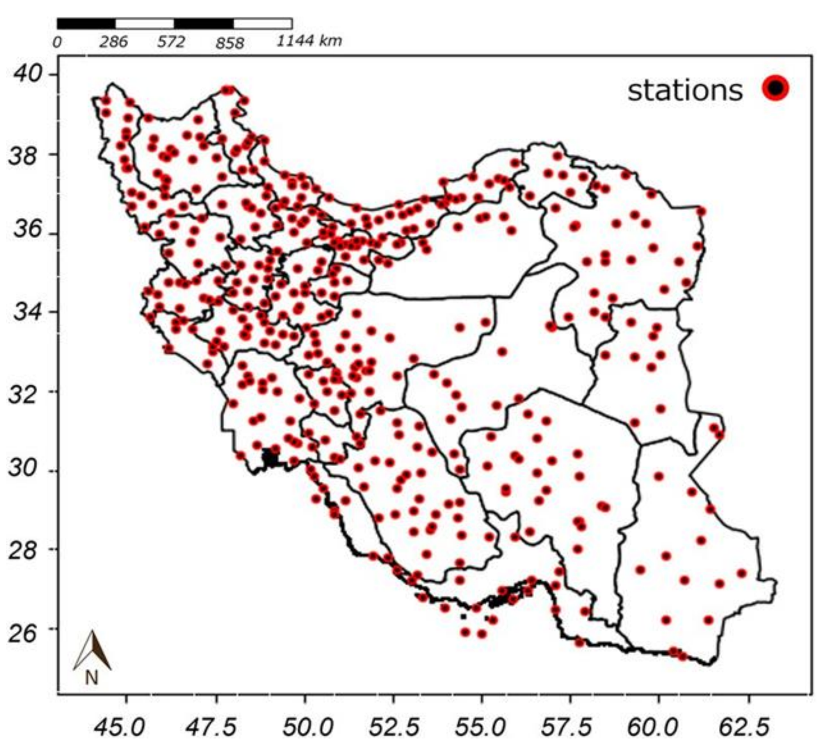

Figure 3.1. The horizontal and vertical axes show the longitude and latitude. The red markers indicate the locations of the weather stations. Total number of the stations is 427, covering the entire country.

Table 3.1. Description of three classes of dust events defined by WMO (World Meteorological Organization).

class **code**	**description**	**Visibility range (VR)**	**Wind speed range (WSR)**
04	Visibility reduced by smoke, e.g. veldt or forest fires, industrial smoke or volcanic ashes	visibility equal to, or greater than, 1 km	Not defined
05	Haze	visibility less than 1 km	Less than 7 m/s
06	Dust is suspended in the air but not raised by the wind at or near the station.	No limit	No limit
07	Sand and dust are raised by the wind at or near the station. The following VR and WSR are considered	Between 1 and 10 km	Between 7 and 15 m/s
08	Well-developed dust whirl(s) or sand whirl(s) seen at or near the station during the preceding hour or at the time of observation, but no dust storm or sandstorm	In visibility above 10 kilometers, it can also be recorded	Not defined
30-32	Slight or moderate dust storm or sandstorm	Less than 1 km	15 m/s
33-35	Severe dusts storms occur with a low VR and strong WSR.	Less than 1 km	More than 15 m/s

3.2.2. Classification Codes of Dust Events

There are several classification codes to represent the dust events based on weather data defined in WMO. Within WMO classification system, numerous codes delineate various dust events based on weather data. However, for the purpose of this study, three primary categories have been selected for analysis: codes 06, 07, and 33-35. For detailed information on additional classification codes and their corresponding definitions, refer to Table 3.1.

Among them, three types were categorized. First, the code for suspended dust (06) represents dust suspended in the air but not raised by the wind near the station at the time of observation. The second, the code for rising dust (07), represents sand or dust raised by the wind at or near the station. The severe dust storms are coded into three categories as 33, 34, and 35, based on the severity of the dust event at the time of observation (WMO Manual on Codes). To record dust events codes at the time of observation, factors such as horizontal visibility, wind speed, relative humidity and precipitation need to be considered. There should be no precipitation at the time of observation and relative humidity levels must be less than 80%. However, the values of wind speed and horizontal visibility may vary depending on the different categories, which are described in Table 1

As previously mentioned, the data were collected every three hours per day, resulting in a maximum of eight dust events being recorded per day. To count the total days experienced with any dust events categorized above, only one reported sand and dust storm was considered as a dusty day in the following statistical analyses. Thus, repeated values from the same class for certain days were omitted, leaving only a single representation of each day's dustiness. After obtaining these values for each station and each dust event category, the frequency of dust events was analyzed annually over a twelve-year period. To provide a clear view of the number of dusty days per year, the data were categorized into 30-day intervals.

In addition, in the dust storm category, all three codes 33, 34, and 35 were considered as one category. Although they represent a dust storm in different intensities, the criteria for recording these events remain the same.

These values then used to analyze occurrence frequency of dust events each year to get general trend of dust events in entire Iran.

3.3. RESULTS

3.3.1. Occurrence Frequency of Dust Events

To statistically understand the general trends of the dust events based on the long- term meteorological dataset, Figure 3.2 depicts the occurrence frequency of dust events in each category. The frequency indicates the expected days per year classified from a month (30 days) to half a year (180 days). The investigation into the occurrence frequency of suspended dust (Fig 3.2 a), rising dust (Fig 3.2 b), and dust storms (Fig 3.2 c) reveals that over 300 stations encounter suspended dust, and a similar number experience rising dust each year among all the stations, whereas nearly 60 stations are affected by dust storms. Although the number of stations that experience suspended dust and rising dust each year is almost identical, the duration and frequency of dust events differ in each category. In most stations, the frequency of dust events in all three categories is 30 days, indicating that 256 stations (74% of stations) experience dust events for almost 30 days each year in the suspended dust category, 91% or 317 stations in the rising dust category, and 100% or 58 stations in the dust storm category. Moreover, 74 stations (22% of stations) experience suspended dust for almost 60 days each year, while only 7% of stations (23 stations) experience rising dust for almost 60 days each year. To summarize these analyses, the mild dust events categorized as suspended and rising dusts occur more frequently, while more severe dust storms also happen, though the frequency is less than that of mild dust events.

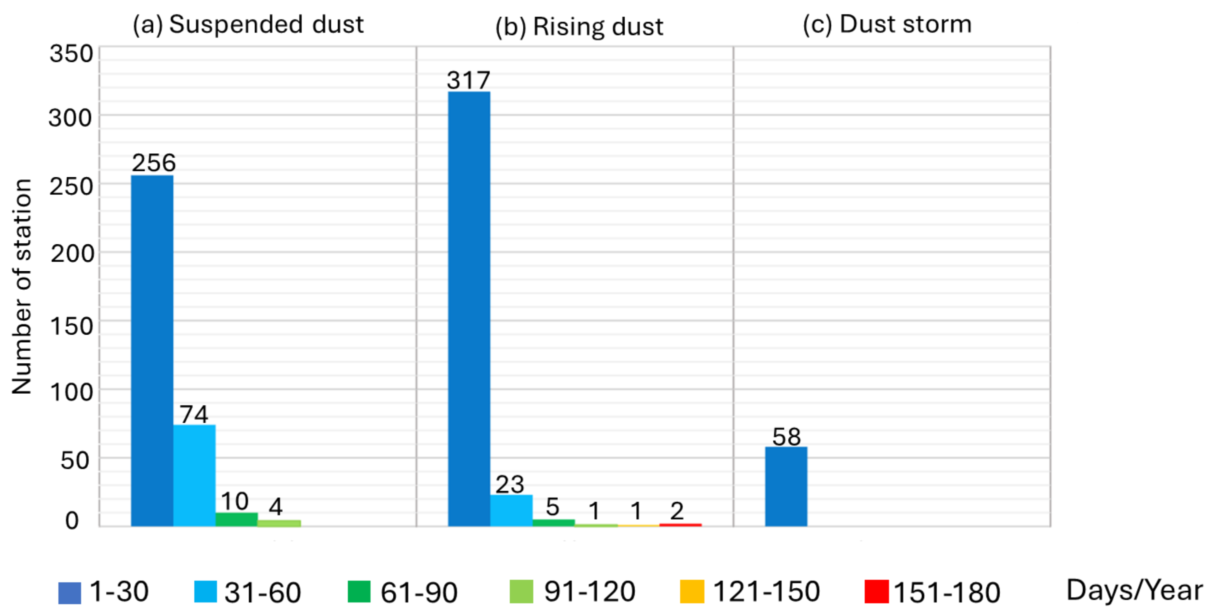

Figure 3.2. The number of stations and occurrence frequency of dust events in each class per year based on 12-year data for (a) suspended dust (06), (b) rising dust (07), and (c) dust storm (33–35).

3.3.2. Spatial Distribution of Dust in Three Categories

Figure 3.3 illustrates the spatial distribution of dust events across Iran, categorized into three types. The sizes and colors of the markers indicate the total days of the dust events per year. It is evident that there are eastern regions where the occurrence frequency of rising dust (Fig 3.3 b) per year surpasses that of the other two categories, aligning with the outcome in Fig 3.2. In the case of suspended dust category (Fig 3.3 a), it is apparent that suspended dust is more prevalent in the western regions of Iran, and the stations in that area experience such events with varying frequencies. Although a few stations experience suspended dust for nearly 100 days annually such as Qasreshirin, Dehloran, Sarpol-E- Zahab, and Bandar-E-Dayyer (Fig 3.3 c, yellow markers), the majority experience it for not more than 60 days per year. Rising dust in (Fig 3.3 b) is predominantly observed in the central, southern, and eastern parts of Iran, with the severity being more pronounced in the eastern region, specifically in the Zabol station. The occurrence frequency of rising dust is approximately 150 days per year in Zabol station (Fig 3.3 c, green markers). Moreover, the occurrence frequency of dust storm does not exceed 10 days per year. While most stations report dust storms for no more than 4 days per year, these events are widespread across Iran and are not confined to specific regions except one station in the east which was mentioned previously.

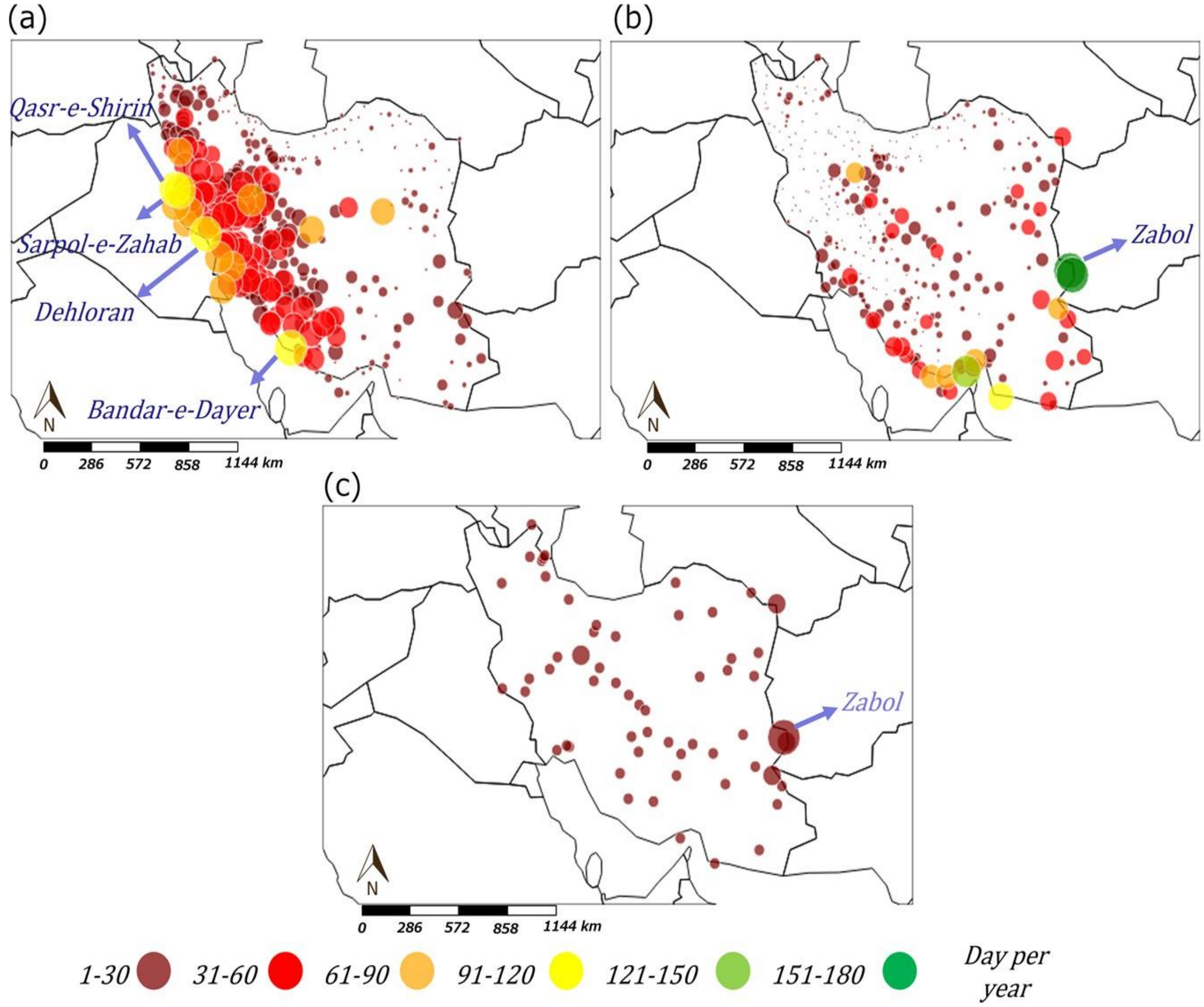

Figure 3.3. Spatial distribution of occurrence frequencies of dust per year for (a) suspended dust, (b) rising dust, and (c) dust storm. The sizes and colors of the marker indicate the frequency.

3.3.3. Spatial Distribution of Standard Deviation of Occurrence Frequencies in Three Categories

Figure 3.4 represents the spatial distribution of the standard deviation of the occurrence frequencies of suspended dust, rising dust, and dust storms over a period of 12 years. In all three categories, the standard deviation of most stations is less than 20 days per year over 300 stations, indicating that the annual averages of each dust event in Figure 3.3 represent the annual occurrence frequencies.

For the suspended dust category (Fig 3.4 a), there are a significant number of stations that recorded the standard deviations between 0 and 40, while only a few stations exhibited higher standard deviation values, such as Sarpol-e Zahab, Sumar, Qasr-e Shirin, Naein, and Tabas, where the frequent dust events were observed. Since the occurrence frequencies of the suspended dust are large (Fig 3.3 a), the variations are also large in some stations near the west regions of Iran. Regarding the rising dust and dust storm categories (Fig 3.4 b,c), enhancing the representativeness of the annual average of the dust days in Figure 3.3.

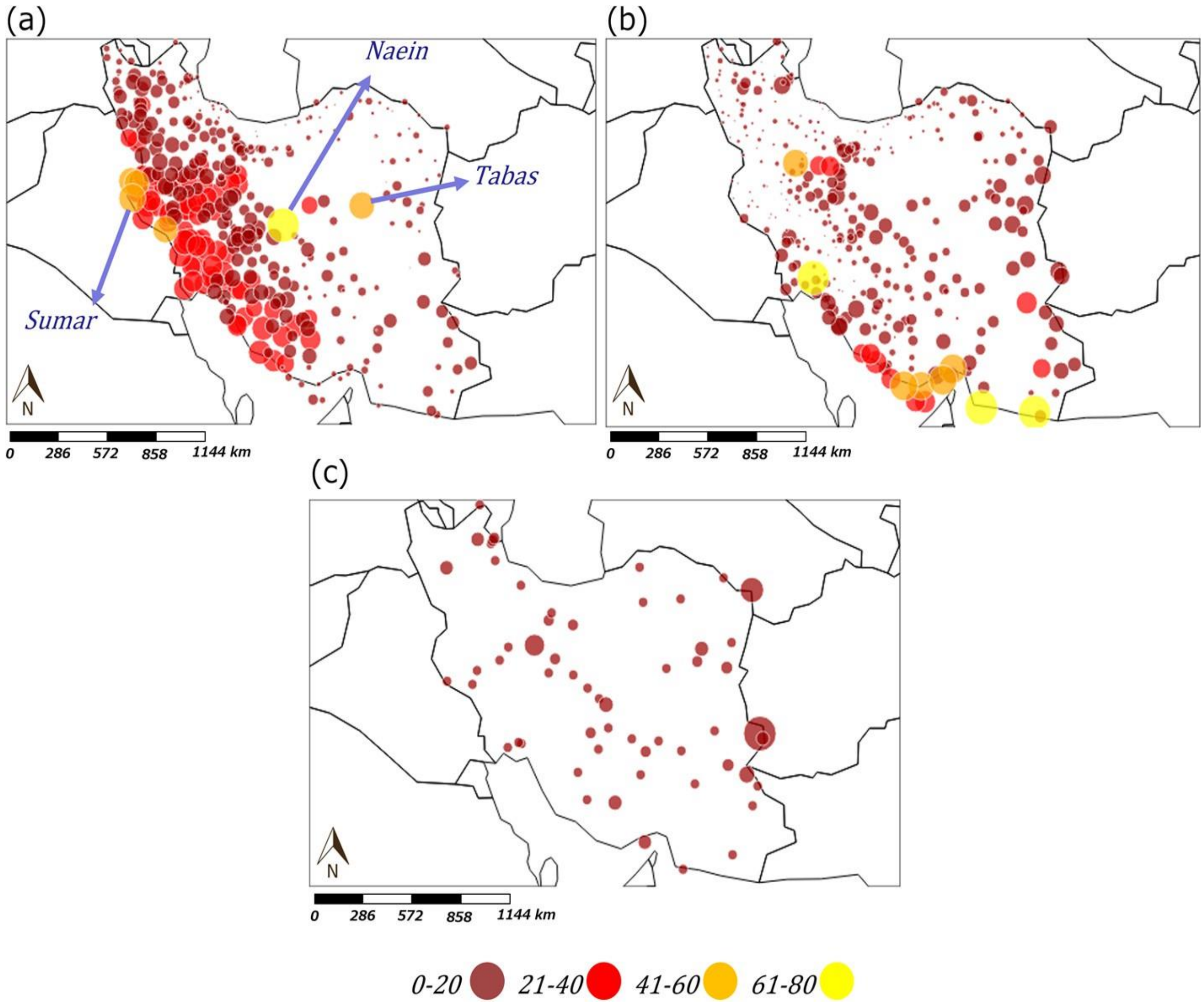

Figure 3.4. Spatial distribution of standard deviation of occurrence frequencies of dust per station for (a) suspended dust, (b) rising dust, and (c) dust storm. The sizes and colors of the marker indicate the frequency.

3.3.4. Breakdown of Occurrence Frequency and Distributions of Dust Events in Less Than 30 Days

Figure 3.5 represents the occurrence frequency of dust events lasting less than 30 days per year in each category. As the frequency of dust events is less than 30 days per year in most stations based on the results from Figure 3.4, this categorization was necessary to provide a more accurate view. In all three categories, the highest frequency of occurrence of dust events is five days, indicating that most stations in all three categories experience dust events for only a few days per year.

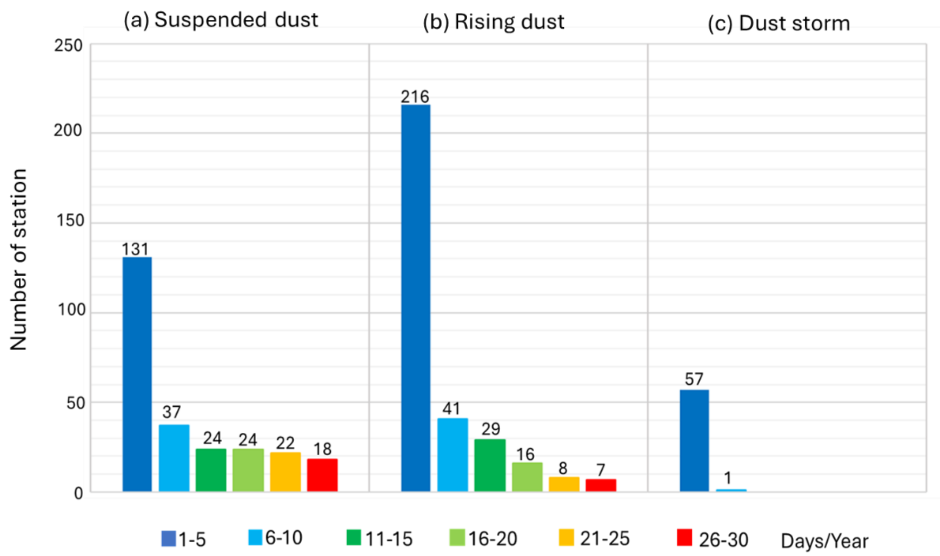

Figure 3.5. Breakdowns of the number of stations and occurrence frequency of dust events less than 30 days per year based on 12-year data for (a) suspended dust, (b) rising dust, and (c) dust storm.

In the suspended dust category (Fig 3.5 a), out of all 427 stations, 344 stations experience suspended dust, and among them, 256 stations experience suspended dust for less than one month. Among these 256 stations, 51% experience suspended dust for almost five days, while 49% experience suspended dust for more than five days. Interestingly, 40 stations experience suspended dust for almost one month each year.

In the rising dust category (Fig 3.5 b), 349 stations experience rising dust each year, and among them, 317 stations experience rising dust for less than one month. Furthermore, 68% of stations experience rising dust for less than five days each year, while 13% of 317 stations experience rising dust for 10 days, and 9% of stations experience rising dust for 15 days. Only 16 stations out of 317 experience rising dust for one month.

In the dust storm category (Fig 3.5 c), 58 stations experience this phenomenon each year, and among them, 98% of stations experience dust storms for less than five days each year. In other words, the frequency of dust storm occurrence is less than five days each year in most stations that experience dust storms, and it is only in a few stations that it exceeds five days. Thus, this figure provides an accurate view of dust events, indicating that the frequency of occurrence of dust events is less than five days in all categories. Only the suspended dust period is longer than the other two categories.

Accordingly, the spatial breakdowns of the occurrence frequency are discussed. Figure 3.6 illustrates the spatial distribution of the number of dusty days with less than 30 occurrences per year across Iran. The three categories of dusty days are uniformly distributed across the country, but their frequency varies. Suspended dust (Fig 3.6 a) is found in all stations, but its highest frequency is observed in the western part of Iran, where the duration of suspended dust is also longer. Stations that expected to experience suspended dust for almost 30 days are 1. Bukan, 2. Javanrud, 3. Kamyaran, 4. Hamedan, 5. Nurabad, 6. Gharaqabad, 7. Salafchegan, 8. Kahak, 9. Delijan, 10. Ardestan, 11. Esfahan, 12. Najafabad, 13. Shahrekord, 14. Sisakht, 15. Nurabad, 16. Bandar-e-Deylam, 17. Khark Island, and 18. Zahedan, respectively (Fig 3.6 a, dark green markers).

Rising dust (Fig 3.6 b), on the other hand, is visible in most stations, but its dura- tion is shorter compared to suspended dust, with an occurrence frequency of less than 10 days. Stations that are expected to have rising dust for almost 30 days per year are 1. Hamedan, 2. Saveh, 3. Qom, 4. Bostan, 5. Naein, 6. Yazd, 7. Gonabad, 8. Hajiabad, 9. Nehbandan, 10. Fasa, 11. Rudan, and 12. Bandar-e-khamir, respectively (Fig 3.6 b, dark green markers). Dust storms (Fig 3.6 c), characterized by a frequency of occurrence of no more than 10 days per year, are observed across the country. As mentioned previously, the only station that experiences dust storms more than other stations are Zabol station, which is expected to have dust storms around 10 days per year.

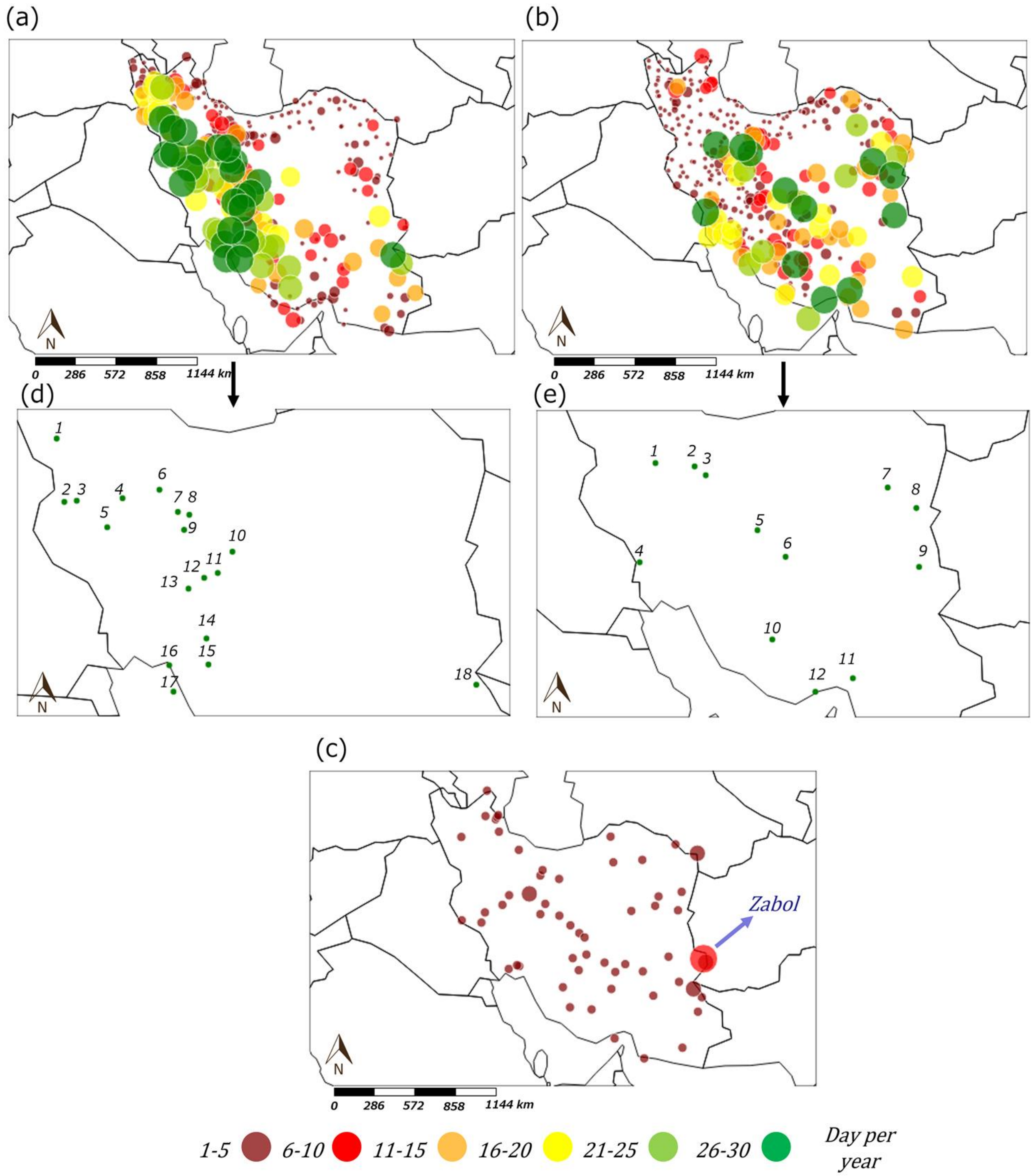

Figure 3.6. Spatial distribution of occurrence frequencies of dust less than 30 days per year for (a) suspended dust, (b) rising dust, and (c) dust storm. The sizes and colors of the marker indicate the frequency. The numbers in (d, e) indicate the locations of the weather stations.

3.3.5. Seasonal Spatial Distribution of Suspended Dust

Figure 3.7 shows the seasonal distribution and the occurrence frequency of suspended dust. The four seasons in Iran are defined as follows: spring from March to May, summer from June to August, autumn from September to November, and winter from December to February. As is evident, the phenomenon of suspended dust is widespread across all areas, with a higher distribution in the western region of Iran. The occurrence frequency of suspended dust varies in each season. In autumn and winter, the frequency of occurrence of suspended dust is approximately 15 days in most stations, with some stations experiencing over 20 days per season. However, the occurrence frequency of suspended dust is higher in spring and summer (Fig 3.7 (spring, summer)) than in autumn and winter (Fig 3.7 (autumn, winter)). In spring, both the frequency of occurrence and the number of stations experiencing suspended dust are higher than in other seasons. Two stations that have higher frequency of occurrence than other stations are Sarpol-e-zahab and Bandar-e-dayer. The occurrence frequency of suspended dust in most stations is around 10 to 40 days per season per year. In summer, although the number of stations experiencing suspended dust is not as high as in spring, the frequency of suspended dust is as high as in spring, and stations such as Arak, qasr-e-shirin, Dehloran, bandar-e-dayer are expected to experience rising dust for more than 30 days and less than 40 days.

3.3.6. Seasonal Spatial Distribution of Rising Dust

Figure 3.8 represents the seasonal distribution and occurrence frequency of rising dust. The average number of stations that experience rising dust is lower than the number of stations that experience suspended dust. The distribution of rising dust phenomenon is widespread, yet it is more visible in the central, south, and east parts of Iran. The highest frequency of occurrence of rising dust is in spring, followed by autumn and summer, respectively, while the lowest belongs to winter.

The occurrence frequency of rising dust is high in spring (Fig 3.8 (spring)), and the number of stations that experience rising dust is higher than in other seasons. However, the number of days that stations experience rising dust does not exceed 10 days in most stations. The only station that experiences high frequency of rising dust in spring is Qeshm Island (Figure

3.8 (spring), dark green markers). The high frequency of occurrence of rising dust is visible in the central, south, and eastern regions.

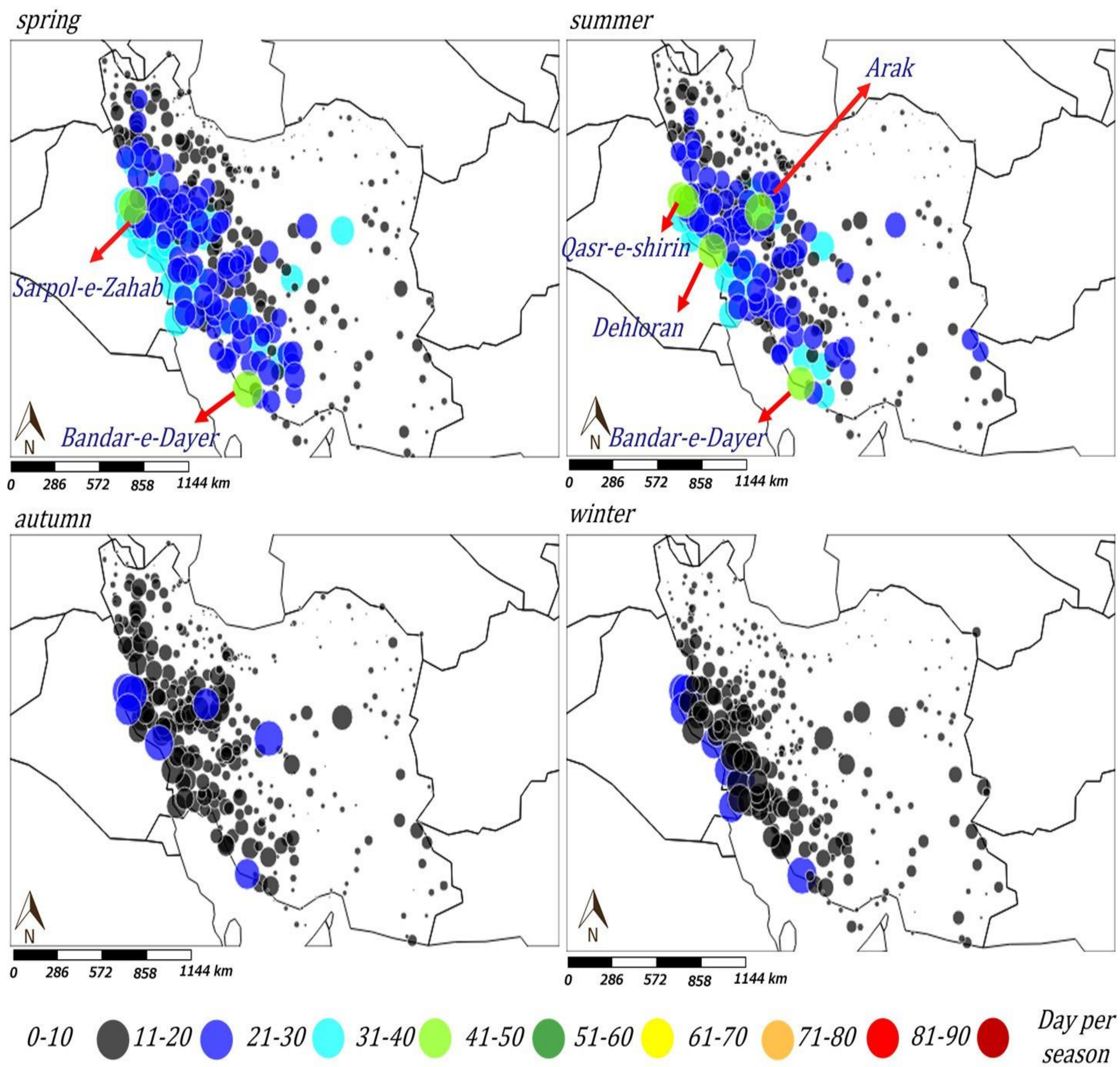

Figure 3.7. Seasonal spatial distribution of the occurrence frequencies per season for the suspended dust. The sizes and colors indicate the frequency. Seasons are defined as follows: spring from March to May, summer from June to August, autumn from September to November, and winter from December to February.

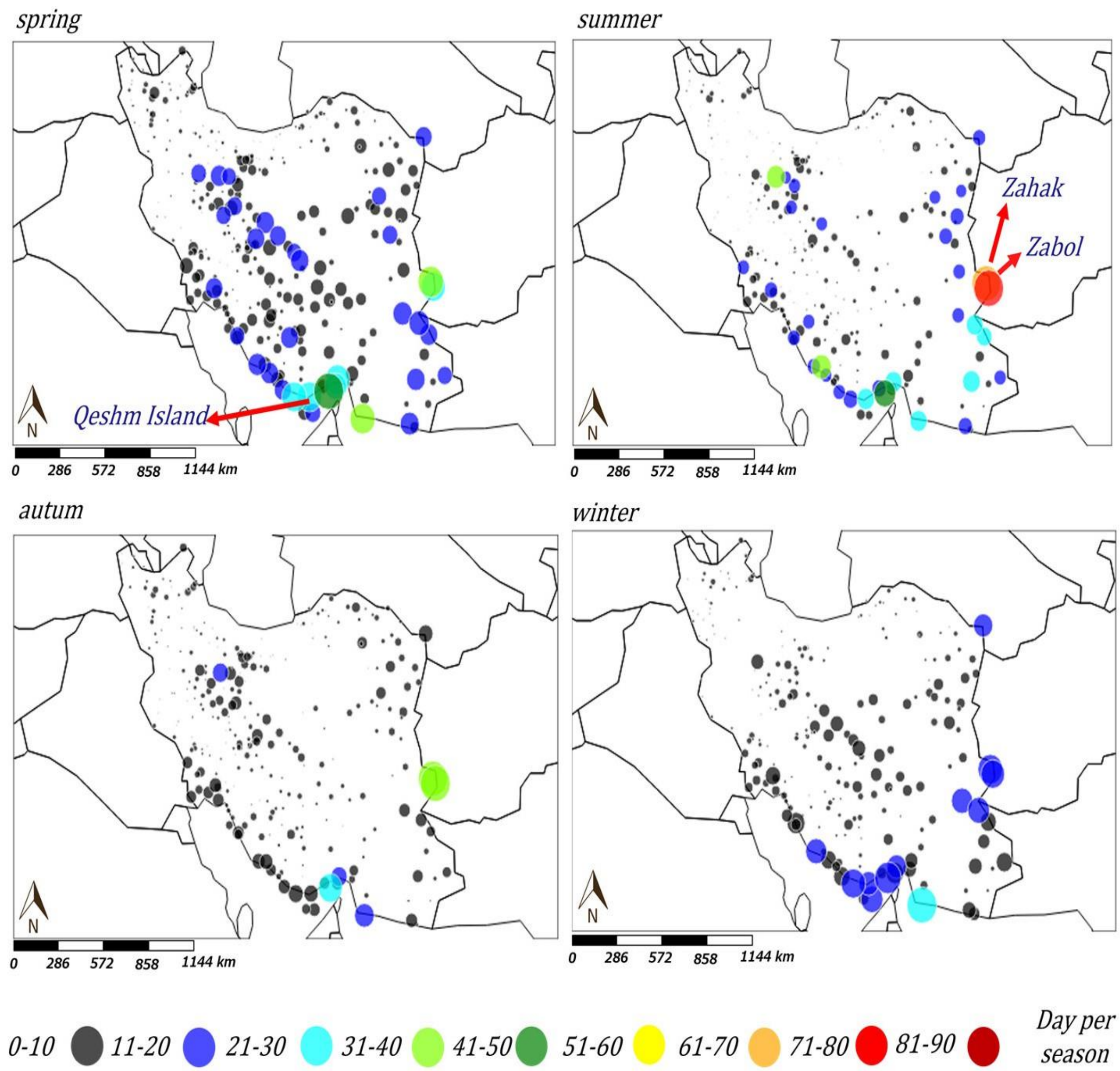

Figure 3.8. Seasonal spatial distribution of the occurrence frequencies per season for the rising dust. The sizes and colors indicate the frequency. Seasons are defined as follows: spring from March to May, summer from June to August, autumn from September to November, and winter from December to February.

In the summer season (Fig 3.8 (summer)), the number of stations that experience rising dust is not as high as in the spring season. However, in several stations, the total day of rising dust is quite large such as Zahak and Zabol stations (Fig 3.8 (summer), red, orange markers), nearly 90 days per season, indicating that these are rising dust events every day in such stations.

In general, the total days of rising dust in the summer season are high in the east, south, and central parts of Iran.

After the spring season, the number of stations that experience rising dust is high in autumn (Fig 3.8 (autumn)). The frequency of occurrence of rising dust in most of them does not exceed 10 days each year, and the recurrence of rising dust is not high in autumn.

In the winter season (Fig 3.8 (winter)), the number of stations that experience rising dust is lower than in other seasons. The frequency of occurrence of rising dust in most stations does not exceed 10 days per season. As can be seen, the frequency of rising dust is high in the south and adjacent to the shoreline and the east part of Iran. Rising dust is also frequent in the central region but with lower recurrence.

3.3.7. Seasonal Spatial Distribution of Dust Storm

Figure 3.9 illustrates the seasonal distribution and frequency of occurrence of dust storms in Iran. The data reveal that the frequency of dust storms does not exceed 10 days in all seasons. Among all the seasons, spring (Fig 3.9 (spring)) has the highest frequency of dust storms, and many stations in central, east, northeast, and northwest parts of Iran experience dust storms during this season. Interestingly, the severe storms categorized as dust storm are uniformly distributed in entire country, and the seasonal trends are less apparent than other categories.

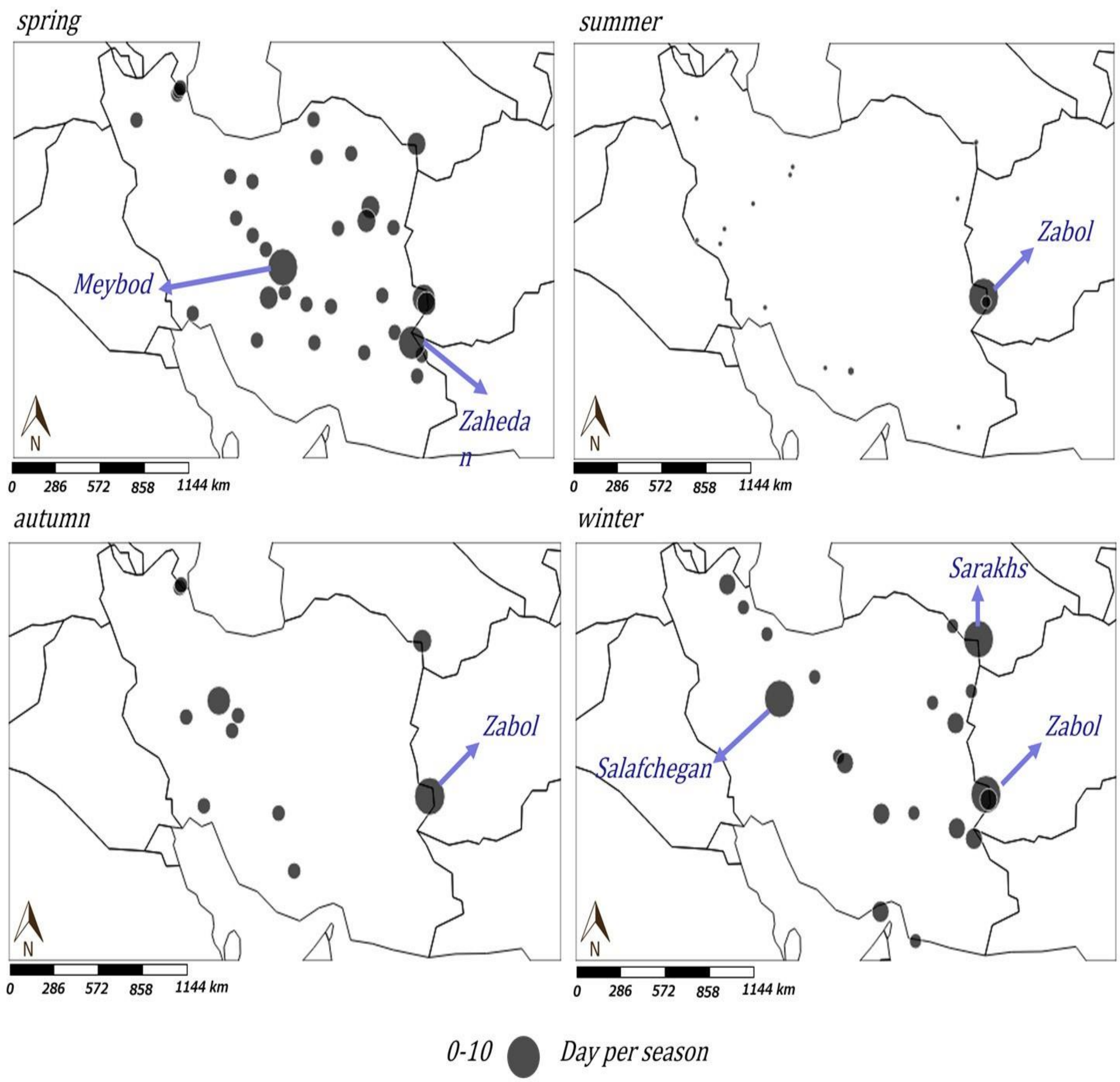

Figure 3.9. Seasonal spatial distribution of the occurrence frequencies per season for the dust storm. The sizes and colors indicate the frequency. Seasons are defined as follows: spring from March to May, summer from June to August, autumn from September to November, and winter from December to February.

In summer (Fig 3.9 (summer)), the frequency of dust storms is low, except in the eastern part of Iran. In this season, dust storms are more prevalent in the south and east of Iran, obviously in Zabol station, but with lower frequency.

Autumn (Fig 3.9 (autumn)) has the lowest frequency of occurrence of dust storms compared to the other seasons, and the number of stations that experience dust storms is numerable, except for some stations where dust storms occur regularly.

After spring, winter (Fig 3.9 (winter)) has the highest frequency of dust storms. Except for the west part of Iran, dust storms are distributed in various parts of Iran, including the islands in the Persian Gulf. However, the number of stations that experience dust storms is few and countable in all four seasons.

3.3.8. Monthly Dusty Days in 12 Years

In addition to the statistical analyses to understand general annual and seasonal trends of the dust events, long-term monthly variation of the dust events is worth investigating to understand the representativeness of the statistical averages. Figure 3.10 illustrates a general overview of the total number of dust events occurred in each month for each year. Rising dust (Fig 3.10 b) has the highest record per month and per year, indicating that it is the most frequently occurring type among the three categories of the dust events. Suspended dust (Fig 3.10 a) is the next most frequently occurring type of the dust events, followed by dust storms (Fig 3.10 c). With regards to monthly frequency, dust events reach their peak frequency in summer, beginning from late spring and decreasing after July as a general trend. The lowest frequency of dust events occurs in winter, particularly in January and December, for both suspended and rising dust categories. Although these general trends can be confirmed for the suspended and rising dust events, as can be seen in previous sections, there is also clear annual variation of less frequent days between 2019 and 2021. In contrast, dust storms do not show any obvious monthly trend because of less frequencies than the other two categories. In the annual analysis, the highest record of dust events occurred in 2012 during the spring season for all three categories.

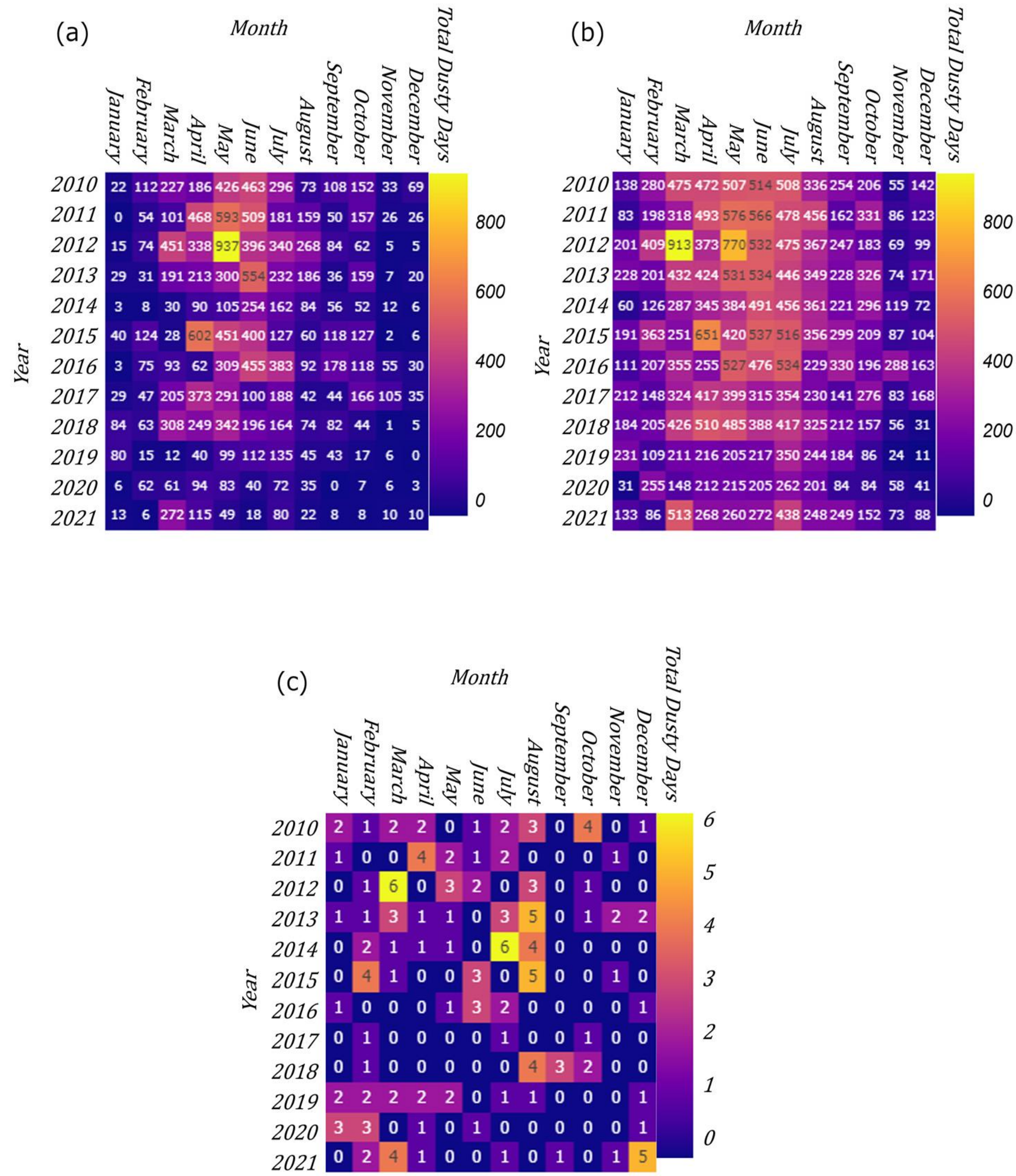

Figure 3.10. Long-term monthly variation of total dusty days for 12 years (a) suspended, (b) rising dust, and (c) dust storm. The numbers indicate the total dusty days per months of all the weather stations.

Regarding suspended dust (Fig 3.10 b), as previously mentioned, the number of occurrences in the spring is higher than in other seasons, but it increases substantially during this season. A slight but considerable high frequency of suspended dust can also be observed in October. From an annual perspective, suspended dust had a high frequency in particular years, such as 2011, 2012, and 2015, but its frequency has decreased significantly after 2018.

Rising dust (Fig 3.10 b) has almost the same pattern as suspended dust but with a higher frequency. The highest frequency of rising dust occurs in the spring and early summer. From an annual perspective, 2012 and 2015 had the highest record of rising dust. However, there is no particular trend in the annual analysis.

Regarding dust storms (Fig 3.10 c), it is evident that they have a very low frequency compared to other categories, and they do not exhibit any obvious trends annually or monthly. The monthly analysis shows that dust storms have a high frequency in the summer compared to other seasons. From an annual perspective, the highest number of dust storms was recorded in 2012 and 2014 during the spring and summer seasons, respectively. Overall, dust storms do not show any particular trend, unlike the other two categories.

3.3.9. Annual and Monthly Frequency of Dust Events for Three Classes

Figures 3.11 and 3.12 illustrate the overall number of dust events that have been recorded across all three categories in all stations. Upon annual analysis, it is evident that the highest number of dusty days and dust events recorded across all stations belong to the rising dust category, with the maximum being observed in 2012 and the minimum in 2020. Following rising dust, suspended dust has the second-highest number of dust events, with a similar trend observed each year, as is the case with rising dust. Although the maximum and minimum number of dust events for this category also occurred in the same years as rising dust, there was a considerable difference in the total number of recorded dust events. The annual analysis of dust storms revealed that the maximum number of recorded dust storms did not exceed 20 events, which occurred in 2013, while the minimum was observed in 2017. In general, it can be concluded that no clear trend can be observed for any of the three dust categories upon annual analysis.

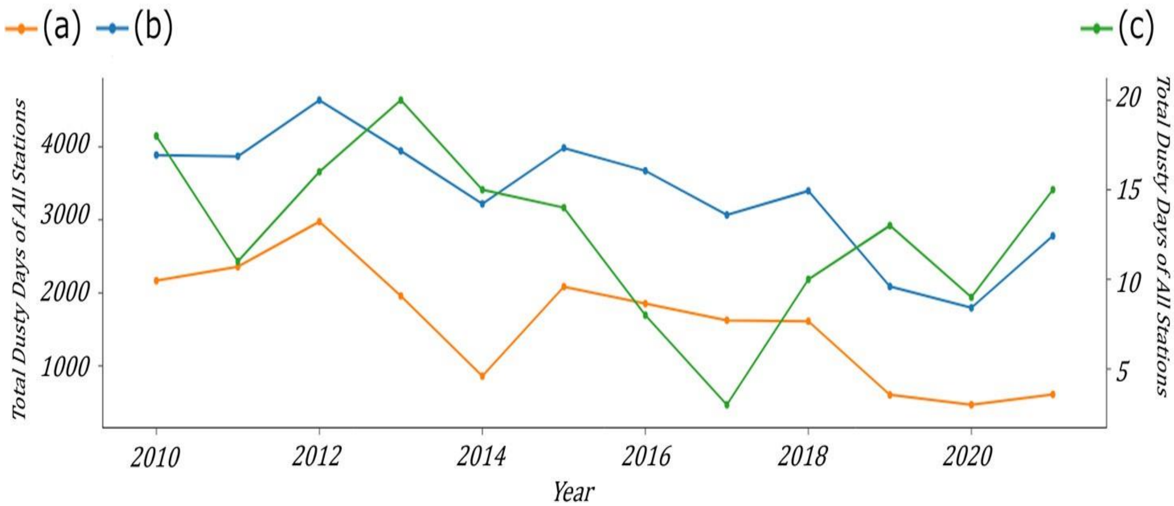

Figure 3.11. Annual variation of the total number of dust events for (a) suspended dust, (b) rising dust, and (c) dust storm.

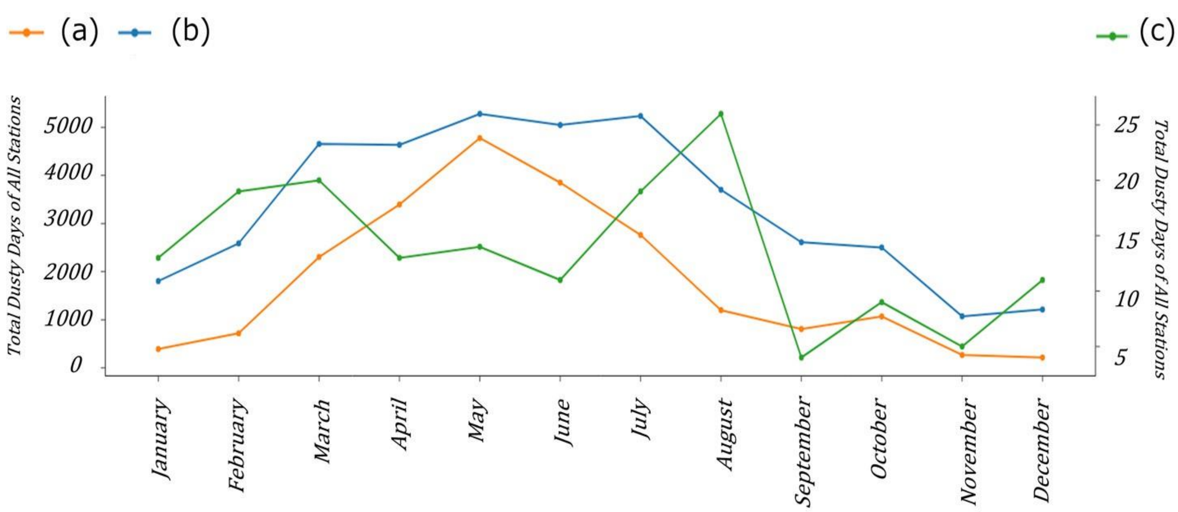

Figure 3.12. Monthly variation of the total number of dust events for (a) suspended dust, (b) rising dust, and (c) dust storm. Each lines indicates the average of 12-year data.

In monthly analysis, the highest recorded of dust events for both suspended dust and rising dust belongs to the spring and summer months, respectively. But for dust storms, it occurs in summer. The lowest frequency for all classes belongs to the winter season.

3.4. CONCLUSIONS

In this chapter, dust events are categorized into suspended dust, rising dust, and dust storms, based on long-term meteorological datasets obtained from 427 stations across Iran over a 12-year period. A single classification of sand and dust storms was found to be insufficient to accurately reflect the varying intensities and indices of this weather phenomenon. Consequently, three classes of sand and dust storms were analyzed across all meteorological stations in Iran.

Among the three classes, rising dust had the highest frequency of occurrence, followed by suspended dust and dust storms. The duration and expected frequency of occurrence of all three categories were found to be less than 30 days per year, with only a few stations experiencing dust events more than 30 days per year. The interannual variation quantified by the standard deviation shows that most stations in all three categories have experienced frequent dust events annually.

The spatial distribution analysis revealed that all three classes were distributed uniformly across all stations. Suspended dust events, however, showed a distinct concentration in the western regions of the country, while rising dust tended to occur more frequently in the southern, eastern, and central parts of Iran. Dust storms, on the other hand, had the lowest frequency of occurrence compared to suspended and rising dust, yet they could still be observed in most parts of Iran.

Seasonal and monthly variations were also quantified. All three classes exhibited higher frequency of occurrence in the spring season. Accordingly, dust events reached their highest peak in late spring to early summer for all three categories, and rising dust was found to be the most frequently occurring type, followed by suspended dust and dust storms. In the annual analysis, the highest record of dust events occurred in 2012, indicating that the annual dust events also have variations.

Given the importance of wind speed in understanding dust events, the next chapter will focus on analyzing wind speed data and predicting wind patterns. This analysis is essential for accurately forecasting dust events and developing early warning systems to mitigate their impacts. By examining wind speed trends and patterns, we can better understand the conditions that lead to different types of dust events and improve our ability to predict their occurrence and intensity.

3.5. REFERENCES

Alizadeh-Choobari O, Ghafarian P, Owlad E. Temporal variations in the frequency and concentration of dust events over Iran based on surface observations. International Journal of Climatology. 2016 Mar 30;36(4):2050-62.

Baghbanan P, Ghavidel Y, Farajzadeh M. Temporal long-term variations in the occurrence of dust storm days in Iran. Meteorology and Atmospheric Physics. 2020 Dec;132:885-98.

Beyranvand A, Azizi G, Alizadeh-Choobari O, Darvishi Boloorani A. Spatial and temporal variations in the incidence of dust events over Iran. Natural Hazards. 2019 May 15;97:229-41.

Boloorani AD, Nabavi SO, Bahrami HA, Mirzapour F, Kavosi M, Abasi E, Azizi R. Investigation of dust storms entering Western Iran using remotely sensed data and synoptic analysis. Journal of Environmental Health Science and Engineering. 2014 Dec;12:1-2.

Climate-Data-Historical. Available online: https://climateknowledgeportal.worldbank.org/about (accessed on 2 June 2023).

Cuevas Agulló, E. Establishing a WMO Sand and Dust Storm Warning Advisory and Assessment System Regional Node for West Asia: Current Capabilities and Needs. Atmosphere 2013, 50, 91–96.

Francis D, Fonseca R, Nelli N, Bozkurt D, Cuesta J, Bosc E. On the Middle East's severe dust storms in spring 2022: Triggers and impacts. Atmospheric Environment. 2023 Mar 1;296:119539.

Ginoux P, Prospero JM, Gill TE, Hsu NC, Zhao M. Global-scale attribution of anthropogenic and natural dust sources and their emission rates based on MODIS Deep Blue aerosol products. Reviews of Geophysics. 2012 Sep;50(3).

Hamzeh NH, Kaskaoutis DG, Rashki A, Mohammadpour K. Long-term variability of dust events in southwestern Iran and its relationship with the drought. Atmosphere. 2021 Oct 15;12(10):1350.

Huang X, Ding K, Liu J, Wang Z, Tang R, Xue L, Wang H, Zhang Q, Tan ZM, Fu C, Davis SJ. Smoke-weather interaction affects extreme wildfires in diverse coastal regions. Science. 2023 Feb 3;379(6631):457-61.

Javadian M, Behrangi A, Sorooshian A. Impact of drought on dust storms: case study over Southwest Iran. Environmental Research Letters. 2019 Dec 6;14(12):124029.

Ke Y, Wang H, Wu Z, Liu S, Zhao T, Yin Y. Quantifying the pollution characteristics of chemical components in PM2.5 in the North China Plain, China: Spatiotemporal variation and health risk. Atmospheric Environment. 2023 Aug 15;307:119860.

Mahmoudi, L.; Ikegaya, N. Present Situations of Dust Storms in Iran for Seeking Numerical Predictions. Proc. Int. Exch. Innov. Conf. Eng. Sci. 2022, 8, 354–359.

Mesbahzadeh T, Miglietta MM, Sardoo FS, Krakauer N, Hasheminejad M. Regional analysis of dust day duration in Central Iran. Applied Sciences. 2022 Jun 20;12(12):6248.

Mesbahzadeh T, Salajeghe A, Sardoo FS, Zehtabian G, Ranjbar A, Krakauer NY, Miglietta MM, Mirakbari M. Climatology of dust days in the Central Plateau of Iran. Natural Hazards. 2020 Nov;104:1801-17.

Middleton N, Kang U. Sand and dust storms: Impact mitigation. Sustainability. 2017 Jun 17;9(6):1053.

Modarres R, Sadeghi S. Spatial and temporal trends of dust storms across desert regions of Iran. Natural Hazards. 2018 Jan;90:101-14.

Rezazadeh M, Irannejad P, Shao YJ. Climatology of the Middle East dust events. Aeolian Research. 2013 Sep 1;10:103-9.

Sivakumar MV, Motha RP, Das HP, editors. Natural disasters and extreme events in agriculture: impacts and mitigation. Berlin, Heidelberg: Springer Berlin Heidelberg; 2005 Dec 6.

The WMO Manual on Codes: International Codes, Volume I.1 Annex II to the WMO Technical Regulations: Part A—Alphanumeric Codes, 2017 ed.;World Meteorological Organization: Geneva, Switzerland, 2019; Volume I.1, ISBN 978-92-63-10306-2.

World Meteorological Organization. WMO Manual on Codes: International Codes, Volume I.1 Annex II to the WMO Technical Regulations: Part A—Alphanumeric Codes, 2017 ed.;World Meteorological Organization: Geneva, Switzerland, 2019; Volume I.1, ISBN 978-92-63-10306-2.

CHAPTER 4: COMPARING ANNUAL EXTREME WINDS IN IRAN PREDICTED BY NUMERICAL WEATHER FORECASTING AND GRAM-CHARLIER STATISTICAL MODEL WITH METEOROLOGICAL OBSERVATION DATA

4.1. INTRODUCTION

Winds, particularly those within the inner atmospheric boundary layers, are strongly influenced by the topography and local surface heating and cooling, making them the most variable and least predictable (Kasai et al. 2018). Iran, a country with four distinct seasons, experiences summer airflow driven by low air pressure and winter winds influenced by high pressure in the northern and northwestern regions. Additionally, it is characterized by well-known wind patterns, such as the 120-day winds in the east, along with local phenomena, such as the north winds along the Persian Gulf, Khoch Abad winds in the Gorgan plain, Deez winds between Mashhad and Nayshabour, and Sham winds in Khuzestan (Mirhosseini et al. 2011). Because Iran is a semi-arid and arid country, strong winds often lead to wind erosion and dust events, and numerous dust events occur annually across Iran. (Mahmoudi & Ikegaya. 2023). Therefore, it is crucial to understand wind behavior due to its significant role in occurrence of sand and dust events (Lackoóvá et al. 2023; Ikegaya et al. 2020; Repetto et al. 2017; Ren et al. 2022).

The prediction of winds and assessment of their impact can be approached using various methods (Li et al. 2023a). Among these, field measurements provide the most reliable wind field data for observing real phenomena. However, this method is costly and is typically used to collect long-term meteorological data. In addition, the number of weather stations is typically limited. Despite its importance, limited studies have been conducted on field measurements in Iran (Panahifar et al. 2020 a; Panahifar et al 2020 b). Another method is numerical weather forecasting (NWF). Numerous NWF models have been optimized to achieve accurate weather predictions (Carvalho et al. 2014; Penchah et al. 2017; Aslam. 2021). Two of the most widely utilized numerical weather forecast models are the Global Forecast System (GFS) and European Center for Medium-Range Weather Forecasts (ECMWF) model. GFS, administered by NOAA through NCEP, is a global forecasting model known for its broad coverage but relatively coarse resolution. The ECMWF model is one of the world's most advanced weather prediction tools, offering global forecasts with particular emphasis on Europe and its surrounding regions (Mathiesen & Kleissl. 2011).

Another well-known NWF model is Weather Research and Forecasting (WRF) Numerous studies have utilized WRF model, often integrating them with various models through a process known as coupling (Skamarock et al. 2019). These integrations consistently yielded promising results (Li et al. 2023b; Cao et al. 2017; Li et al. 2021; Hågbo & Giljarhus. 2024; Mortezazadeh et al. 2021; Wang et al. 2023). For instance, Zhang et al. (2022) conducted a comparative study of a coupling method based on the WRF to investigate its accuracy and efficiency. The results showed that WRF achieved excellent performance in both probabilistic and deterministic assessments. Gholami et al. (2021) also acknowledged the importance of WRF strategies in meteorological forecasting and their reliability for certain coupling methods, whereas others utilized the WRF model output for comparison with observational data. Penchah et al. (2017) evaluated observational data against the WRF output and employed a Weibull distribution to reconstruct the wind speed distribution. However, the accuracy of predictions from the WRF model remains uncertain, with several studies indicating a tendency to overestimate wind speed (Prósper et al. 2019; Saadatabadi et al. 2023; Hamzeh et al. 2023), particularly during extreme wind events (Mohammadi et al. 2024). In addition, most of these studies were limited to analyses of a few stations located in Iran.

To examine the outcomes derived from NWF approaches, many statistical models or parametric methods have been developed to estimate wind speed probability density and extreme wind speeds by assuming a certain shape of the probability density functions (PDFs). These methods describe the PDFs of wind-speed data based on empirical parameters obtained from the wind-speed data (Ammari et al. 2015). The Weibull distribution is well-known and the most frequently used distribution function for the distributions of the magnitude of wind speeds because it can express long-tail positively skewed distribution functions. For example, Alavi et al. (2016a) employed the Weibull and Nakagami distributions, which are modified gamma distributions, to analyze the PDFs at five stations using data collected at 10-minute intervals. Accordingly, Alavi et al. (2016b) analyzed four PDFs, including the Weibull distribution of wind-speed data gathered at five stations in Kerman Province, Iran. Nedaei et al. (2018) comprehensively evaluated wind resources by employing various statistical approaches to analyze extreme wind events at higher altitudes for wind turbines. Although numerous studies have investigated the characteristics of wind speeds based on PDFs, most have focused on the applicability of the Weibull distribution with different parameters to estimate background meteorological wind conditions. Although many dust events are associated with strong winds, few studies have focused on the occurrence of extreme annual wind events.

Furthermore, an alternative approach to modeling the PDF of wind speeds, a modified Gaussian distribution known as the Gram-Charlier series (GCS), has recently been employed. The GCS is recognized as a series expansion of the Gaussian distribution function with higher-order statistics to accurately estimate PDFs. (Wang and Okaze, 2022) proposed GCS models to enhance the applicability of statistical models for predicting the PDF of pedestrian-level winds. Their research suggests that GCS models can be tailored to any order based on the available statistical data. Seta et al. (2023) developed GCS models to demonstrate progressive improvements in higher-order modeling. Zainol et al. (2022) investigated the PDF of wind using GCS models and validated their applicability for strong wind prediction. Similarly, Li et al. (2024) validated the GCS models by analyzing the relationship between higher-order statistics and strong and weak wind speeds. Although these statistical model applications focus on the prediction of PDFs for instantaneous wind distribution, it is worth understanding whether such statistical models can be employed for the prediction of annual extreme wind events.

According to the review of these studies, which provide valuable perspectives on wind distribution in various situations, certain aspects need to be studied. First, to validate the WRF models, these studies were mostly applied to datasets obtained from few stations. Therefore, a comprehensive analysis of stations covering Iran is required. In addition, previous studies have mostly focused on the reproduction of the mean wind speeds; however, the higher-order statistics of the averaged wind speeds, which largely affect the PDFs of the occurrence of annual extreme wind events, have not been assessed. Second, although a few statistical distributions were employed to show the PDFs of the wind speeds of the meteorological data (e.g., the Weibull distribution), the predicted PDFs were not used to estimate extreme values. In addition, recent statistical models, such as GCSs, have only been used in idealized city models; hence, their performance for meteorological data remains uncertain.

Under these circumstances, this study aims i) to validate the WRF model using a comprehensive observation dataset covering the entire Iran; ii) to compare the fundamental statistics of mean, standard deviation, skewness, and kurtosis; iii) to apply the GCS method to model the PDFs of the wind speeds for both observational data and WRF-model output; and iv) to evaluate the applicability of that method for the annual peak values of the wind speeds. Our approach expands WRF-model by showing the relationship between observational data, the WRF model output, and the application of statistical methods.

In Section 2, the details of the datasets and numerical simulations are provided, and the study regions, numerical weather forecast model, physical parameterization, and statistical model employed are discussed. In Section 3, the relationship between the WRF model output and the observational data is explored through a comparison of the fundamental statistics, followed by an analysis of the peak values between the two datasets. In Section 4, the correlation between the two datasets is discussed, followed by an analysis of the predictive accuracy of the probability density using the GCS model for both datasets. The main conclusions of this study are summarized in Section 5.

4.2. METHODOLOGY

4.2.1. Study region

Figure 4.1 shows the study region for the NWF and the locations of the meteorological weather stations. With a total area of 1.648 million km2, Iran spans latitudes between 25 and 40º N and longitudes between 44 to 64º E. The color in Figure 4.1 (a) indicates the altitude. The country comprises diverse regions influenced by various structural units, including the Persian Gulf, Caspian Sea, Zagros Mountains, and Alborz Mountains, with elevations ranging from minus 24 to 5609 m. Iran exhibits both arid and semi-arid climates, resulting in a wide range of climate features across its territories (Najafi et al. 2023). To apply both the NWF and a statistical method for predicting the wind speeds for such varieties in climate zones, our datasets from the observation and NWF cover the entire region of Iran, as shown in Figure 4.1 details of the NWF and meteorological stations are explained in the following sections.

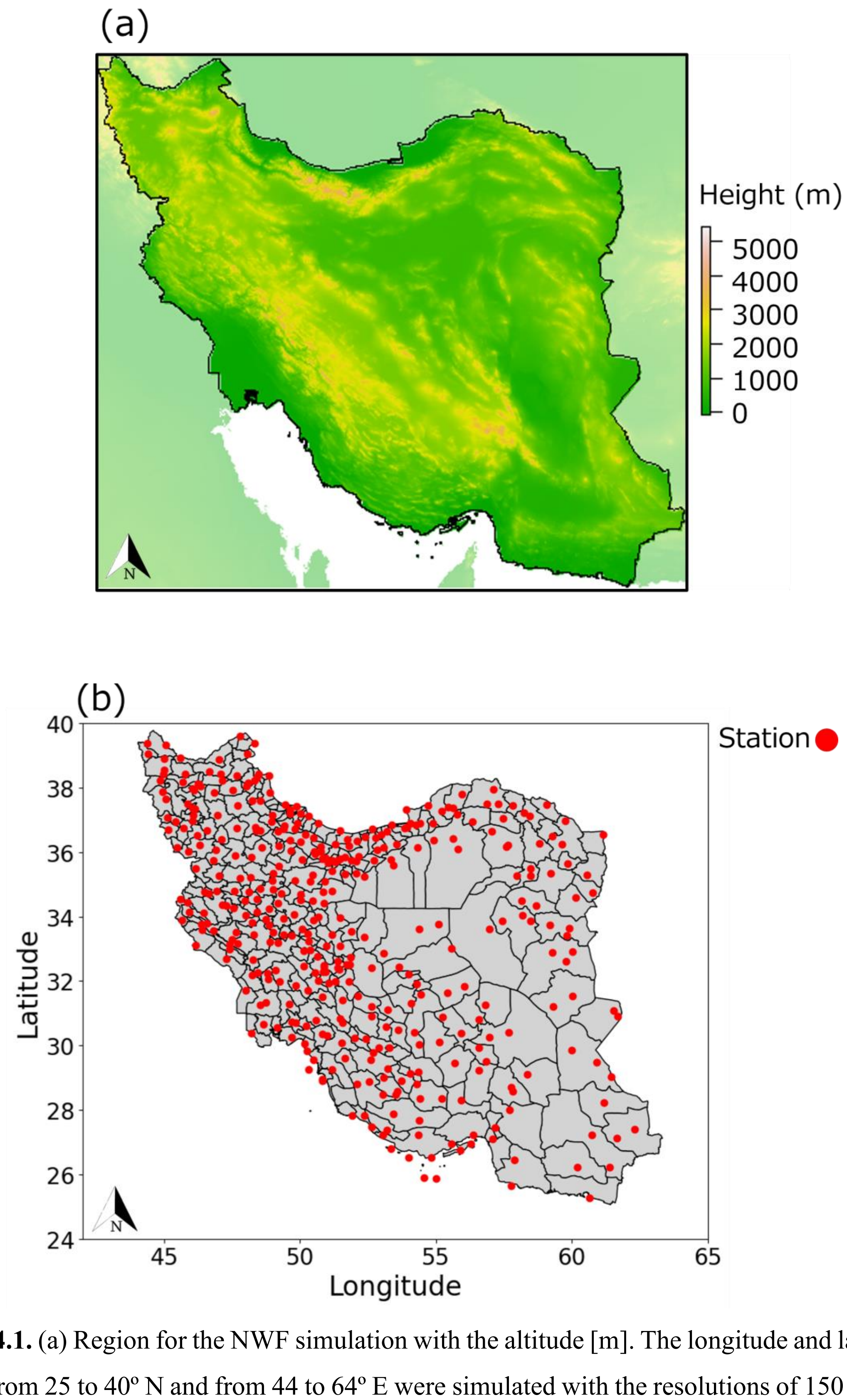

Figure 4.1. (a) Region for the NWF simulation with the altitude [m]. The longitude and latitude ranges from 25 to 40º N and from 44 to 64º E were simulated with the resolutions of 150 × 130,

respectively. (b) Locations of the weather stations provided by the meteorology organization of Iran.

4.2.2. Weather station datasets

Meteorological data for the period of 2021 were obtained from January 1, 2021, to December 31, 2021, with a three-hour interval at 427 stations from the meteorology organization of Iran (Islamic Republic of Iran Meteorological Organization, IRIMO). In most stations, wind speeds are measured using three-armed cup anemometers (LAMBRECHT meteo GmBH), while only at airport stations, ultrasonic anemometers (Vaisala) are employed for measurements as standard instruments with a sampling frequency of 4 Hz. Figure 4.1 (b) shows the locations of these stations. The datasets included the three-hour averaged wind speed, temperature, relative humidity, precipitation, soil temperature, and cloud height, along with the altitude and longitude of the stations. This chapter focuses on a dataset of wind speed measured at 10 meters above the ground. Stations with more than 50% missing wind speed data were excluded from the analysis. Consequently, data from 390 stations were used for further analyses. The latitude and longitude of each station were used to extract data from the WRF simulation.

4.2.3. Numerical weather forecasting model

For the NWF, the WRF version 4.1.2 was employed to cover the entire region in Figure 4.1 (a) for a one-year simulation to identify both diurnal and seasonal fluctuations (Giannaros et al. 2017; Prieto-Herráez et al. 2021). Alternative studies assessing the accuracy of WRF predictions have contributed to confidence in the reliability of the model for a region in Mexico and the US (Cuevas-Figueroa et al. 2022). They showed that the root mean squared error (RMSE) of the wind speeds between the meteorological data and WRF output can become over 20% at maximum and mostly less than 15%, although the RMSE of the PDFs were rather small (less than 3%). The numerical domain was defined with the grid resolution of 13 km in both lateral directions, resulting in 150 x 130 grid numbers in longitude and latitude, respectively. The vertical levels were discretized by 44 grid points and top pressure were 5000 hPa. The fifth-generation reanalysis data (ERA-5) of European Centre for Medium-Range Weather Forecasts (ECMWF) with 0.25-degree latitude-longitude horizontal resolution was used as the input data of the reanalysis data for the WRF simulation. The initial conditions were generated by the WRF preprocessing system (WPS) form the reanalysis dataset. The WPS also generate the time-dependent boundary conditions from the reanalysis data for every three hours. The time integration was based on the Runge-Kutta 3rd order scheme with the time step of 60s. The governing equations of the WRF model include the following:

$$\partial_t U + (\nabla \cdot \mathbf{V}u) + \mu_d \alpha\, \partial_x p + \left(\frac{\alpha}{\alpha_d}\right) \partial_\eta p\, \partial_x \phi = F_U \qquad (1)$$

$$\partial_t V + (\nabla \cdot \mathbf{V}v) + \mu_d \alpha\, \partial_y p + \left(\frac{\alpha}{\alpha_d}\right) \partial_\eta p\, \partial_y \phi = F_V \qquad (2)$$

$$\partial_t W + (\nabla \cdot \mathbf{V}w) - g\left[\left(\frac{\alpha}{\alpha_d}\right) \partial_\eta p - \mu_d\right] = F_W \qquad (3)$$

$$\partial_t \Theta_m + (\nabla \cdot \mathbf{V}\theta_m) = F_{\Theta_m} \qquad (4)$$

$$\partial_t \mu_d + (\nabla \cdot \mathbf{V}) = 0 \qquad (5)$$

$$\partial_t \phi + \mu_d^{-1}[(\mathbf{V} \cdot \nabla\phi) - gW] = 0 \qquad (6)$$

$$\partial_t Q_m + (\nabla \cdot \mathbf{V}q_m) = F_{Q_m} \qquad (7)$$

The set of equations from 1 to 7 constitutes the fundamental governing equations utilized in the Weather Research and Forecasting (WRF) model. Equations 1 to 3 pertain to momentum conservation, capturing the dynamics of wind motion in the horizontal and vertical directions. Equation 4 governs the evolution of potential temperature, reflecting the thermal energy distribution within the atmosphere. Equation 5 represents mass conservation, ensuring continuity of air mass throughout the simulation. Equation 6 addresses the evolution of geopotential height, a crucial parameter in atmospheric dynamics. Finally, equation 7 accounts for the conservation of moisture content, which plays a vital role in the formation of clouds and precipitation. Collectively, these equations form the backbone of the WRF model, providing a comprehensive framework for simulating atmospheric processes and phenomena.

The physical parameterizations of the simulation are listed in Table 4.1. Since the purpose of this paper is not to optimize the WRF model to choose best planetary boundary layer and physical schemes, the configuration was adapted based on a previous study showing the optimized configurations of the physical parameterizations (Saadatabadi et al. 2023). Thompson option was selected for microphysics, which significantly enhanced winter precipitation forecasts through advanced bulk microphysics schemes. The long-wave and shortwave radiation options are rapid radiative transfer model (RRTM) and Dudhia, respectively. The RRTM scheme is specifically designed for quick calculation of radiative transfer, while Dudhia suggests a simple approach to integrate various factors for more accurate predictions. The Quasi-Normal Scale Elimination option was chosen for planetary boundary layer and surface layer physics. Additionally, the Noah Land Surface Model has been incorporated for land surface schemes, providing soil temperature and moisture data across multiple layers. Although a sensitivity study of the parameterization of the WRF simulation was not performed, the simulated data were carefully compared with weather station data (Skamarock et al. 2019).

The WRF simulation was conducted for the year 2021 and the data were stored for 3-hours interval and spin up period is not used. After simulation horizontal velocity components, u, and v, were extracted based on geographical coordination of observatory stations at 10 m for further analysis. The horizontal wind speed was defined by $v_a = \sqrt{u^2 + v^2}$.

Table 4.1. Physical parameterization for the WRF simulation

Physical parameterizations	Schemes	Description
Micro-physics	Thompson model	Including refined saturation adjustment variable cloud water droplet shape parameter (Thompson et al. 2008).
Cumulus parameterization	Kain–Fritsch scheme	The Kain-Fritsch convective parameterization scheme shares a fundamental closure assumption with the Fritsch-Chappell (1980) scheme, assuming that convective effects remove convective available potential energy in a grid element within an advective time (Berg et al. 2013).

Longwave radiation	Rapid Radiative Transfer Model	Efficient look-up tables to ensure accuracy, considering multiple bands, trace gases, and microphysical species in its calculations (Mlawer et al. 1997)
Shortwave radiation	Dudhia model	A straightforward downward integration method to efficiently estimate cloud and scattering effects, as well as clear-sky absorption and scattering (Dudhia, 1989).
Planetary boundary layer surface layer physics	Quasi–normal Scale Elimination Scheme	new spectral model for stratified turbulence for the atmospheric boundary layer over sea ice (Sukoriansky et al. 2005).
Land surface	Noah Land Surface Model	A unified scheme developed by NCEP/NCAR/AFWA, incorporating soil temperature and moisture data across four layers (Saadatabadi et al. 2023).

4.2.4. Statistical model

In addition to the NWF prediction of the annual wind speed distribution, A statistical model (Wang et al. 2022) was employed to confirm its suitability for predicting annual extreme wind events. The Gaussian distribution (or normal distribution) is a standard distribution with a symmetric bell-shape, along with skewness and kurtosis values of 0 and 3, respectively. However, in various probability distributions of wind speeds, it is very rare for the distribution of wind speeds to follow a Gaussian distribution; therefore, the skewness and kurtosis values may deviate from these values because of the occurrence of infrequent strong wind speeds. In order to better approximate these PDFs, a modified Gaussian distribution can be used by incorporating higher-order statistics. The third-order GCS uses several statistics, such as the mean, standard deviation, and skewness, to modify the Gaussian distribution using the following equation:

$$p(\zeta) = \frac{1}{\sqrt{2\pi}} e^{\frac{-\zeta^2}{2}} \left\{1 + \frac{S_k}{6}(\zeta^3 - 3\zeta)\right\} \tag{8}$$

Here, $\zeta = \frac{u-\mu}{\sigma}$ is the standardized random variable, μ and σ are the mean and standard deviation, respectively. S_k represents the third-order moment or skewness.

To assess the precision of the annual extreme events based on the GCS model, the 99.9th, 99th, and 90th percentiles of the three-hourly averaged wind speed in one year were computed in the following analyses based on the GCS, WRF, and field observations for the selected 390 stations.

4.3. RESULTS

4.3.1. Comparison between observation and WRF-model outputs

The PDF is dominantly characterized by its first three statistics of mean, standard deviation, and skewness when the distributions are modeled using the third-order GCS in Eq. (1). In addition, the skewed shape of the PDFs largely depends on skewness. Comparisons of these variables between observations and the WRF model are pivotal for reproducing PDFs. Figure. 4.2 illustrates the comparison between the observational and WRF model outputs for the mean (Fig. 4.2 (a)), standard deviation (Fig. 4.2 (b)), and skewness (Fig. 4.2 (c)) of the three-hour averaged wind speeds for one year at 390 weather stations. This comparison is crucial for scrutinizing and selecting stations with high correlations for further analysis.

The mean wind speed in the observational output typically ranged from 1 to 4 m/s, whereas in the model output, it increased to 3–7 m/s. Notably, the model tends to overestimate the mean wind speed, which is consistent with the findings of prior research (Gholami et al. 2021; Penchah et al. 2017).

The standard deviations of the wind speed for both the observational and model outputs were relatively low, hovering around 2 m/s for the observation and approximately 3 m/s for the model. Note that the small value of the standard deviation is because the values are defined by the standard deviation of the three-hour mean wind speed. This means that, on average, the averaged three-hour wind speeds were consistent over one year, without much variation.

The skewness value for both datasets was positive and fluctuated between zero and two for the output data. This suggests an asymmetric distribution in the wind speeds, indicating that the occurrence of strong three-hour mean wind speed is relatively low, but the magnitude is large.

According to the fact that the WRF can cause the overestimation of the mean values, the current simulation results also exhibited similar tendencies in terms of the reproduction of the mean values. However, to the authors best knowledge, other statistics such as the standard deviation and skewness have never been compared in previous studies. Their inclusion is not only helpful but also necessary for further analysis in our study. This study also shows that the standard deviation was overestimated. By contrast, the skewness values showed relatively good agreement because of the nature of dimensionless statistics. Although it was possible to improve the reproduction of the simulation datasets, further statistical analyses were performed to scrutinize the relationships between the statistics and peak wind speeds.

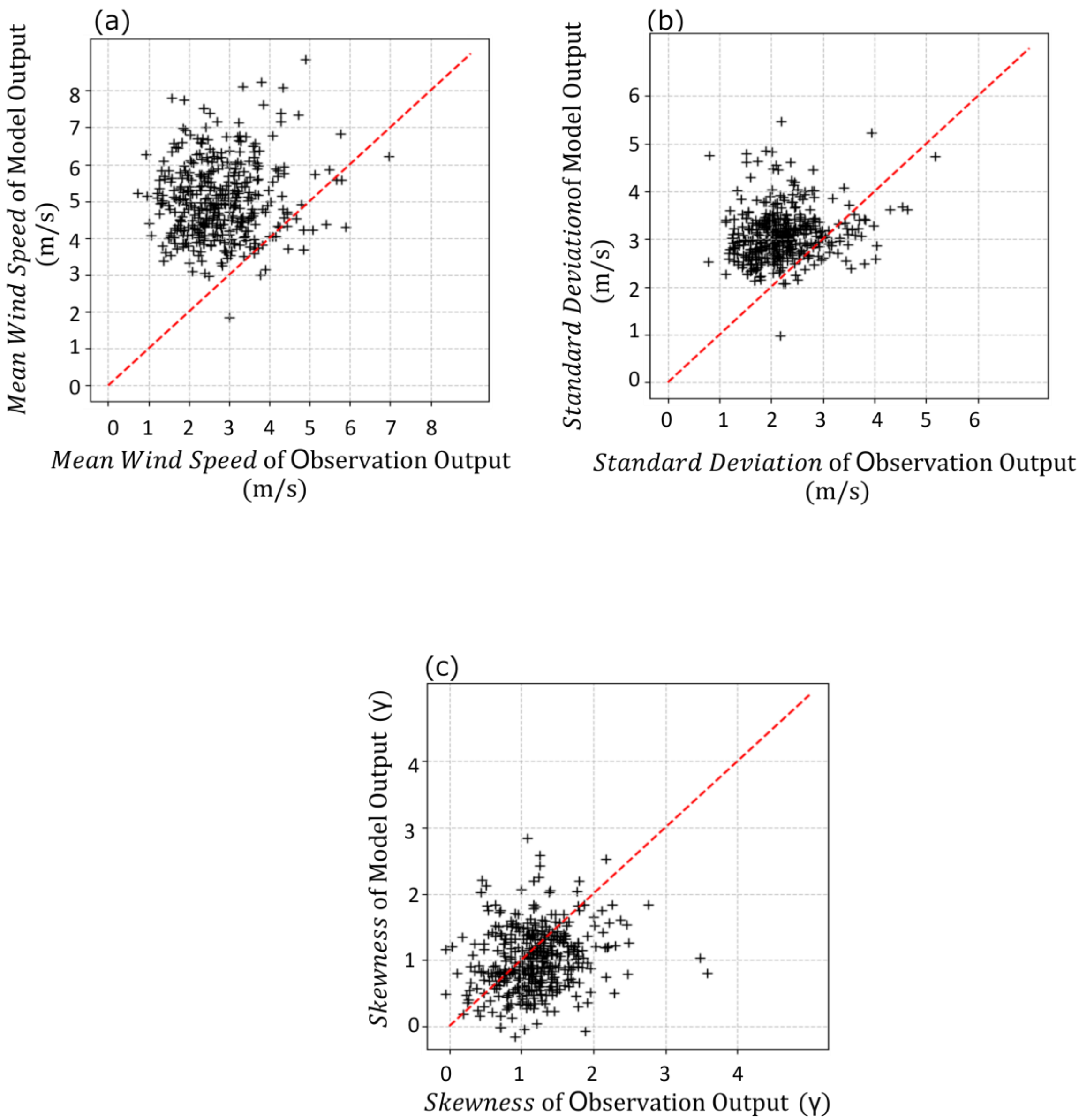

Figure 4.2. Relation of the statistics of the three-hour averaged wind speeds determined by the observation and WRF-model outputs over a year period for the 390 weather stations. (a) Annual mean wind speed [m/s], (b) standard deviation [m/s], and (c) skewness of the three-hour averaged wind speeds.

Highlighting the distinctive relationship between the mean, standard deviation, skewness, and kurtosis can clarify the consistency between the observation and WRF model outputs. Figure 4.3 shows the relationship between the mean wind speed and the other three statistics: standard deviation, skewness, and kurtosis of the three-hour averaged wind speed. As shown in Figure 4.3, across all three variables, the mean wind speed in the observational data was consistently lower than the WRF model output. However, a noticeable consistency exists between the two datasets in terms of the relationship between the mean and the other statistics (Fig. 4.3 (a, b)). Although there is a certain deviation between the observations and WRF model predictions in terms of the range of the mean wind speed, it is interesting to observe a similar tendency among the statistics for both outputs. Figure 4.3 (c) shows the kurtosis distributions of both outputs as functions of mean wind speed. For both outputs, the kurtosis values were predominantly distributed between three and five. This suggests that the PDFs are sharper than the Gaussian distribution because the kurtosis values exceed three.

According to Figures 4.2 and 4.3, the comparisons indicated that the prediction accuracy was not high, resulting in overestimation of the WRF output. However, these comparisons still provided satisfactory results compared to the observations from the WRF model in terms of the relationship between mean wind speeds and other statistics. Therefore, an improvement in the overall prediction using the NWF is required. However, the relationship between the statistics, PDFs, and extreme-averaged wind speed can be discussed based on the observational and WRF model outputs.

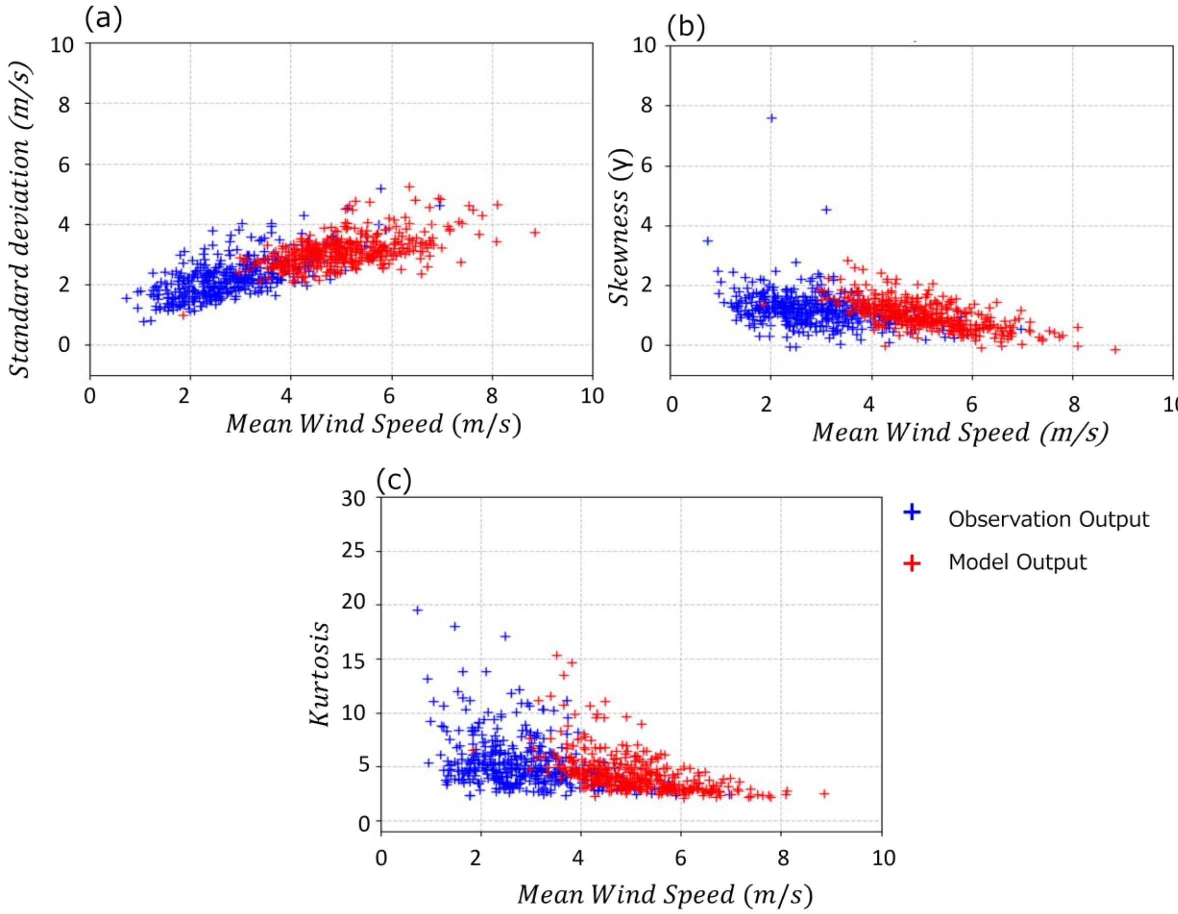

Figure 4.3. Comparison of the relationship between statistical variables of observation and WRF-model outputs with mean wind speed [m/s]. Blue crosses represent observation output and red crosses show model output. (a) standard deviation [m/s], (b) skewness, and (c) kurtosis of the three-hour averaged wind speeds.

4.3.2. Relation between statistics and peak values

In this section, the relationship between mean values and statistics, such as 99.9th, 99th, and 90th percentile wind speeds, along with their corresponding peak factors, coefficient of variation, and skewness of the three-hour averaged wind speeds, are explored to understand the distribution and better predict extreme wind speeds. Figures 4.4, 4.5, 4.6, and 4.7 show these relationships for both the observational and WRF model data.

Figure 4.4 (a) and (b) illustrate the relationship between the mean and three percentiles of wind speeds for the WRF model and observational outputs, respectively. The red, green, blue, and black circles represent wind speeds at the 99.9th, 99th, and 90th percentiles, respectively, and the maximum wind speed of the three-hour averaged wind speeds to highlight the infrequent occurrence of strong mean wind speeds annually. The 90th–99.9th percentiles represent strong mean winds during the observation year at each station. In addition, each category was regressed by a linear line to show the increasing trend of the percentiles with the mean wind speed. The distribution of the mean wind speed for the observational output ranged predominantly from 1 m/s to 4.5 m/s. Conversely, for the WRF model output, this value was elevated, ranging from 3 m/s to 7.5 m/s. As shown in Figures 4.2 and 4.3, the model overestimates the wind speed, as explained in the previous section.

Regarding strong mean wind speeds, it is evident that the percentile values increase simultaneously with an increase in the mean wind speeds across all percentiles, although the degrees of deviation from the regression lines vary. This observation suggests that as the mean wind speed increases, the magnitude of infrequently observed strong winds also escalates; however, this tendency becomes more pronounced for the 90th percentile than for the 99.0th and 99.9 th percentiles. This linear relationship indicates that the PDF of wind speed expands with an increase in wind speed (Ikegaya et al. 2020). Notably, the deviation from the regression line was comparatively lower for the 90th and 99th percentile values than for the 99.9th percentile. The deviation from the regression lines indicates that the variations in the magnitude of wind speeds increased for larger percentiles. Despite deviations from the regression lines, establishing a relationship between these variables implies a possible approximate prediction of strong wind speeds based on a simple linear relationship. Although the range of the mean wind speed differed between the two datasets, it is intriguing that the trend was similar regarding the relationship between the mean and extreme wind speeds.

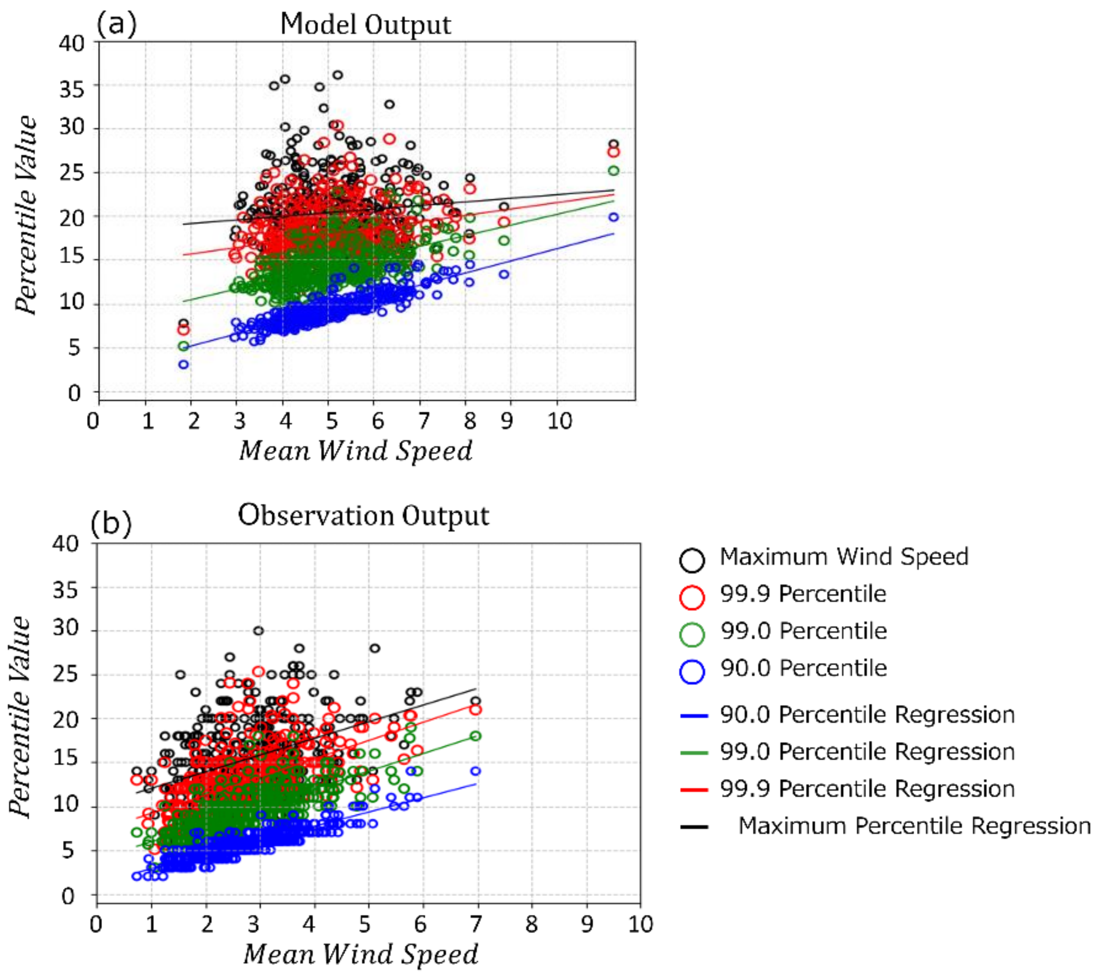

Figure 4.4. Relation between percentile values and mean wind speed. (a) WRF-model output, (b) observation. Black circles represent maximum wind speed [m/s] and red, green, and blue circles represent 99.9, 99.0 and 90.0 percentiles, respectively. Lines represent regression lines based on each percentile.

Figure 4.5 illustrates the relationship between the mean wind speed and peak factors for the 99.9th, 99th, and 90th percentiles of three-hour averaged wind speeds. The peak factor, PF, is defined as $PF = (v_{a_F} - \mu)/\sigma$, where v_{a_F} indicates the F-th percentile value of v_a. Therefore, the PF defined here is similar to the values of the standardized random variable ζ (Ikegaya et al. 2020). To define PF, the maximum wind speed and the 99.9th, 99th, and 90th percentiles were selected as the low-occurrence strong mean wind speeds. PFs are commonly used to estimate instantaneous extreme values from wind speed statistics; However, the same strategy was employed to estimate the strong mean wind speed during the one-year observation period. The horizontal lines in Figure 4.5 represent the PFs determined by the Gaussian distribution (i.e., the values of ζ at each cumulative probability).

For the 90th percentile, the PFs aligned with the value of the Gaussian distribution for both the model (Fig. 4.5 (a)) and the observations (Fig. 4.5 (b)). However, for the 99th and 99.9th percentiles, the PFs deviated from the Gaussian distribution. Specifically, the values for PFs at the 99th and 99.9th percentiles exceeded those determined by the Gaussian distribution, particularly when the mean wind speed was small. This deviation is less pronounced for the model output (Fig. 4.5 (a)) but more prominent for the observational output (Fig. 4.5 (b)). Furthermore, the PFs of the 99.9th and 99th percentiles approached the horizontal lines with an increase in the mean wind speed.

Notably, the 90th percentile can be estimated using the PF determined from the Gaussian distribution. In addition, the PFs of the 99.9th and 99th percentiles approached Gaussian distributions. These findings are consistent with those of previous studies (Ikegaya et al. 2020; Hirose et al. 2022; H'ng et al. 2022; Li et al. 2024), although they discussed the relationship between the mean and instantaneous wind speeds. The common tendency of the 90 percentiles to be approximated by the PF of the Gaussian distribution highlights the robustness of the PF for a relatively high occurrence frequency by employing the mean and standard deviation as statistical values.

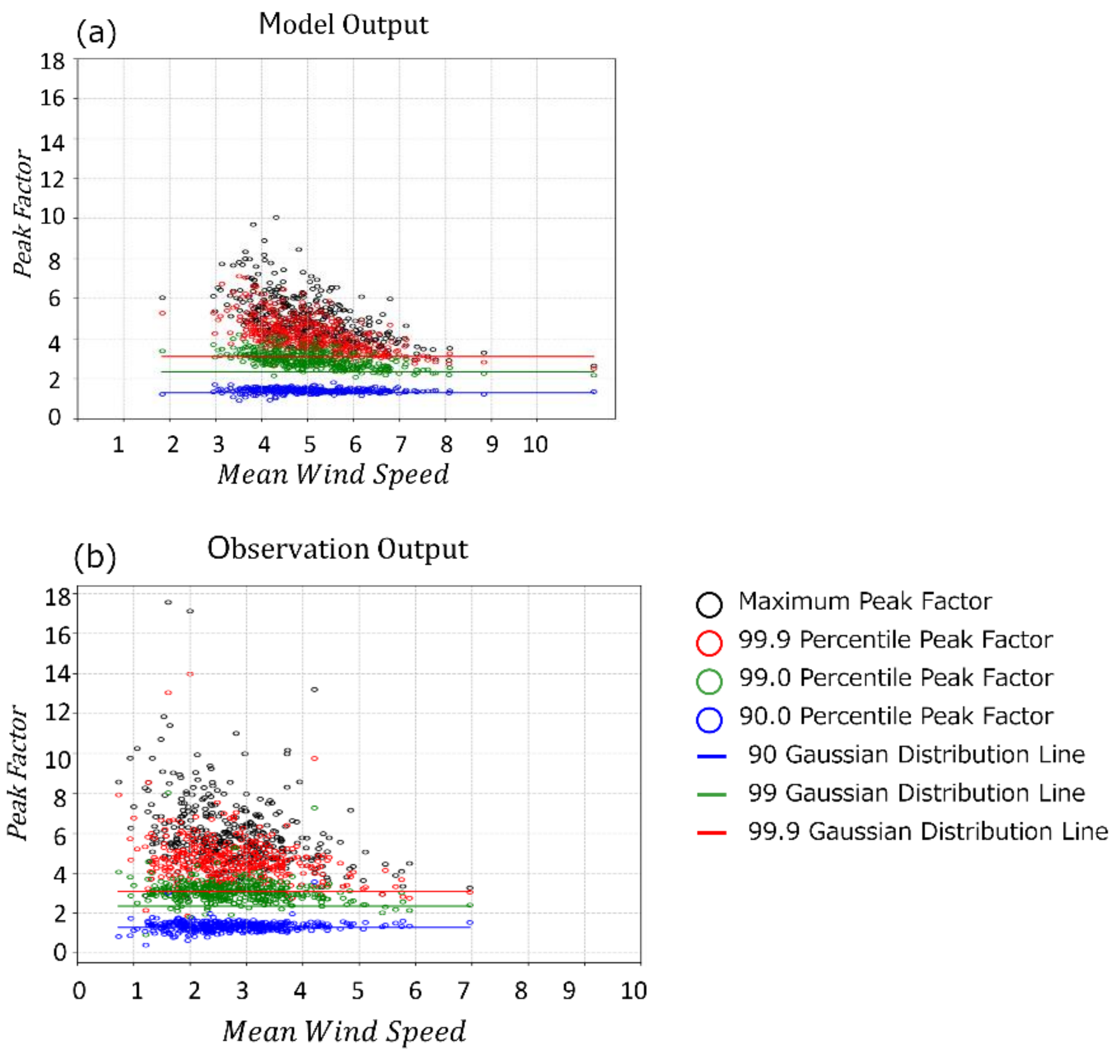

Figure 4.5. Relationship between PFs of each percentile with mean wind speed for (a) WRF-model output, and (b) observation output. Black circles represent maximum PF and red, green, and blue circles represent 99.9, 99.0, and 90.0 percentiles peak factor, respectively. Lines represent PFs determined by normal distributions.

Figure 4.6 illustrates the coefficient of variation, $CV(=\sigma/\mu)$, with higher values indicating greater deviation from the mean, versus PF for each percentile of the WRF-model output (Fig. 4.6 (a)) and observation data (Fig. 4.6 (b)). Because the effect of the standard deviation on the PFs was not considered in Figure 4.5, CV was used to express PFs in Figure 4.6. In addition, Wang and Okaze (2022) employed the CV of the wind speed to predict extreme values. They concluded that PF could be estimated from CV based on a two-parameter Weibull distribution.

In the WRF output (Fig. 4.6 (a)), the CV values were consistently below 1.0, across all three categories (i.e., the standard deviation was less than the mean). However, in the observational data (Fig. 4.6 (b)), the CV values can exceed 1.0 and some can reach 2.0. Furthermore, the PFs of the 90th percentile in both outputs aligned with the values of the Gaussian distribution, implying that the wind speeds for the 90th percentile could be estimated. However, for the PFs of the 99.0th and 99.9th percentiles, there is a noticeable tendency towards overestimation, which means that the wind speeds for the 99.0th and 99.9th percentiles cannot be estimated, particularly for the observation output.

In this analysis, the effect of variations in three-hour averaged wind speeds was considered by employing the standard deviation. However, the deviation in the PFs did not improve. This means that the variation in the PFs cannot be explained well by the CV.

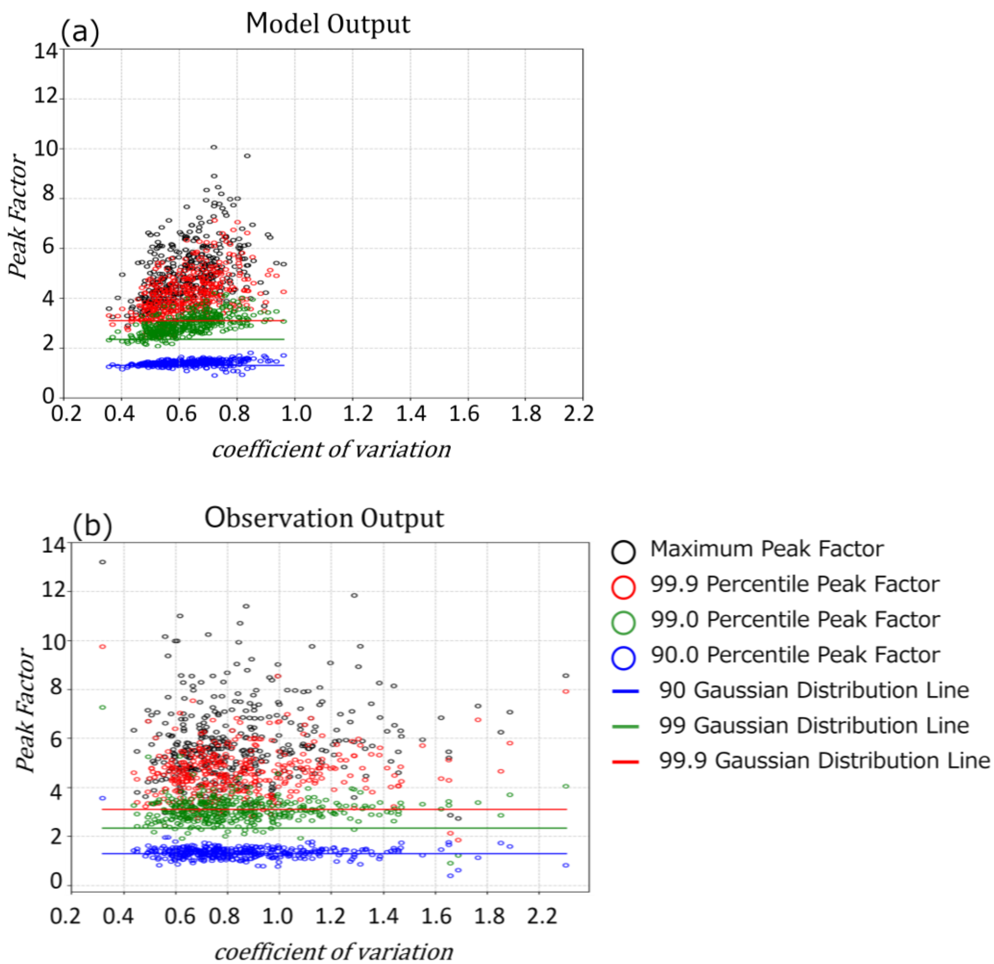

Figure 4.6. Relationship between PFs of each percentile with coefficient variation. (a) model output, (b) observation output. Black circles represent maximum PF and red, green, and blue

circles represent 99.9, 99.0, and 90.0 percentiles PF, respectively. Lines represent PFs determined by normal distributions.

Figure 4.7 shows the relationship between the PFs defined by the 99.9th, 99th, and 90th percentile values and the skewness of three-hour averaged wind speeds. Skewness, being a higher-order statistic than the CV, is probably a suitable parameter for showing a clearer relationship between PFs and statistics. This leads to better predictions of the PDFs and spatially dependent wind speed distributions.

As shown in Figures 4.7 (a) and (b), the skewness values mostly vary between 0 and 2 for both outputs. A positive skewness indicates that extreme winds contribute to the PDF having a long-tailed shape on the positive side while shortening the edge of the PDF on the other side, consequently increasing the PF of strong wind speeds. Figure 4.7 shows good agreement between the PFs of the 90th percentile by the Gaussian distribution line, suggesting that strong winds with the 90th occurrence frequency can be estimated if the PF values are determined. This tendency is more pronounced for the WRF model output as the observation output deviates more. The good agreement between the PFs of the 90th percentile and those of the Gaussian distribution in Figures 4.5, 4.6, and 4.7 indicate that the PFs of the 90th percentile are not associated with these statistics but can be predicted by the Gaussian distribution.

On the other hand, for the values of the 99.0th and 99.9th percentiles show an overestimation from the Gaussian distribution. However, the deviation of the PFs was smaller than those shown in Figures 4.5 and 4.6. This implies that skewness is an influential parameter for PFs as the skewness correlation with strong wind speeds is strong.

In terms of the differences between the model and observation, the skewness ranges differed between the datasets, as in the mean and CV.

Although discrepancies were observed between the observations and WRF model outputs, the relationship between the statistics and PFs was maintained for both datasets. Therefore, the consistent tendencies observed between the two datasets justify the following analyses based on both outputs. In addition, the current simulation covers the entire region of Iran to identify holistic trends in statistics and peak values, which can produce ample datasets rather than observations.

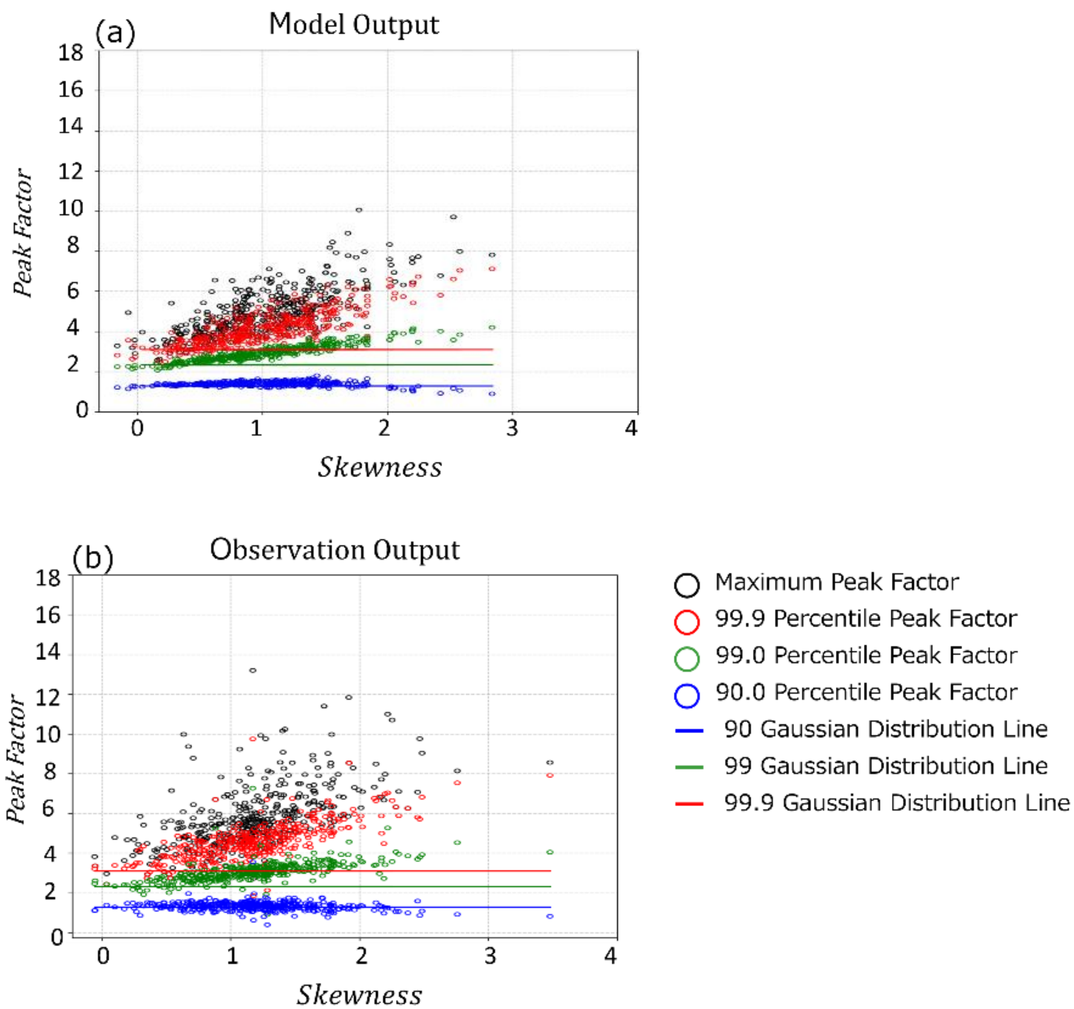

Figure 4.7. Relationship between PFs of each percentile and Skewness. (a) model output, (b) observation output. Black circles represent maximum PF and red, green, and blue circles represent 99.9, 99.0, and 90.0 percentiles PF, respectively. Lines represent PFs determined by normal distributions.

4.3.3. Prediction of probability densities and peak values

In this section, observational data and WRF model outputs are compared to discuss the accuracy of the local measurement positions based on the spatial distribution of the correlation coefficient of the mean wind speed. In addition, the PDFs and percentiles of the GCS model were compared between the WRF model output and the observational data.

4.3.3.1. Correlation coefficient distribution

Figure 8 illustrates the spatial distribution of the correlation coefficient C between the observed and WRF model outputs of three-hour averaged wind speeds for one year. Figure 4.8 (a) depicts the overall spatial distribution of all stations, whereas Figures 4.8 (b) and (c) highlight the spatial distribution of stations exhibiting high ($C > 0.4$) and low ($C < 0.2$) correlations, respectively. Most stations displayed C ranging from 0.3–0.5. Notably, even higher values of C do not surpass 0.7 and are widely distributed in the western and eastern regions of the country (e.g., Fig. 4.8 (d,e)). In contrast, stations such as Zabol, Zahak, Taybad, and Khaf in the east; Aghajari, Hezarkaniyan, Golpayegan, Bukan, and Arak in the west; and Bushehr, Manjil, Varzaneh, and Mobarakeh in the south, north, and central regions exhibited C values exceeding 0.6, showing relatively better predictions than other stations. Most of these stations are considered to have high annual wind speeds (the average wind speeds of these stations ranged from 3 to 6 m/s). and some of them host wind farms (Mirnezami & Mohseni Cheraghlou. 2022). These results indicate that an acceptable prediction of wind speeds can be achieved for stations in the western and eastern regions where there are certain demands for numerical prediction. Conversely, certain stations demonstrated low C, with some even displaying negative C.

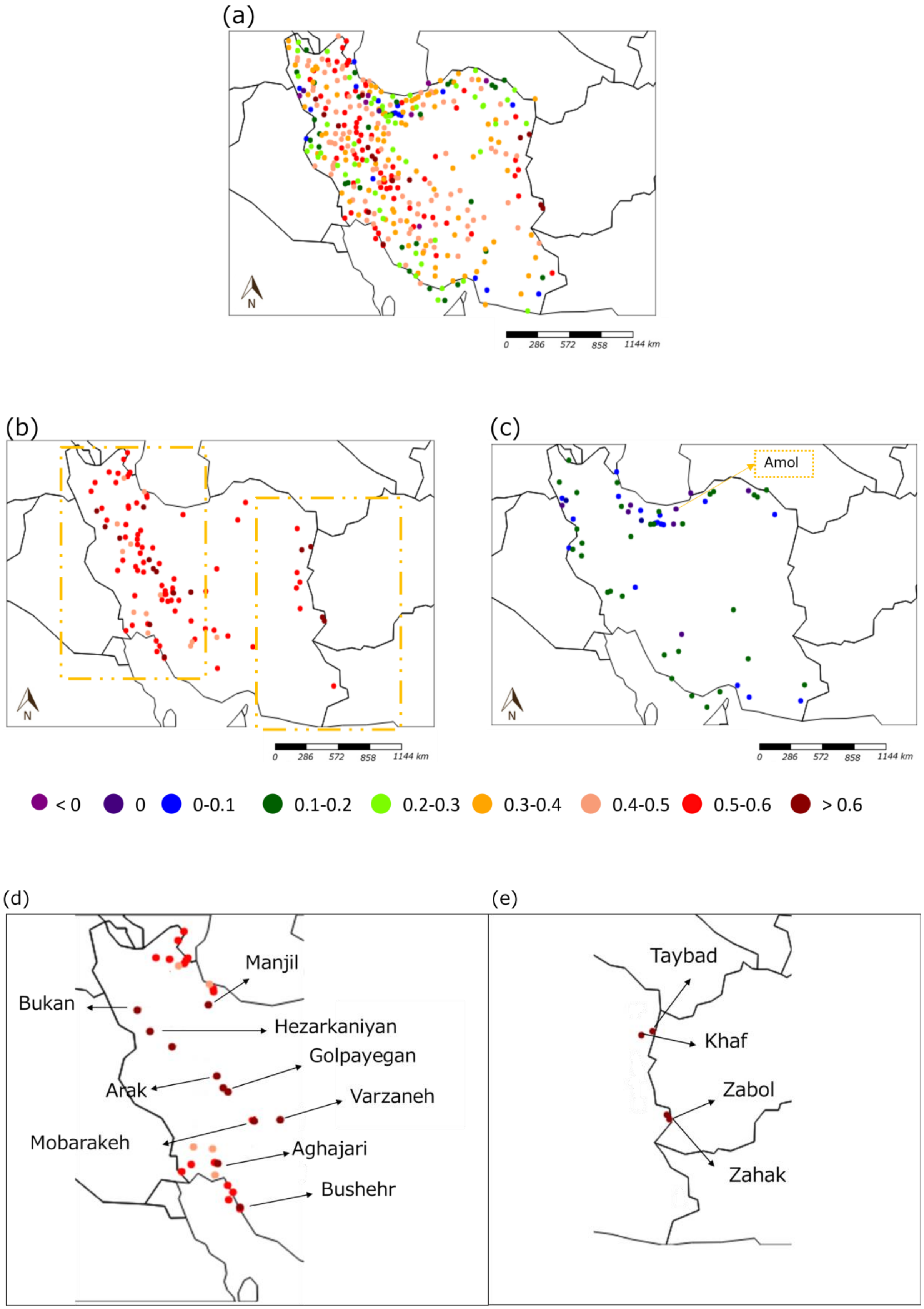
(a)
0
286
572
858
1144 km
(b)
(c)
Amol
< 0
0
0-0.1
0.1-0.2
0.2-0.3
0.3-0.4
0.4-0.5
0.5-0.6
> 0.6
(d)
Manjil
Bukan
Hezarkaniyan
Golpayegan
Arak
Varzaneh
Mobarakeh
Aghajari
Bushehr
(e)
Taybad
Khaf
Zabol
Zahak

Figure 4.8. Spatial distribution of correlation coefficient C of wind speeds between observation output and WRF-model outputs for (a) all stations, (b) stations with high correlation ($C > 0.4$), and (c) stations with low correlation ($C < 0.2$). Enlarged figures in (d) west and (e) east regions with high correlation ($C > 0.4$).

4.3.3.2. Comparison of PDF at specific stations

According to the distribution of the correlation coefficients, most stations showed acceptable correlations. Along with the numerical predictions, specific stations with high correlation values were chosen for the GCS model analysis to demonstrate the applicability of the statistical model.

(a) Zabol

Figure 4.9 shows a histogram and scatter comparison of the mean wind speeds at the Zabol meteorological station. The Zabol meteorological station is positioned at 31º, 08′ and 61º, 54,' standing at an elevation of 489.2 m above sea level. This station, situated in a province known for its robust summer wind patterns (Alizadeh-Choobari et al. 2014), exhibited the highest annual mean wind speed among all the stations analyzed. In addition to this comparison, Figure 4.9 (a, b) shows the predictions of the PDFs using the Gaussian distribution and GCS models. The values at the top-right corner indicate the skewness, standard deviation and mean values for both the observation and WRF-model outputs, and the C analysis between the observed wind speed at the Zabol station and the WRF output yields a value of 0.66, as depicted in (Figure 4.9 (c)).

The wind speeds ranged from 0 to 18 m/s. However, there was a slight disparity in the densities of the outputs. Although the density of wind speeds at 3 m/s was notably high in both outputs, it was slightly higher in the WRF model output than in the observation output. This finding corroborates the earlier observation that the WRF model tends to overestimate the mean wind speeds. This tendency was also observed at the station.

In terms of the PDF distributions, both outputs exhibit positively skewed PDFs, with the WRF output demonstrating higher values of 0.68 and observation with 0.54. Despite the positive skewness values, the Gaussian distribution deviated slightly from the PDFs of the third-order models. However, the GCS model can express positively skewed PDFs obtained from the WRF output and observations. The smaller distinction in the observed output occurs because the skewness of the wind speed aligns more closely with those of the random variables following a Gaussian distribution. Therefore, the GCS model is well-suited for describing skewed PDFs, and this model effectively predicts the skewed tail; however, for better prediction, other higher-order statistics should be evaluated.

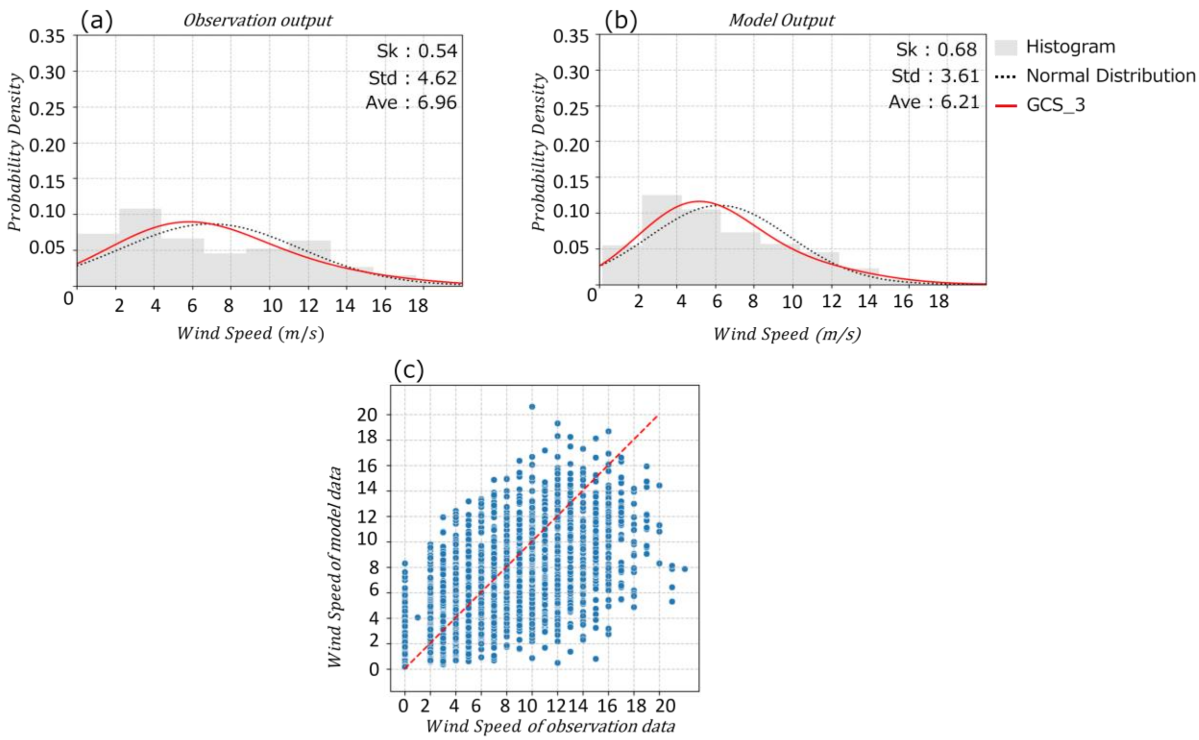

Figure 4.9. Comparison of PDF of wind speed times series (grey zone) and GCS third order model for Zabol station. (a) observation output, (b) model output. (c) correlation coefficient between observation output and model output with a value of 0.66.

(b) Aghajari

Aghajari is another station demonstrating a high correlation coefficient between the WRF-model and observation outputs, positioned at 30º, 69´ latitude, and 49º, 82´ longitude, with an elevation of 143 m above ground.

The mean wind speed in 2021 stood at 2.58 m/s. In the observation output, the wind speed distribution ranged between 1 and 7 m/s, with a peak occurrence frequency between 1 and 2 m/s. Conversely, for the WRF model output, the distribution spanned from 1 to 10 m/s, with a peak density observed at 4 m/s. Notably, at Aghajari station, the WRF output overestimated the wind speed. Thus, there is a discrepancy in the predictions of the occurrence frequencies of the two outputs.

Additionally, regarding the analysis of GCS model prediction, with a tiny discrepancy, it shows a close prediction of the PDF for both datasets. The skewness values for both the observation and WRF outputs were in good agreement. Hence, the PDF of the WRF and observation outputs show similar long-tail shapes. Therefore, analyzing the accurate prediction of skewness values separately can help us understand the variations in strong winds reaching high values. However, for more accurate results, other higher-order statistics should also be analyzed.

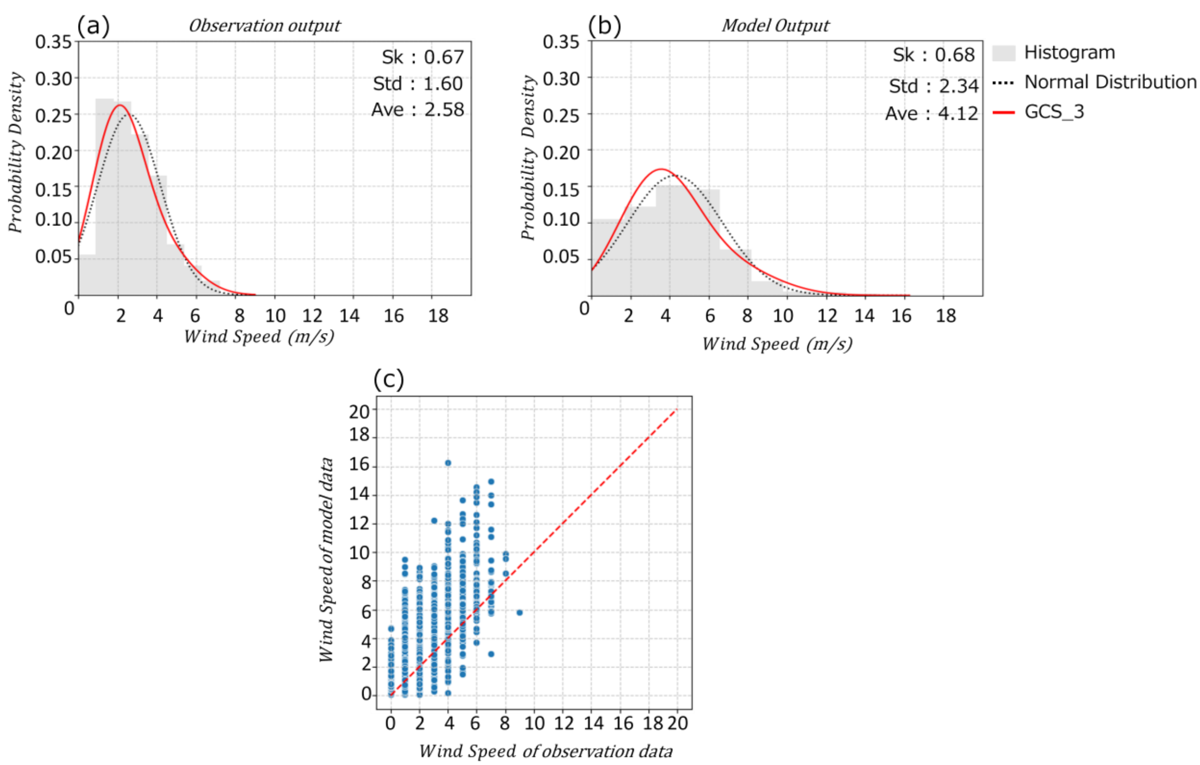

Figure 4.10. Comparison of PDF of wind speed times series (grey zone) and GCS third order model for Aghajari station. (a) observation output, (b) WRF-model output. (c) correlation coefficient between observation output and model output with a value of 0.66.

(c) Amol

One of the stations exhibiting a low correlation coefficient between the WRF model and observation outputs is the Amol station, as shown in Figure 4.11 Positioned in the northern part of Iran, it has latitudes and longitude of 52º, 38´ and 36º, 46°, respectively, with an elevation of 76 m above sea level. During the analysis period, Amol station recorded a mean wind speed of 1.76 m/s. The wind speed density in the observation output fluctuated between 0 and 8 m/s, with peak concentrations between 0 and 2 m/s. By contrast, the density of the model output varied between 0 and 12 m/s. Additionally, there was a higher frequency of occurrence between 2 and 6 m/s in the WRF model output. The skewness values between the two outputs showed a considerable discrepancy, with the WRF output having a higher value of 1.34 and the observation output showing a lower value of 0.17.

Regarding the prediction by the statistical model, it is evident that there is a discrepancy between the prediction by the GCS model and the Gaussian distribution in both outputs, which shows a weak prediction of the PDF by the GCS model, especially for the observational data compared to the WRF output.

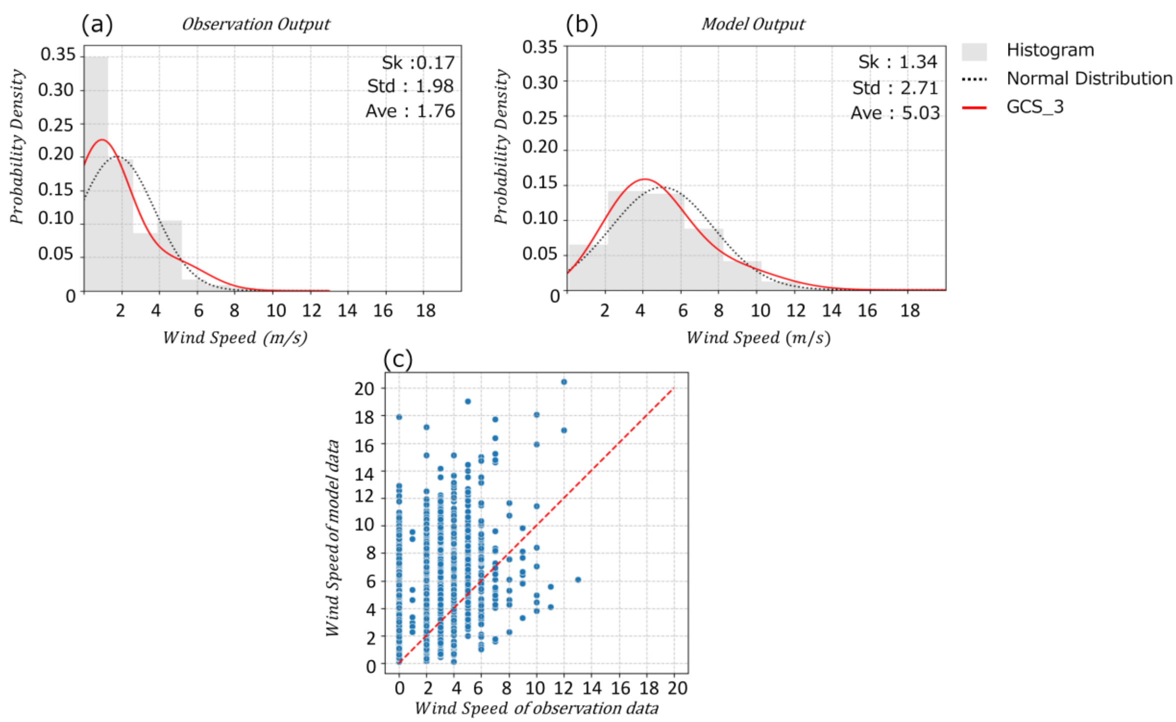

Figure 4.11. Comparison of PDF of wind speed times series (grey zone) and GCS third order model for Amol station. (a) observation output, (b) model output. (c) correlation coefficient between observation output and model output with a value of 0.31.

4.3.3.3. Extreme value prediction by statistical model

Figure 4.12 illustrates the relationship between the percentiles determined by the third-order GCS model for both the WRF model (Fig. 4.12 (a)) and the observation output (Fig. 4.12 (b)). This comparison aimed to validate the GCS model for predicting the peak values for both the WRF and observation outputs.

The diagonal line in the figures indicates a perfect prediction. Figure 4.12 shows a moderate correlation between the two outputs, although this does not imply a strong linear relationship. Notably, the percentile value of 90.0 exhibits a slightly better linear correlation for both the WRF and observational outputs. However, this trend was not as evident for the higher percentile categories of 99.0 and 99.9. As shown in Section 3.2, the peak factor of the 90th percentile was accurately predicted by the Gaussian distribution. Therefore, an accurate prediction of the 90th percentile is possible compared to the other rare percentiles.

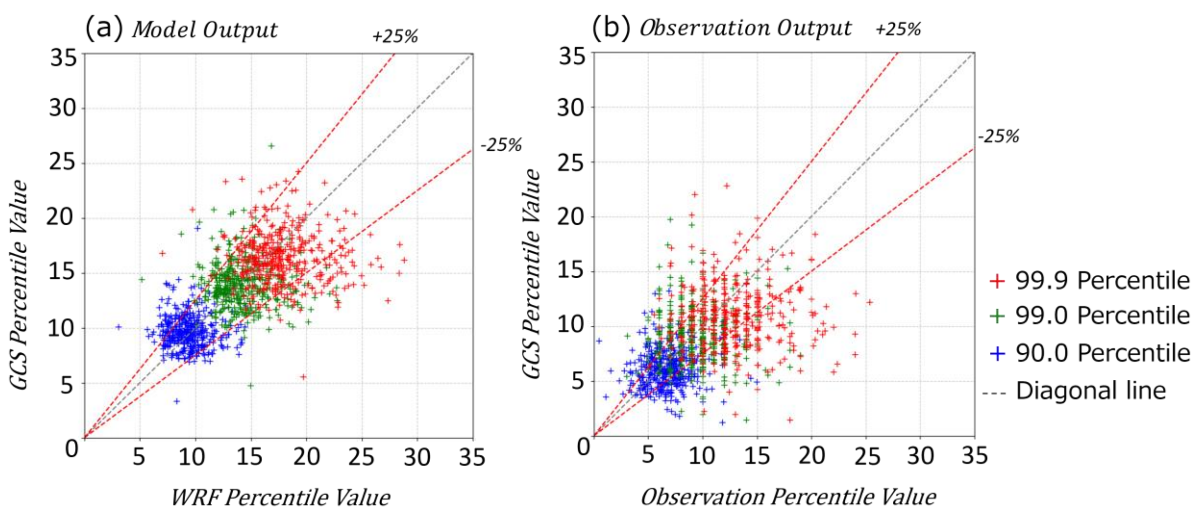

Figure 4.12. Comparison of WRF model output percentiles with observational and GCS percentiles at various levels. Red crosses represent percentile value of 99.9, green represents the 99.0 percentile and blue crosses show the 90.0 percentile values.

4.4. CONCLUSION

This chapter compared the three-hour averaged wind speeds for one year across 390 stations of the WRF model output with observational data in terms of fundamental statistics, peak factors, and probability density distribution. The aim was to assess the WRF simulation for reproducibility of rare annual wind events by scrutinizing the PDF, peak values of wind speeds, and occurrence frequency of extreme winds. Subsequently, a statistical model using the Gram-Charlier series expansion of the PDF for peak value prediction was proposed. The following conclusions were drawn.

First, in the comparison between the observed and WRF model outputs, the model tended to overestimate the mean wind speeds and standard deviations. In contrast, skewness shows a better agreement, probably because of the nature of dimensionless statistics. Additionally, both datasets showed similar patterns of positive skewness, indicating an asymmetric distribution of the probability density for wind speeds. Despite the discrepancy in the prediction by the WRF simulation for the mean and standard deviation, there was a noticeable consistency between the two datasets regarding the relationship between the mean, standard deviation, skewness, and kurtosis. This result justifies the latter analysis by scrutinizing the relationship between the peak factor and statistics for both datasets.

Second, analyzing extreme winds across three categories—the 90th, 99th, and 99.9th percentiles—revealed that the prediction of the 90th percentile was more stable than that of other categories using the PF. It is noteworthy that the 90th percentile can be easily predicted by assuming Gaussian distributions for annually strong wind speeds. Additionally, analyzing the relationship between the PFs and CV , and PF, and skewness clarified skewness as an influential parameter in the prediction of strong winds.

Third, to confirm the overall reproducibility of the WRF output for stations with a high correlation coefficient between the WRF model output and observations, the GCS model was applied to predict the PDFs of wind speed. Despite a slight disparity between the GCS model and the WRF-model output or observation output, the comparison of the percentiles showed that the GCS model acceptably captured the positively skewed PDFs of the wind speed distributions. However, there were some stations with a low correlation coefficient, for which the GCS model prediction was weaker. This weakness was also influenced by mean wind speeds at the stations. Thus, stations with higher mean wind speeds performed better in the analysis of the PDFs using the GCS model.

4.5. REFERENCES

Alavi, O., Mohammadi, K. and Mostafaeipour, A., 2016a. Evaluating the suitability of wind speed probability distribution models: A case of study of east and southeast parts of Iran. Energy Conversion and Management, 119, pp.101-108.

Alavi, O., Sedaghat, A. and Mostafaeipour, A., 2016b. Sensitivity analysis of different wind speed distribution models with actual and truncated wind data: A case study for Kerman, Iran. Energy conversion and management, 120, pp.51-61.

Alizadeh-Choobari, O., Zawar-Reza, P. and Sturman, A., 2014. The "wind of 120 days" and dust storm activity over the Sistan Basin. Atmospheric research, 143, pp.328-341.

Ammari, H.D., Al-Rwashdeh, S.S. and Al-Najideen, M.I., 2015. Evaluation of wind energy potential and electricity generation at five locations in Jordan. Sustainable Cities and Society, 15, pp.135-143.

Aslam, M., 2021. A study on skewness and kurtosis estimators of wind speed distribution under indeterminacy. Theoretical and applied climatology, 143(3), pp.1227-1234.

Berg, L.K., Gustafson, W.I., Kassianov, E.I. and Deng, L., 2013. Evaluation of a modified scheme for shallow convection: Implementation of CuP and case studies. Monthly weather review, 141(1), pp.134-147.

Cao, J., Man, X., Liu, J., Liu, L. and Shui, T., 2017. Preliminary assessment of the wind power resource around the thousand-meter scale megatall building. Energy and Buildings, 142, pp.62-71.

Carvalho, D., Rocha, A., Gómez-Gesteira, M. and Santos, C.S., 2014. WRF wind simulation and wind energy production estimates forced by different reanalyses: Comparison with observed data for Portugal. Applied Energy, 117, pp.116-126.

Cuevas-Figueroa, G., Stansby, P.K. and Stallard, T., 2022. Accuracy of WRF for prediction of operational wind farm data and assessment of influence of upwind farms on power production. Energy, 254, p.124362.

Dudhia J. Numerical study of convection observed during the winter monsoon experiment using a mesoscale two-dimensional model. Journal of Atmospheric Sciences. 1989 Oct 15;46(20):3077-107.

Gholami, S., Ghader, S., Khaleghi-Zavareh, H. and Ghafarian, P., 2021. Sensitivity of WRF-simulated 10 m wind over the Persian Gulf to different boundary conditions and PBL parameterization schemes. Atmospheric Research, 247, p.105147.

Giannaros, T.M., Melas, D. and Ziomas, I., 2017. Performance evaluation of the Weather Research and Forecasting (WRF) model for assessing wind resource in Greece. Renewable Energy, 102, pp.190-198.

Hågbo, T.O. and Giljarhus, K.E.T., 2024. Sensitivity of urban morphology and the number of CFD simulated wind directions on pedestrian wind comfort and safety assessments. Building and Environment, p.111310.

Hamzeh, N.H., Abadi, A.R.S., Kaskaoutis, D.G., Mirzaei, E., Shukurov, K.A., Sotiropoulou, R.E.P. and Tagaris, E., 2023. The Importance of Wind Simulations over Dried Lake Beds for Dust Emissions in the Middle East. Atmosphere, 15(1), p.24.

Hirose, C., Nomichi, T. and Ikegaya, N., 2022. Distributions of gust and peak factors at a pedestrian level in a simplified urban canopy obtained by particle image velocimetry. Building and Environment, 222, p.109350.

H'ng, Y.M., Ikegaya, N., Zaki, S.A., Hagishima, A. and Mohammad, A.F., 2022. Wind-tunnel estimation of mean and turbulent wind speeds within canopy layer for urban campus. Urban Climate, 41, p.101064.

Ikegaya, N., Kawaminami, T., Okaze, T. and Hagishima, A., 2020. Evaluation of exceeding wind speed at a pedestrian level around a 1: 1: 2 isolated block model. Journal of Wind Engineering and Industrial Aerodynamics, 201, p.104193.

KASAI, K., KIMURA, K., SHIOMI, K., KONNO, A., TADONO, T. and HORI, M., 2018. Analysis of the Strong Local Wind in Northwestern Hokkaido, Japan. Geographical Studies, 92(1), pp.17-36.

Lackoóvá, L., Lieskovský, J., Nikseresht, F., Halabuk, A., Hilbert, H., Halászová, K. and Bahreini, F., 2023. Unlocking the Potential of Remote Sensing in Wind Erosion Studies: A Review and Outlook for Future Directions. Remote Sensing, 15(13), p.3316.

Li, F., Hirose, C., Wang, W., Liu, C.H. and Ikegaya, N., 2024. Correlations among high-order statistics and low-occurrence wind speeds within a simplified urban canopy based on particle image velocimetry datasets. Building and Environment, 247, p.111050.

Li, F., Xie, Z., Yang, Y. and Yu, X., 2023a. Investigations of synoptic wind profile patterns in complex urban areas based on LiDAR measurements. Building and Environment, 242, p.110573.

Li, N., Yang, J. and Tang, X., 2023b. Spatiotemporal scale-dependent effects of urban morphology on meteorology: A case study in Beijing using observations and simulations. Building and Environment, 240, p.110383.

Li, S.H., Sifton, V., Lundgren, J., McClellan, C. and Gibbons, M., 2021. Extreme wind climate of the Arabian Peninsula characterized by using WRF simulation. Weather and Climate Extremes, 33, p.100330.

Mahmoudi, L. and Ikegaya, N., 2023. Identifying the Distribution and Frequency of Dust Storms in Iran Based on Long-Term Observations from over 400 Weather Stations. Sustainability, 15(16), p.12294.

Mathiesen P, Kleissl J. Evaluation of numerical weather prediction for intra-day solar forecasting in the continental United States. Solar Energy. 2011 May 1;85(5):967-77.

Mirhosseini, M., Sharifi, F. and Sedaghat, A., 2011. Assessing the wind energy potential locations in province of Semnan in Iran. Renewable and Sustainable Energy Reviews, 15(1), pp.449-459.

Mirnezami, S.R. and Mohseni Cheraghlou, A., 2022. Wind Power in Iran: Technical, Policy, and Financial Aspects for Better Energy Resource Management. Energies, 15(9), p.3230.

Mlawer EJ, Taubman SJ, Brown PD, Iacono MJ, Clough SA. Radiative transfer for inhomogeneous atmospheres: RRTM, a validated correlated-k model for the longwave. Journal of Geophysical Research: Atmospheres. 1997 Jul 27;102(D14):16663-82.

Mohammadi, M.H., Meshkatee, A.H., Ghader, S. and Azadi, M., 2024. Wind gust forecasting by post-processing the WRF model outputs using ANN. Dynamics of Atmospheres and Oceans, 105, p.101425.

Mortezazadeh, M., Jandaghian, Z. and Wang, L.L., 2021. Integrating CityFFD and WRF for modeling urban microclimate under heatwaves. Sustainable Cities and Society, 66, p.102670.

Najafi, M.S. and Alizadeh, O., 2023. Climate zones in Iran. Meteorological Applications, 30(5), p.e2147.

Nedaei, M., Assareh, E. and Walsh, P.R., 2018. A comprehensive evaluation of the wind resource characteristics to investigate the short-term penetration of regional wind power based on different probability statistical methods. Renewable energy, 128, pp.362-374.

Panahifar, H., Moradhaseli, R., Bourzoie, H., Gholami, M. and Khalesifard, H.R., 2020a. Lidar Measuremnt on Dust Transport from the Saharan Desert to the Iran Plateau. In EPJ Web of Conferences (Vol. 237, p. 02020). EDP Sciences.

Panahifar, H., Moradhaseli, R. and Khalesifard, H.R., 2020b. Monitoring atmospheric particulate matters using vertically resolved measurements of a polarization lidar, in-situ recordings and satellite data over Tehran, Iran. Scientific reports, 10(1), p.20052.

Penchah, M.M., Malakooti, H. and Satkin, M., 2017. Evaluation of planetary boundary layer simulations for wind resource study in east of Iran. Renewable Energy, 111, pp.1-10.

Prieto-Herráez, D., Frías-Paredes, L., Cascón, J.M., Lagüela-López, S., Gastón-Romeo, M., Asensio-Sevilla, M.I., Martín-Nieto, I., Fernandes-Correia, P.M., Laiz-Alonso, P., Carrasco-Díaz, O.F. and Sáez-Blázquez, C., 2021. Local wind speed forecasting based on WRF-HD Wind coupling. Atmospheric Research, 248, p.105219.

Prósper, M.A., Otero-Casal, C., Fernández, F.C. and Miguez-Macho, G., 2019. Wind power forecasting for a real onshore wind farm on complex terrain using WRF high resolution simulations. Renewable energy, 135, pp.674-686.

Ren, H., Dudhia, J., Ke, S. and Li, H., 2022. The basic wind characteristics of idealized hurricanes of different intensity levels. Journal of Wind Engineering and Industrial Aerodynamics, 225, p.104980.

Repetto, M.P., Burlando, M., Solari, G., De Gaetano, P. and Pizzo, M., 2017. Integrated tools for improving the resilience of seaports under extreme wind events. Sustainable cities and society, 32, pp.277-294.

Saadatabadi AR, Hamzeh NH, Kaskaoutis DG, Ghasabi Z, Penchah MM, Sotiropoulou RE, Habibi M. Optimization and evaluation of the Weather Research and Forecasting (WRF) model for wind energy resource assessment and mapping in Iran. Applied Sciences. 2024 Apr 14;14(8):3304.

Seta, K., Wang, W. and Ikegaya, N., 2023. Modeling probability density functions of instantaneous velocity components at the pedestrian levels of a building array by Gram–Charlier series. Journal of Wind Engineering and Industrial Aerodynamics, 239, p.105427.

Skamarock, W.C., Klemp, J.B., Dudhia, J., Gill, D.O., Liu, Z., Berner, J., Wang, W., Powers, J.G., Duda, M.G., Barker, D.M. and Huang, X.Y., 2019. A description of the advanced research WRF version 4. NCAR tech. note ncar/tn-556+ str, 145.

Sukoriansky, S., Galperin, B. and Perov, V., 2005. Application of a new spectral theory of stably stratified turbulence to the atmospheric boundary layer over sea ice. Boundary-layer meteorology, 117, pp.231-257.

Thompson, G., Field, P.R., Rasmussen, R.M. and Hall, W.D., 2008. Explicit forecasts of winter precipitation using an improved bulk microphysics scheme. Part II: Implementation of a new snow parameterization. Monthly weather review, 136(12), pp.5095-5115.

Wang, W. and Okaze, T., 2022. Statistical analysis of low-occurrence strong wind speeds at the pedestrian level around a simplified building based on the Weibull distribution. Building and Environment, 209, p.108644.

Wang, J., Wang, L.L. and You, R., 2023. Evaluating a combined WRF and CityFFD method for calculating urban wind distributions. Building and Environment, 234, p.110205.

Wang, W., Seta, K. and Ikegaya, N., 2022. Modelling probability density functions based on the Gram–Charlier series with higher-order statistics: Theoretical derivation and application. Journal of Wind Engineering and Industrial Aerodynamics, 231, p.105227.

Zainol, M.A., Ikegaya, N. and Mohamad, M.F., 2022. Stochastic and statistical characteristics of artificially generated turbulent flow following Karman spectrum in a wind-tunnel experiment. Journal of Wind Engineering and Industrial Aerodynamics, 229, p.105148.

Zhang, Y., Cao, S., Zhao, L. and Cao, J., 2022. A case application of WRF-UCM models to the simulation of urban wind speed profiles in a typhoon. Journal of Wind Engineering and Industrial Aerodynamics, 220, p.104874.

CHAPTER 5: CONCLUSION

SUMMARIZE AND FUTURE WORK

The West Asia region, often referred to as the Middle East, is characterized by its climatic sensitivity and vast desert landscapes. Stretching from the eastern Mediterranean Sea to the Arabian Peninsula, the region encompasses countries like Syria, Iraq, Iran, and others. Its climatic conditions, including low precipitation and extensive desert areas, make it highly susceptible to dust storms.

Several factors contribute to the development of dust events in the region. Climatic parameters, such as low precipitation and vegetation coverage, play a significant role. Decreased precipitation affects vegetation rates and soil moisture, making the surface more susceptible to wind erosion. Increased cohesion of soil particles due to higher soil humidity can mitigate wind erosion. Wind speed and particle size are also crucial factors determining the distance and area over which dust storms occur.

Anthropogenic activities, particularly changes in land use and water management, contribute to dust emissions. Hydrologic dust sources, including ephemeral water bodies, contribute significantly to worldwide dust emissions, with a large portion being anthropogenic. Vegetated surfaces, desert shrublands, and agricultural lands also contribute to dust emissions, influenced by land use and hydrological cycles.

Iran, located within the dry belt of West Asia, faces significant challenges related to dust storms. It is surrounded by countries with large deserts, such as the Karakum desert in Turkmenistan and the Margo and Registan deserts in Afghanistan. Iran itself is home to deserts like Dasht-e Kavir and Dasht-e Lut, recognized as major sources of dust storms.

Moreover, dry lakebeds, such as Hamoun, Hawr-al-Azim, Jazmurian, and Urmia lakes, contribute to dust events when they dry up due to water scarcity and drought conditions. The desiccation of these lakes, influenced by climatic factors and water management practices, leads to the uplift of deflatable soil material by intense local winds, exacerbating dust storm activity in the region.

Dust storms have diverse impacts on human health, the environment, and the economy. They increase the risk of respiratory diseases, affect cloud lifetime and climate, impair plant growth, damage infrastructure, and reduce agricultural productivity. Studies in Iran have demonstrated the correlation between dust storms and increased mortality rates, hospital admissions, and respiratory emergencies.

Monitoring and forecasting dust storms is crucial for early warning and mitigation efforts. Various methods, such as satellite remote sensing, ground-based lidars, radar systems, and numerical modeling, are employed for monitoring and predicting dust events. However, challenges persist in accurately modeling dust emission processes and understanding their complex dynamics, necessitating further research and development of comprehensive monitoring and forecasting systems. Wind, which exhibits significant variability both spatially and temporally, and soil characteristics, which vary widely and are not consistently well-defined, pose particular challenges in this regard.

In chapter 3, long-term meteorological data from 427 stations in Iran covering the period from 2010 to 2021, with a three-hour interval were analyzed. The data included various meteorological parameters and classifications of dust events based on World Meteorological Organization criteria. The analysis categorized dust events into suspended dust, rising dust, and dust storms, considering the frequency and spatial distribution of each category.

The occurrence frequency varies among the categories, with most stations experiencing around 30 days of dust events per year. Suspended dust is prevalent in western Iran, while rising dust is more common in central, southern, and eastern regions, especially pronounced in areas like Zabol. Dust storms, although less frequent, are widespread across the country.

The spatial distribution analysis showed uniformity in the occurrence of dust events, with suspended dust being more prevalent in the west and rising dust in the central and eastern parts. Dust storm occurrences were relatively rare, except for one station in the east.

The seasonal variation of dust events across Iran reveals distinct patterns: suspended dust is widespread, particularly in the western region during spring and summer, while rising dust peaks in spring and is more visible in central, south, and east Iran. Dust storms, less frequent but observed nationwide, are most prevalent in spring and less so in summer and autumn, with winter showing an increase but still limited occurrences. Overall, spring stands out as the season with the highest frequency of dust storms.

Annual variations analysis showed that Rising dust was the most common type, followed by suspended dust and dust storms. Annual trends showed fluctuations, with certain years like 2012 and 2015 witnessing higher occurrences.

The findings illustrate the occurrence of all three categories of dust events across various regions of Iran, each exhibiting distinct intensity and frequency patterns. These phenomena are predominantly active during the spring and summer seasons.

Although the study analyzed records from all meteorological stations in Iran to study dust events, the period of analysis was limited, and a longer timeframe would be necessary to obtain a more comprehensive understanding of these phenomena.Furthermore, it is important to note that the categories selected for the analyses did not encompass all possible dust classes. Therefore, for future studies, it would be beneficial to consider all dust classes to gain a more complete picture of sand and dust storms in Iran. This would enable us to identify any additional trends or patterns that may have been overlooked in our analysis.

In Chapter 4, the comparison between observational data and WRF model outputs for three-hour averaged wind speeds across 390 weather stations revealed several key findings. Further analysis highlighted a consistent relationship between the mean wind speed and fundamental statistics such as standard deviation, skewness, and kurtosis across both datasets. Despite some deviations, there is noticeable consistency in the tendencies among statistics for both outputs. However, the prediction accuracy of the WRF model was not high, indicating the need for improvement in overall prediction using the WRF. The WRF model tends to overestimate the mean wind speeds. The standard deviations of wind speeds are relatively low for both datasets, suggesting consistency over one year without significant variation. Both observational and model outputs exhibit positive skewness, indicating an asymmetric distribution of wind speeds with relatively low occurrences of strong three-hour mean wind speeds.

The analysis of extreme winds across different percentiles, including the 90th, 99th, and 99.9th percentiles, indicates varying levels of stability in prediction using peak factors. Notably, the prediction of the 90th percentile emerges as more reliable compared to other categories when employing peak factors. This finding underscores the potential for relatively straightforward prediction of the 90th percentiles, particularly for annually strong wind speeds.

In the next step, the GCS model was applied as a statistical method to assess the outcomes derived from the WRF model and observational output for analyzing the PDF of both outputs. It is applied for stations with a high correlation coefficient between the WRF model and observational output. While there was a slight variation, the comparison revealed that the GCS model adequately captures the positively skewed PDFs of wind speed distributions. However, it is noted that stations with a low correlation coefficient exhibited weaker predictions by the GCS model, influenced partly by the mean wind speed of the stations. Consequently, stations with higher mean wind speeds demonstrated better performance in the analysis of PDFs using the GCS model.

In summary, despite the coarse resolution of the simulation domain, significant statistical correlations were found between the WRF model and observational data. The GCS model has been approved as a new and reliable model for assessing the PDF. Besides, previous studies using the GCS model typically analyzed datasets with durations of only a few seconds. However, this experiment employed a one-year period of meteorology dataset, demonstrating that the GCS model also works effectively for longer dataset.

However, regarding modeling of wind by using weather prediction model of WRF, it is suggested to scrutinize the WRF model to attain more accurate simulations for analyzing PDFs of wind speed. Additionally, examining wind speeds across different seasons is recommended, as the intensity varies across seasons, leading to potentially more diverse and precise results. More fundamental studies based wind-blown sand flux should be done to achieve accurate.